A Deep-Learning Approach

for

Marker-less Stride Parameters Analysis

with Two Cameras

Masoud Dorrikhteh

Thesis submitted to the Faculty of Engineering
in partial fulfillment of requirements for the degree of

Master of Science

In

Digital Transformation and Innovation

School of Electrical Engineering and Computer Science

Faculty of Engineering

uOttawa

University of Ottawa

Ottawa, Ontario

Abstract

Human gait analysis is an essential indicator for physical and neuroglial health of an individual. Recent developments in deep-learning approaches to computer vision make possible new techniques for body segment and joint detection from photos and video frames. In this thesis, we propose a deep learning approach for non-invasive video-based gait analysis using two RGB cameras that would be suitable for routine gait monitoring in senior care and rehabilitation centers. Due to modularity and the low cost of implementation, it is considered an affordable solution for such centers. Furthermore, since the solution does not require any markers or sensors to be worn, it is a pervasive and easy method for daily usage. Our proposed deep-learning approach starts by calibrating both the intrinsic and extrinsic parameters of the cameras. Next, video streams captured from two RGB cameras are used as input, and OpenPose and HyperPose deep-learning frameworks are used to localize the main body key points, including the joints and skeleton based on Body 25 and COCO models, respectively. The 2D parameter outputs from the frameworks are triangulated into 3D vector spaces for further analysis. In order to reduce the noises in our data, we applied median and dual pass butter worth filters to the data. Finally gait parameters has been extracted measured and compared to the manually evaluated ground truth data which has been capture via manual measurement of a domain expert.

The approach was evaluated in a laboratory setting similar to an institutional hallway in five types of trials: walking back and forth in a straight line while turning out of frame, walking back and forth in a straight line while turning in frame, circular walking, walking with a cane

and a walker. The method brings promising results compared to more expensive and restrictive approaches that use up to 16 cameras and require markers or sensors.

Table of Contents

List of Figures

List of Tables

Abbreviations and Definitions

Abbreviation	Definition
AR	Augmented Reality
CNN	Convolutional Neural Network
COCO	Common Objects In Context
CPU	Central Processing Unit
EMG	Electromyography
GPU	Graphics Processing Unit
IC	Initial Contact
IMU	Inertial Measurement Unit
LSTM	Long Short-Term Memory
NCBI	National Center for Biotechnology Information
PAF	Part Affinity Fields
CRRD	Center of Rehabilitation Research And Development
RNN	Recurrent Neural Network
TC	Terminal Contact
TOHRC	The Ottawa Hospital Rehabilitation Centre

Acknowledgments

My sincere appreciation to my supervisors, Prof. Liam Peyton, Prof. Natalie Baddour, and Prof. Edward Lemaire, for trusting my abilities and providing this research opportunity. The pandemic of COVID-19 has brought many unexpected challenges for me and to this project. Yet, I was lucky enough to have such supportive and caring supervisors and have the utmost support and encouragement from them. I am deeply thankful for the thorough revisions and feedback provided to me on the research papers and thesis, which enabled me to take my work to completion in the most professional manner.

I am genuinely grateful to my family, my dear parents, and brothers, and I would always be indebted to them for any achievement in my life.

I am very grateful to Prof. Edward Lemaire, a leader in Physical Medicine and Rehabilitation, for the opportunity given and access to Rehabilitation Lab at the Ottawa hospital and the full breadth of his expertise. I would also like to thank Prof. Natalie Baddour for all her support and funding provided during my thesis and access to lab facilities at the Ottawa university after COVID-19 restricted our access to the hospital. And this research could not prosper without continuous support of Prof. Liam Peyton. Moreover, my gratitude extends to Mr. Connor McGuirk for his collaboration in data collection, while both of us were working on our respective master theses, amid the pandemic restrictions and its challenges.

Finally, I feel privileged to be part of the CREATE-BEST program and receive funding from the Natural Sciences and Engineering Research Council of Canada (NSERC). The journey

has been enriching, and I truly cherish the time spent at University of Ottawa and The Ottawa Hospital.

1 Introduction

1.1 Research Context & Scope

Human gait analysis is an essential indicator of physical and neuroglial health for an individual. Recent developments in deep-learning approaches to computer vision make possible new techniques for body segment and joint detection from photos and video frames.

In this thesis, we propose a deep learning approach for non-invasive video-based gait analysis using two RGB cameras that would be suitable for routine gait monitoring in senior care and rehabilitation centers. Due to modularity and the low cost of implementation, it is considered an affordable solution for such centers. Furthermore, since the solution does not require any markers or sensors to be worn, it is a pervasive and easy method for daily usage. The work for this research was conducted in partnership with The Centre for Rehabilitation Research and Development (CRRD) of The Ottawa Hospital Rehabilitation Centre (TOHRC). Our research approach was developed by combining deep learning-based methods presented in a survey called "Deep learning for sensor-based activity recognition" [1]and a marker-less posture analysis method proposed in "Real-time Multi-Person 2D Pose Estimation using Part Affinity Fields"[2]. By merging these two novel state-of-the-art papers, we hope to achieve a hybrid approach, which will result in a marker-less method for human gait analysis based on deep-learning techniques.

Gait analysis is known as an essential element for individuals health monitoring since it is a good representative of a person’s neurological and physiological status[3]. Accurate and reliable posture measurements also can be used for care preparation. Quantitative posture measurements, in addition to clinical evaluation, provides insights required to better evaluate

sensory issues related to exteroception, proprioception, stereognosis, two-point discrimination, and motor impairments affecting muscle strength, range of motion, and spasticity[4][5]. Moreover computer vision combined with machine learning has shown promising results for the clinical applications such as pain [6] or fall detection[7].

The current posture measurement systems involve multiple motion analytical components (i.e., inertial and optical). These complex lab setups are necessary to determine anatomical points, body segments, and biomechanical models. However, these systems can have high development and installation costs and require a considerable footprint allocation[8].

1.2 **Rationale**

Gait analysis is a continuous requirement for the elderly's health; however, current approaches require human intervention and specialized equipment. Besides, these approaches are highly time-consuming, especially if it needs to be implemented in the highly demanding locations such as long-term care centers. A traditional method is to make these measurements manually, using a goniometer, tape, or other specialized tools. However, visual observation can be affected by human error [9]. This may lead to a risk for patients since not accurate results can cause long-term damages. Additionally, advanced technologies such as x-ray and marker-based motion analysis systems (e.g., Vicon) are costly and hard to access. As another challenge, these systems required dedicated space in clinical environments to set up the system and allow people to move through or run the tests.

Considering the limitations of these methods, our research targets creating a marker-less system for tracking human-pose while moving through an institutional hallway. Our goal is to design an automated and pervasive process for recording the data with minimum human

intervention while providing high-quality input to give good quality analysis and reports. The successful implementation of the system results in reduced financial cost and time.

1.3 Research Questions and Objectives

The main question to be answered is whether two cameras supported by deep learning algorithms could provide useful gait parameters to be used in clinical settings. Having two cameras is defined as an objective since that is the minimum requirement for having a stereo vision for 3-D motion analysis[10]. The target is to detect and analyze the posture without any physical markers. Next, and after detecting the key points on a body, a deep-learning algorithm would be used to predict and correct the key points' location for the next frames. The research is considered novel in this domain since the hybrid approach has never been tested and validated.

Research question 1:

Would it possible to extract clinically usable gait parameters in 3-D from two cameras installed in an institutional hallway?

Objective 1:

Create and evaluate a viable system for 3-D pose key-point identification from video captured with two mid-ceiling placed cameras.

Research question 2:

Which pose estimation model would provide the most accurate result for the planned setup with the considered restrictions?

Objective 2:

Evaluating outcomes of different pose estimation models in 3-D from videos of individuals walking through a hallway.

1.4 Thesis Outline

This thesis is organized as follows: Chapter 1 presents an introduction, context, and rationale of the research. Chapter 2 reviews the related literature. The technologies and tools used by these research are analysed and compared. Chapter 3 elaborates on our proposed research model and measurement criteria and measurement parameters and methods. Based on these criteria, in Chapter 4 we report the calculated results. Chapter 5 we discuss and analyze the results. Finally in Chapter 6 we explore the future possibilities and provide a summery.

1.5 Thesis Methodology

Due to the nature of the research, the methodology to be used is Design Science Research [11] as shown below. After identifying a potential objective-centered solution based on a review of the literature, relevant works, and desired techniques we performed a series of design and development centered iteration as we refined our artifact (deep-learning approach for marker-less stride parameters analysis with two cameras based on experiments and evaluation of 5 trial types (walking in a straight line with a turn in or out of the frame, or a circle, walking with crutches or a walker).

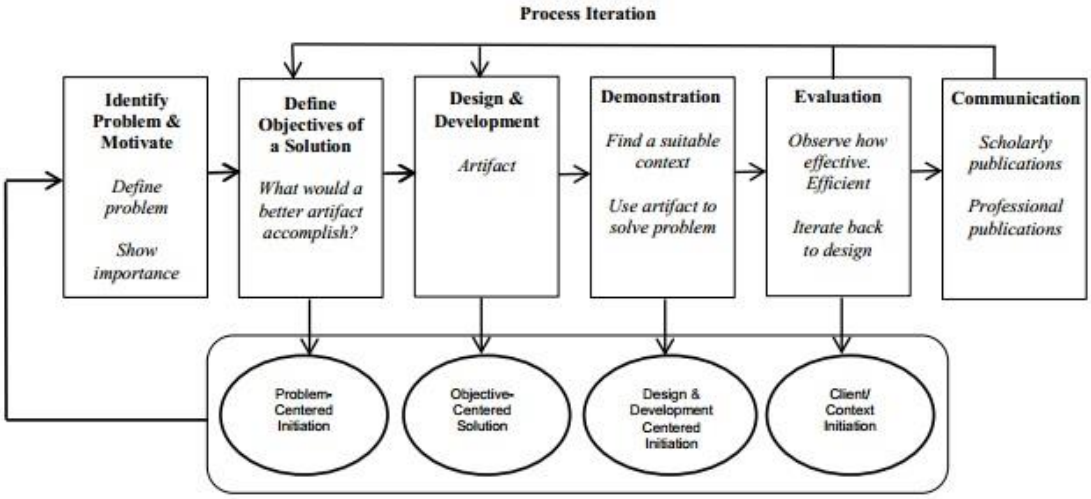

Figure 1 The Design Science Research Methodology Process Model [11]

The following iterations are followed to meet the objectives:

1. Iteration 1: March 2020
    a. HyperPose – Camera Origin – Median Filter, Cubic Spline – Subset of Spatial Parameters
2. Iteration 2: August 2020:
    a. HyperPose- Lab Origin – Median Filter, Butterworth Filter, Subset of Temporal and Spatial
3. Iteration 3: October 2020:
    a. OpenPose- Lab Origin – IQR Outlier remover, Butterworth Filter, Complete Temporal and Spatial
4. Final Iteration: April 2021
    a. OpenPose – Lab Origin – RANSAC, Butterworth Filter – Complete Temporal, Spatial and Spatial-Temporal

2 Literature Review

2.1 Overview

This chapter studies the significance of human posture measurement, gait analysis and reviews related measurement methods to determine the requirements for a marker-less stride parameters analysis with two cameras in a smart hallway. Moreover, the chapter introduces several technologies to gain insights for developing the most compatible solution for routine gait monitoring in senior care and rehabilitation centers.

2.2 Method

Our literature review surveyed the following sites for relevant literature: Google Scholar, ScienceDirect, NCBI, and PLOS One. The following search terms were used: Marker-less gait analysis, openPose+gait, DeepLearning+posture measurement, posture measurement + LSTM, gait database, pose estimation, pose capturing and 3D Pose Estimation. Search results were narrowed to those published after 2010; however, some exceptions have been made for older papers related to the research's key concepts. All articles chosen were required to meet the following criteria:

- Must include mention of the following primary search terms: posture measurement, gait analysis, accuracy, and marker.
- Must be peer-reviewed.

2.3 Analysis of Human Movement

To classify healthy walking and measure anomalies that may occur due to disease or accident, gait analysis is widely performed [12] [5] [4], The gait cycle is defined as the time interval between two consecutive occurrences of one of the recurrent walking events, often

beginning with the initial contact (IC) of the foot and ending with the subsequent IC. [13]. In healthy populations, the synchronisation of IC and terminal contact (TC), known as heel strike and toe off, is important to mark the transition between swing phase and stance phase of gait. These two events are important to evaluate the variables of temporal gait, such as phase time, double and single support periods , and to examine forces, moments, and joint angles through several strides [14].

The separation of the gait cycle often helps physicians, by offering a consistent overview of the normal actions of the lower extremity during each step of the gait cycle, to determine deviations of pathologic gait and progress made with recovery. Figure 3 indicate numerous activities, times, tasks, and stages in the gait cycle of the right leg. It splits a gait cycle into two stages. The stance stage is from the IC event of a leg to its instant toe off event. The swing step is identified from the foot off event to the subsequent foot strike event of the same leg. In determining the stride parameters, foot off and foot strike activities are critical.

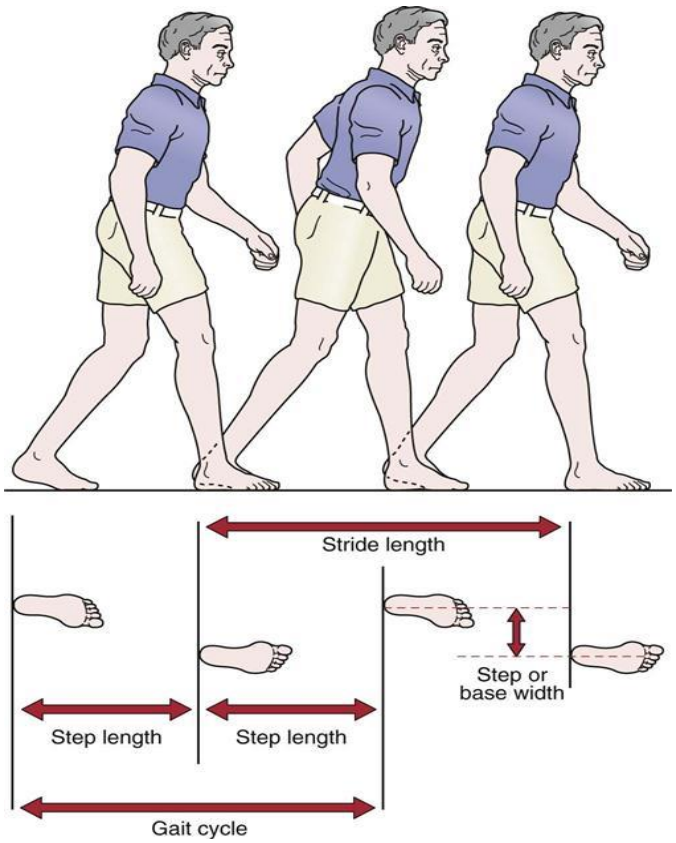

Figure 2 Gait cycle, stride length, and step length and width. adopted from [25]

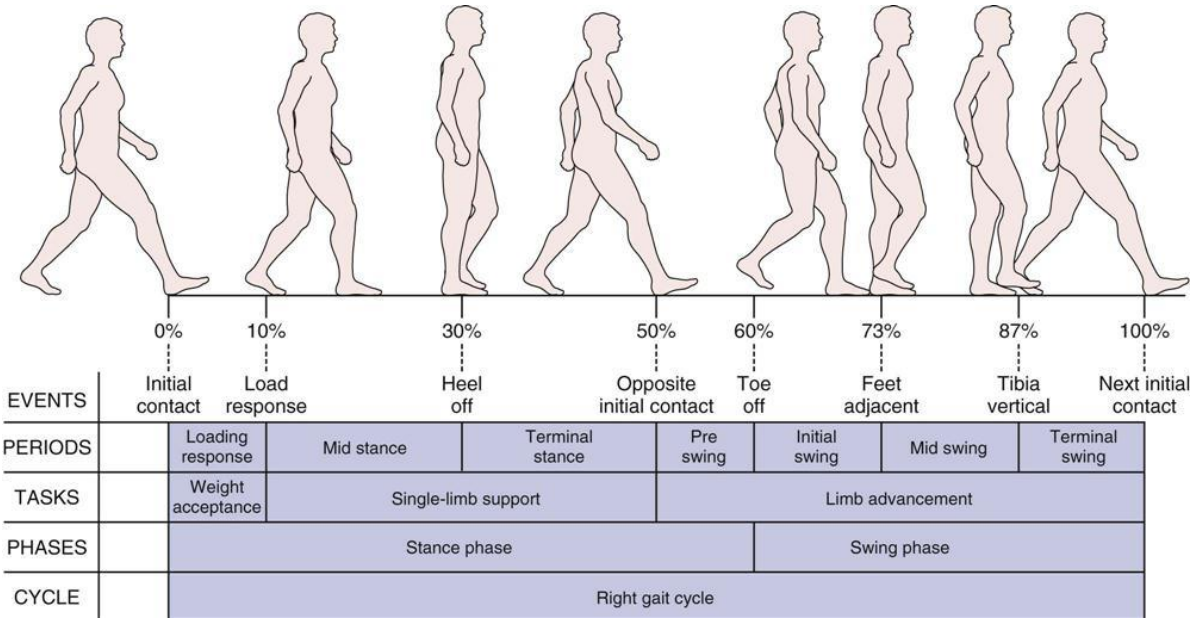

Figure 3 gait cycle phases. adopted from [25]

Regarding the various modalities, all of the studies evaluated fall into two major groups for gait analysis: 1) sensor-based 2) vision-based. The "gold standard" [15] for doing a comprehensive anatomical examination of gait characteristics is a gait or motion capture laboratory equipped with force plates or instrumented treadmills and cameras, with gait event identification as a vital component. Gait laboratories, on the other hand, require complex motion capture equipment, an expert, ample time, and analytical tools [16]. While laboratory-based research is regarded the gold standard for gait anatomical analysis, laboratory-based analysis, particularly for patient groups, is not always indicative of walking in real-world conditions [17].

Outside of the typical instrumented motion analysis laboratory, a revolution in the development of video and wearable sensor-based approaches for gait analysis in ‘real-world' circumstances has occurred recently. These systems do not use kinetic parameters or data from force plates to assess gait occurrences such as Initial Contact (IC) and Terminal Contact (TC) in their simulations (TC). Rather than that, camera data or sensor signals from gyroscopes [18][19][20][21] , accelerometers [22][23], Electromyography (EMG)[24][25], and force-sensitive resistors[26][27], are used to forecast gait accidents. Gait event prediction using sensor data has been used in sensor-based rehabilitation systems.

Identification of gait occurrences such as IC and TC is critical for evaluating the use of therapeutic diagnosis and treatment, particularly when functional electrical stimulation is used to synchronise stimulus distribution or actuator activation to specific gait stages. While time identification and error prediction are inherent in methods of kinematic-based gait phase

detection, the strategy employed to record gait events has an effect on the timing discrepancies discovered. Quantifying gait event delays [13] and subsequently developing compensation algorithms for gait event timing errors are crucial for applications where gait occurrences contribute to assistive applications. This methodology enables for effective correction and compensation of gait event prediction errors in order to decrease timing problems for assistive applications, this methodology enables for effective correction and compensation of gait event prediction errors in order to decrease timing problems for assistive applications.

The first study we evaluated in terms of gait analysis was "Walking speed" as a basis for measuring normal and pathological gait.[28]. It explores time distance measurements and records parameters of ground reaction force relative to walking speeds. In this descriptive, quantitative research, regression analysis is used to create essential functional relationships between amplitudes and walking speed. Basic time-distance tests observed over various walking speeds can be seen to be strong indicators of knee-disabled gait abnormalities.

To deal with the issue of gait analysis Hausdorff et al., [29] conducted a 1-year study known as “Gait Variability and Fall Risk in Community-Living Older Adults: A 1-Year Prospective Study”. The objective of the paper is to test a hypothesis. The mentioned hypothesis is that the increase in gait variability is linked to falls among older adults. Three outpatient geriatric clinics were considered to perform this test. Fifty-two patients aging over 70 participated in this study. The participants were asked to walk at an average pace while wearing insoles that were force sensitive. The insoles could measure the rate on a stride-to-stride basis. Then, they reported their fall status in a week for a year.

The most important outcomes were, first, any association between fluctuations recorded in gait rhythm, secondly, subsequent fallings that were reported during a follow-up year, and lastly, any potential factor contributing to the fall. While previously, it was assumed that increased gait variability is not necessarily included in the aging process, after conducting the research, it was proven that any change observed in gait variability is likely to show a method for underlying disease rather than changes related to aging. Before this result, researchers used to believe that exercise might decrease gait variability and help to restore physiological capacity. They also thought that a certain exercise Tai Chi and its similar could minimize the risk of falls. However, further study is required so as to determine the various factors contributing to gait variability and how it is related to fall risk. This paper argues that the measures considered for the stride-to-stride fluctuations might help researchers pave the way for older adults to benefit from state-of-the-art interventions.

Later in 2018, Prakash et al., [30] wrote a paper “Recent developments in human gait research: parameters, approaches, applications”, machine learning techniques, datasets and challenges proposing that with the advancement of new technology, the human gait can be examined subjectively and objectively and empirically to provide a better life quality. After giving a literature review of the past survey on gait analysis, this paper discusses several gait analysis methods. According to this research, for body poses estimation, vision-based human motion analysis can potentially offer a non-obstructive, inexpensive solution.

This is followed by a discussion on data parameters for gait analysis, and after that, preprocessing steps are taken. Then, machine learning techniques are explained in considerable detail. The main objective behind this research was to give a comprehensive analysis of the-state-of-the-art gait analysis. In other words, the presented paper introduces a

framework including available datasets, techniques, parameters, machine learning techniques for the later researchers to realize which area in gait analysis is infertile.

The authors of this paper believe that the overview provided in this paper will help researchers whose area of interest is gait analysis. An introduction to human gait taxonomies on the basic level is presented. Several applications for this field are categorized into biometrics, rehabilitation, clinical diagnosis, care for seniors, sports, and industrial areas. Many machine learning techniques, along with their available gait analysis datasets, are introduced. Finally, the authors give their opinion on what they think for the future prospective gait analysis.

Although human gait usually refers to leg and foot movements, the complete human motor system is involved. Another research, in 2016, by Nieto-Hidalgo et al., [31] hypothesized that some parameters for movement could help characterize gait singularities to identify abnormalities or any potential diseases, and the paper was named “A vision-based proposal for classification of normal and abnormal gait using RGB camera” [31] These movement parameters include dynamic balance and movement harmony for each body element, namely, thorax, head, and arms.

As this paper mostly relates to the preliminary problem, which concerns the classification of normal and abnormal gait, this research was mostly based on the lower part of the body. The proposal introduces a gait specification, which is functional, and in that only kinematic aspects of observation are explained.

The derived specification is open enough to be used for various gait analysis problems, ranging from rehabilitation to children's motor skills. For carrying out the final specification, an extraction system is developed. Through this system, image sequences are analyzed for the

purpose of gait system identification. Not only does the resultant prototype let the researchers determine the dynamic parameters, such as heel strike, length of the stride, and time, but it also helps them to distinguish between the normal and abnormal gait properly. The study has been performed on a dataset with a sample size of 30.

Nevertheless, M. Nieto-Hidalgo et al. faced some limitations while working on this project. These problems were mostly concerned with the algorithm, size of the room, and camera. Regarding future work, it could be said that the used algorithm (FASE) can be improved to alleviate the issue of readily locating both arms and each leg.

Later in 2019, paper “Normal and pathological gait classification LSTM model. Artificial intelligence in medicine” [32] stated that while clinical gait analysis, as an essential subset of computer vision problems, has been the topic for permanent research, there are not enough publicly available datasets. Consequently, comparing the current methods is rather complicated. Even when there is a publicly open dataset available, they often include very few subjects with only one modality measurement, which is a limitation for using. In this paper, Le2i et al. first tried to offer a new publicly available database resulted from Kinect v.2 camera for gait analysis purposes. Secondly, it was adapted to use a new orientation data called skeleton joint for calculating kinematic gait parameters.

The objective behind using this orientation data is to match the gold standard, motion capture (MOCAP) solutions. A novel feature set based on 3D low-limbs flexion dynamics for assessing the gait symmetry is introduced. This research's last contribution is designing a Long-Short Term Memory (LSTM) ensemble model for creating a new tool for classification, which is unsupervised. Results prove that joint orientation data offered through Kinect v.2 camera can then be applied in an inexpensive monitoring system for gait while having

slightly better results than those reported the state-of-the-art techniques for three abnormal/regular gait classes.

2.4 Gait Analysis

2.4.1 Inertial measurement unit

One of the popular posture estimations is using Inertial Measurement Unit (IMU) systems. An IMU typically includes a gyroscope, accelerometer, and sometimes magnetometer. Data from these sensors (rotational velocities, accelerations, heading by tracking magnetic-north) can be combined to determine the device's [33].

IMU has shown good accuracy in monitoring normal activities, such as gait or sports performance, and outcomes of a rehabilitative process in patients. For instance, in a study[34], The researchers determined the angle of the knee joint using an IMU that is coupled to a sensor alignment tool that is manually aligned to the individual's anatomy. This is referred to as the reference orientation. The individual next takes the IMU from the alignment tool and secures it to their thigh and shank using the sensor casings. The angle between the thigh and shank orientations in relation to the reference orientation is calculated and used to convert the data to an anatomical coordinate system. Additionally, most smart phone devices include IMU sensors for a variety of applications, including orientation and movement acceleration detection.

Although having vast uses in biomechanics, IMU can produce errors for position determination since double integration is required, thereby enhancing drift and noise in the system[33]. Furthermore, maintaining a durable interconnection between sensors and joints remains challenging, especially for dynamic measurement trials.

2.4.2 Marker based systems

Marker based system, mainly divide into two categories: Active and Passive. In passive, marker-based systems typically use retro-reflective balls that are illuminated using infrared (IR) lights mounted on the cameras. Systems include Motion Analysis Corporation (Santa Rosa, CA), Qualisys (Göteborg, Sweden), Vicon (Oxford, England).

Ezeh, C., Holloway, and C., & Carlson in their paper[35] mention that while passive marker-based motion monitoring systems that attach independent retroreflective markers to clothing or skin are convenient, passive markers worsen post-processing issues for markers that are near together. Manual editing may be required to rename markers. Background reflective surfaces may also be misinterpreted as markers, necessitating careful background masking or relabeling. The distances between markers were utilised to determine the precision (0.015 mm) and accuracy (0.15 mm) of motion caption systems. Due to the higher resolution, the closer the camera is to the dynamic object, the better the motion capture performance. While passive marker systems are accurate, their use in clinical practise is limited due to motion laboratory space requirements, system cost, and patient setup and data processing time requirements.

Active systems use light-emitting diodes (LED) as markers, with each marker having a predefined frequency to assist in marker differentiation [36]. However, individuals need to carry several cables and other components that may affect their movements. Active markers systems include Codamotion (Rothley, England), Optotrak (Northern Digital, Inc., Waterloo, Ontario, Canada), Qualysis (Göteborg, Sweden), Selcon (Selspot Systems, Ltd., Southfield, Michigan)[37]. Active markers can eliminate errors due to marker misidentification and therefore marker sorting time during post-processing [38].

Neelesh, Nissa, Amod, and Sohi's [39] evaluated an active marker system using LED-based markers to compute spatiotemporal and kinematic parameters through LabVIEW. A study of 19 healthy participants and 39 patients with lower back pain revealed that patients with lower back pain demonstrated a rigid (less flexible) pelvis-thorax coordination compared to healthy participants [40] . Lamoth [41]noted that active markers enhance distractibility and reduce gait alteration since the cable system responsible for powering and controlling the LED lags behind the participant as they walk. New Optotrak markers have in-line batteries that eliminate the need for a tether following the person, but wires are still needed for limb markers on the body.

The Selspot system taped active markers to the participant's limbs [42]. Drawbacks of the Selspot system included errors due to reflections, the need to carry apparatus and cables, and a trade-off between the number of markers and sampling rate. Since distance influences image resolution, as LEDs are moved away from Selspot cameras the amount of light intercepted per light pulse decreases [43] and increasing the aperture to capture more IR light can distort image.

In next decade, future developments of active marker systems will employ radio-frequency active emitters as gait analysis hardware. Radio-frequency signals are applied in the military. Due to their lightweight nature and low cost, implementation of a similar approach in clinical practice settings requires further research and development. However, research and development of hardware and software entail costs that are significantly below the costs attributed to passive marker systems [42].

2.4.3 Marker-less systems

Motion analysis systems that do not require markers could be used in movement analysis to reduce preparation time and encourage natural movement. To deal with the human pose estimation approaches, the first paper that which has been reviewed in this area was written in 2011. The study proposes a new method that uses a single depth image and no temporal information to swiftly and efficiently determine 3D positions of the body joints[44].

An object recognition approach allowed the authors to construct an intermediate body parts representation that could deal with difficult position problems by converting them into more specific per-pixel classification problems. Moreover, because of using a comprehensive and diverse training dataset, the proposed method could effectively cope with body parts invariant to pose, body shape, clothing, etc. This paper's findings show that the accuracy of the proposed approach is high on both synthetic and real test sets. This work should be completed by further studying the variability of the source mocap data, the generative model's properties underlying the synthesis pipeline, and the particular part definitions. Human 2D pose estimation — the challenge of identifying anatomical key-points or "sections"—focused primarily on discovering individual body parts.

The paper “Articulated Human Detection with Flexible Mixtures-of-Parts”[45] describes a method for detecting articulated human and estimating human pose in static images. This method is derived from a novel representation of deformable part models. Instead of modeling articulation based on a family of wrapped, either in rotated or foreshortened templates, a mixture of small and non-oriented parts is applied. A general mixture model, which is flexible, is described. This can capture spatial relations between locations of components and connections of co-occurrence between part mixtures. This

function helps augment structure models for standard pictorial, which can only encode spatial relations.

The models have some notable properties

5. They model articulation efficiently through sharing the computation across wraps that are similar to each other
6. They model a set of global mixtures of enormous size efficiently by composing the local mixtures.
7. They determine the dependency on local appearance for global geometry, meaning that the parts look different at various locations.

As relations are in a tree's structure, the models in this paper can be optimized efficiently using dynamic programming. All other parameters are learned, ranging from spatial relations, local appearances, and co-occurrence relations through a Support Vector Machine (SVM) solver, which is structured. Since the model presented here has enough efficiency to be applied as a detector, which searches over image locations and scales, new criteria are proposed to evaluate pose estimation and detect humans, both on the individual and joint levels.

In conclusion, this paper shows that evaluation criteria, which are common currently, might conflate some issues. Many previous techniques model limbs that had articulated and rigid templates. These models were trained each one separately. However, the presented model in this paper provides an extensive diagnostic evaluation. This argues that joint training and flexible structure are essential for performance. Later, on a standard benchmark, experimental

results were derived, which suggested that this paper's method is considered state-of-the-art for pose estimation.

Later in 2014, M.Andrilkuka et al. conducted research and wrote a paper to contribute to this problem. The article “2D Human Pose Estimation: New Benchmark and State of the Art Analysis”[46] has proposed a new benchmark, entitled "MPII Human Pose," that could advance the future human body models. Covering more than 800 human activities, this benchmark is more comprehensive than previously studied benchmarks. It includes different recreational, occupational, and household activities and captures people from a broader range of viewpoints.

This paper's authors provided a full list of labels consisting of body joints, whole 3D torso and head orientation, occlusion labels for joints and body parts, and activity labels. A video frame facilitates the application of motion information for each tag. This paper finally provides informative insights for the success and failures of human pose estimation approaches. In my opinion, an exciting extension to this study would be the investigation of joint pose estimation for multiple people and in image sequences.

In another work[12], it suggested a deep-learning based approach to infer 3D patient pose from deep pictures dynamically. To this end, they focus on a mixture of Convolutional Neural Network (CNN) and Recurrent Neural Network (RNN)), trained on a comprehensive database covering a variety of hospital bed motions. They compare a state-of-the-art action recognition method trained on the same data and show their method's superior result. Their method can also estimate the joint positions under a simulated occluding blanket with an average joint error of 7.56 cm. I believe the further assessment of the machine learning

algorithm would elaborate more on their result's validity. Moreover, deep learning might add to the accuracy of joint detection on the occluding blanket.

The paper Realtime Multi-Person 2D Pose Estimation using Part Affinity Fields [2] focusing on pose estimation in the year 2017, presents an effective method detect multiple people's 2D pose in an image. The technique uses a non-parametric model, called Part Affinity Fields (PAFs), to learn to associate body parts with individuals in the picture. Architecture encodes global meaning, enabling a greedy bottom-up parsing stage that retains high precision while maintaining real-time efficiency regardless of the number of people in the picture. The architecture is designed to co-learn part locations and associations through two branches of the same sequential prediction process. Evaluating the accuracy using gold-standard tools such as motion capture cameras (Vicon) could elaborate more on the accuracy between actual pose (using Vicon) and their method.

Motion measurement is usually used in a variety of hospital diagnostic procedures. Although automated pose estimate from RGB-D input has reached the hospital in the recovery and gait assessment domain, no such approach is required for bed-ridden patients. However, in some parts, including sleep labs, epilepsy testing, and intensive care units, patient pose estimates in bed are needed.

In a work by Tang et al.[47], hierarchical patterns of parts and sub-parts that are meaningful are represented through compositional models. The compositional models' ability to characterize the high-order relationships among different parts of the body has prepared a bedrock to solve low-level ambiguities in estimating human pose. Nevertheless, previously proposed compositional models have made some assumptions on the part-subpart relationship that is unrealistic; thus, they seem to be incapable of characterizing compositional patterns

with high complexity. Furthermore, the higher-level parts' state spaces can be immense, which makes the learning and the inference complex.

Therefore, to alleviate these problems, W.Tang et al. proposed a new framework called "Deeply Learned Compositional Model (DLCM)", which was designed for Human Pose Estimation (HPE). The DLCM model uses deep neural networks to learn the human body's compositionality, leading to a new network with hierarchies. The network includes the top-down/bottom-up inferences stages. Additionally, a new representation based on bone is introduced. Not only does it encode orientations, shapes scales of each part, but it also helps to avoid the potentially large spaces for each state. The approach presented in this paper outperforms the state-of-the-art techniques when tested on the three datasets benchmark.

3 Research Design

3.1 Design Criteria

As the first point, the equipment for our system is targeted to cost less than $5000. The system is capable to record 3D coordinates all 25-body key-points based on COCO and MPII data models. The system is capable of being installed in the mid-ceiling of an institutional hallway. While the subject is walking at any point in time, initially, the error is targeted to be less than 2 cm measurement error between any two key points. Also, the system should be designed in a way that it can detect the posture of patients who deal with canes and walkers. The analysis of movement is done using 60 frames per second videos. Instant reporting needs to be available within 5 minutes, but this might change by advancements in the technology. The system will not require an external server, meaning that it will be based on a local processing unit. It will have the ability to detect any changes, minimum of 1 cm.

3.2 Lab Setup

In order to simulate an institutional hallway, two cameras parallel are installed in middle of our research lab, with three feet distance between them to capture the movement in sagittal plane[48] of subject's body while he walks through a simulated hallway. First, the cameras are intrinsically and extrinsically calibrated to remove unnecessary distortions and calculate transformation matrixes between them.

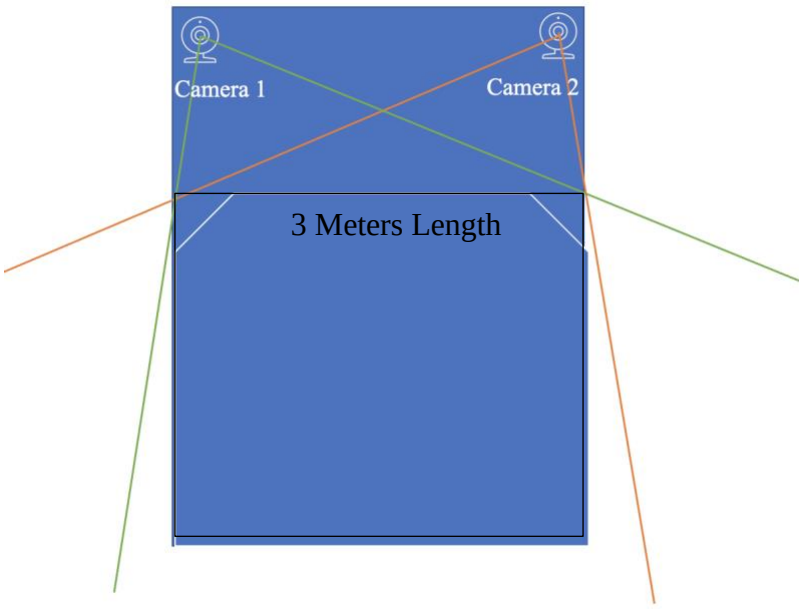

Figure 4 Cameras' Setup

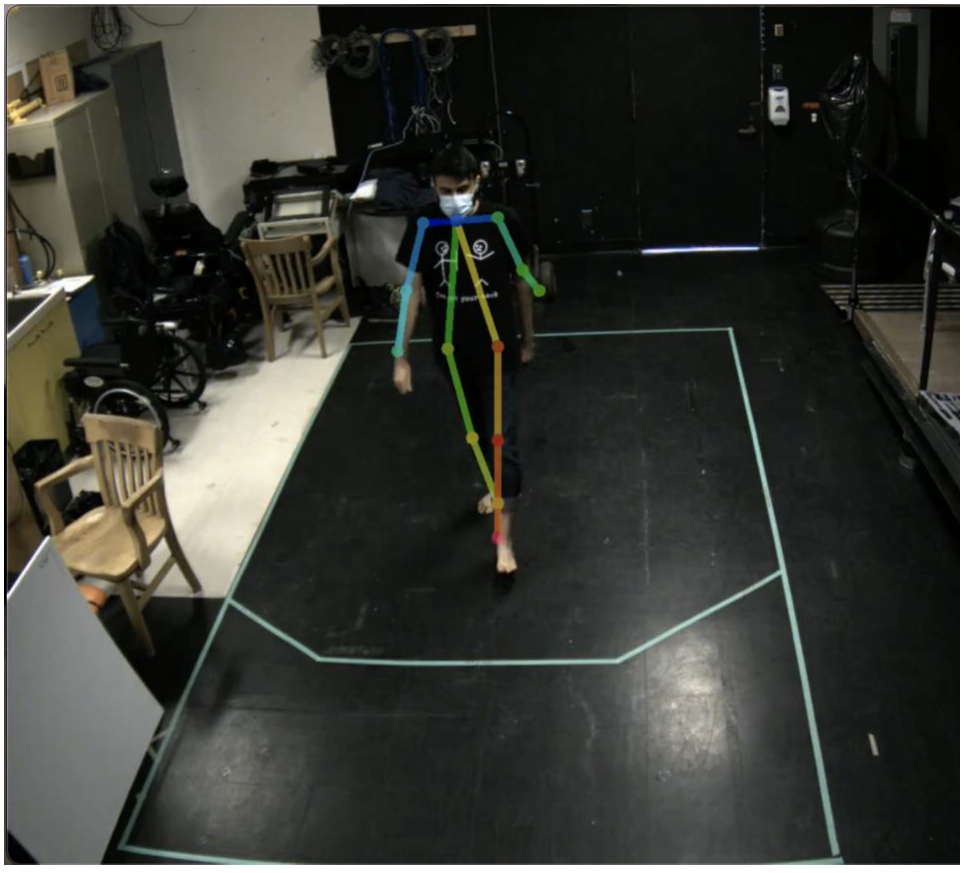

3.2.1 Camera Specification

Our video recording and analysis approach is based on stereo camera system that can record and recognize 3-D pose on semi real-time manner. We integrate the camera system into our labs at the Ottawa Hospital and University of Ottawa. The cameras are mounted to mid ceiling of the labs using adjustable arms with three feet distance from each other. The cameras are precisely positioned and adjusted in the corners of the pathway to have a 45° angle to cover of the entire walking path sized at 3m x 2m. We use FLIR BlackFly vision cameras with sensors that produce images with the size of 1280 x 1024 pixels that can record videos up to 120 frames per second, although in practice we only recorded up to 60 fps to have a closer setup to the cameras that are being used in institutional hallways. Each camera is equipped with a 1/2" sensor size format, 4.8 μm pixel size[49] and a global shutter. Fujinon Fisheye lenses with 3–4mm focal length are used as our primary lens for the trials. This setup result in a subject with a 1.8m size appearing at ~150X400 pixel image patch from the farthest distance to each camera. The cameras are placed in a way that at each point in time, the whole subject's body is visible to both cameras while walking throughout the pathway. This resolution is sufficiently high enough to allow our selected framework to recognize the key points on body.

3.2.2 Recording and Processing

With each camera producing each frame with a JPEG lossless compression at 60 Hz, the raw output of our system can reach up to 240 MB/s. To handle this data stream, we used a dual band PCI express USB hub controlled by Jetson AGX Xavier. The data streams from 2 cameras are routed to Nvidia AGX Xavier (8-Cores ARM 64-Bit CPU, 8 MB L2 Cache and 4

MB L3 Cache). The data streams are compressed and stored in a solid-state drives (NVMe SSD) of the local machine. In order to have a precise multi-view 3-D reconstruction of a static scene, having an accurate frame synchronization is required [50]. An external 5 V synchronization trigger that uses TTL pulse to open and close the shutters of both cameras simultaneously through General Purpose Input/Output (GPIO) is used. The accuracy of the synchronization technique has been tested several times and it remains accurate to sub millisecond.

3.3 **Participants**

We initially intended to ask 30 patients to participate in our research; however, this had to be changed due to COVID-19. Based on the initial protocol, all the participants should have been able-bodied. There were some inclusions criteria for that, such as they should have been able to walk 100 meters. As for their age, they must have been over 19 and receive cognitive status to understand the instructions. Regarding the exclusion criteria, we were not looking for people with balance problems and people under medication that affects their balance and mobility.

However, it all had to be reconsidered due to social distancing measures and limited access to our research lab at Ottawa Hospital Research Institute. For this thesis's sake, the subject is only the researcher, who satisfied all the inclusion and exclusion criteria.

3.4 **Trials**

In this research we aim to address the requirements of a typical institutions hallway and cameras were setup to simulate a hallway or a room. Next, we wanted to find out how accurate the approach is in five different moving scenarios. Each subject performed two attempts per trial and we video captured the attempts.

Prior to COVID-19 pandemic, we had designed an informed consent sheet for the subjects, however we could not use it since we had to implement changes to our protocol. This sheet includes information such as ID, age, sex, weight, height, limb lengths using an anthropometer (foot, shank, thigh, hip-width, upper arm length, lower arm length, shoulder width)- key points length, test date.

The start line for the trial is 150 cm before the capture volume, and the end line is located 50 cm after the capture volume. Next, we start the hallway system and ask the person to stand in the middle of the capture volume. After that, the person stands at the start line, before the capture volume, and ask the person to walk through the middle of the hallway, pass the end line, turn, and return to the start line. The walking distance is 3 meters, and with 1.5 meters per foot strikes, it takes about 15 seconds. Then, we ask the person to stand at the start line, 1 meter before the capture volume, once with a cane, and once with a walker. Finally, they will be asked to stand at the start line, walk through the middle of the hallway, mark the floor halfway through the capture volume, turn, and walk back to the start line. Repeat ten times, walking with turns to the left and right.

3.5 Movement Types

3.5.1 Walking with a cane

Similar to the first trial, the subject walks back and forth in a straight line, while using a cane. The subject turn out of frame.

3.5.1 Walking in a Straight Line – Turn Out of Frame

In this trial the subject walks with good posture in a straight line, 3 meters forward, turn, and backward. The turn happens out of frame.

3.5.1 Walking in a Straight Line – Turn in Frame

In this trial the subject walks with good posture in a straight line, 3 meters forward, turn, and backward. The turn happens visible to the cameras.

3.5.2 Circular Walking

For the second trial the subject walks in an imaginary circle with the diameter of ~3 meters.

3.5.3 Walking with Walkers

Similar to the first trial, the subject walks back and forth in a straight line, while using a walker.

3.6 Gait Parameter Extraction

Video segments for processing will be extracted. The raw input move for the pre-processing stage, which includes more details after the design phase. Then we will apply a key-point detection algorithm and extract inter-key points measurements. Through that, we will extract gait parameters. After extracting the postural information from the captured videos of trials, we measured and extracted the gait features listed below. The parameters are mainly based on as the parameters listed in “Clinical gait analysis ”[51], “Computational Musculoskeletal Analysis of Human Lower Extremities” [52] review papers and Biomechanics and Gait Analysis book [53].

Table 1 Gait Parameters

Gait Parameters	Temporal Parameters	Swing Phase
		Stance Phase
		Stop Phase
	Spatial Parameters	Left Arm Length
		Left Forearm Length
		Right Arm Length
		Right Forearm Length
		Left Thigh Length
		Left Shank Length
		Right Thigh Length
		Right Shank Length
		Left Ankle to Heel Length
		Left Ankle to Big Toe Length
		Left Ankle To Small Toe Length

		Right Ankle to Heel Length
		Right Ankle to Big Toe Length
		Right Ankle to Small Toe Length
		Shoulder Width
		Hip Width
		Chest Height
		Heels Vertical Position
		Toe Vertical Position
		Knee Vertical Position
	Spatial-Temporal Parameters	Stride Length
		Stride Times
		Stride Speeds
		Step Length
		Step Time
		Cadence
		Stance Time
		Swing Time
		Stance to Swing Ratio
		Double Support Time
		Shank Center of Mass Vertical Velocity
		Thigh Center of Mass Vertical Velocity
		Heel Vertical Velocity
		Toe Vertical Velocity
		Knee Vertical Velocity
		Thigh Angular Velocity
		Leg Angular Velocity

3.6.1 Temporal Parameters – Gait Cycles

The gait cycle is the time interval between two consecutive occurrences of one of the locomotion's repeating events. The human gait cycle is divided into two distinct phases: the stance phase, during which the foot is in touch with the ground, and the swing phase, during which the limb is not in contact with the ground.

1) Stance Phase: begins with the first contact of the foot with the ground and concludes with the same foot leaving the ground. Around 60% of the gait cycle is spent in the stance phase.

2) Swing Phase: The time during which the foot lifted off the floor and swung forward in the air until the heel landed again on the floor.
3) Stop Phase: Despite not officially being a part of a gait cycle, determining it helps in having more precise detection of start and ending a cycle.

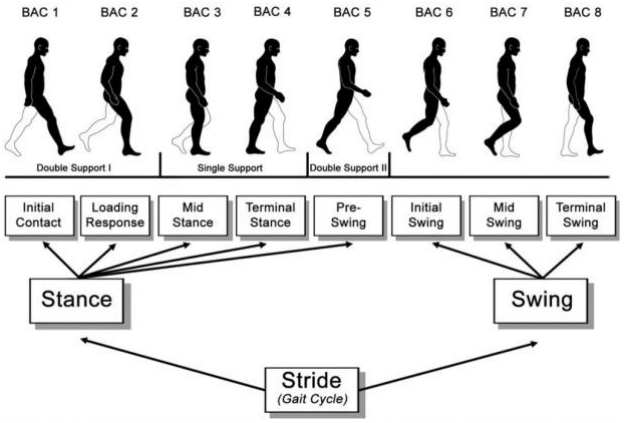

Figure 5 Gait Cycle [54]

A full gait cycle is made of the following events:

8. Heel-strike: The initial contact of one foot with the ground, also referred to as HS or foot-strike, is the initiating moment of the gait cycle.
9. Foot-flat: The point at which the remainder of the foot makes contact with the ground, which is often when the leg is supporting the entire body weight.
10. The term "midstance" refers to the position of the centre of mass exactly above the ankle joint centre. This is also the instant when the hip joint centre is higher than the ankle joint centre.
11. Heel-off happens when the heel of the foot begins to lift off the ground in preparation for the body's forward propulsion.
12. Toe-off occurs during the stance phase as the final point of contact.

3.6.2 Spatial Parameters

A. *Length, Height and Width*

To spatial parameters including Lengths, Heights and Widths we refer to the formal definition of each body segment provided in “Body segment parameters” paper published in Artificial limbs Journal [55]. Based on the definition of each body segment, we measure the distance between the two contact points detected by our deep-learning framework and report the average calculated value throughout all frames of each trial.

B. *Vertical Position of Feet Key Points*

The vertical position of feet key points (changes relative to z-axis in the framework coordinate system) in the 3-D space are used to determine each gait cycle event.

3.6.3 Spatial-Temporal Parameters

A. *Stride Length*

Based on the definition of a stride provided in section 3.6.1, stride length is the distance between the initial points of contact of successive toes of the same foot. Normally, the lengths of the right and left strides are equal.

B. *Stride Times*

Based on the definition of a stride provided in section 3.6.1, we measure the average duration from starting a stride until ending it.

C. *Stride Speeds*

Based on the definition of a stride provided in section 3.6.1, we calculate the distance and time taken by a stride and divide them to calculate the speed.

D. *Step Length*

Based on the definition of a step provided in section 3.6.1, step length is he distance between one foot's initial point of touch and the opposing foot's initial point of contact. In normal gait, the lengths of the right and left steps are comparable.

E. *Step Time*

Based on the definition of a step provided in section 3.6.1, we measure the duration from starting a step until ending it.

F. *Cadence*

Also known as walking rate, is calculated as the number steps taken per minute.

G. *Stance Time*

Based on the definition of a stance phase provided in section 3.6.1, the average duration taken from starting the stance phase until ending it is reported.

H. *Swing Time*

Based on the definition of a stance phase provided in section 3.6.1, the average duration taken from starting the swing phase until ending it is reported.

I. *Stance to Swing Ratio*

Based on the definition of a stance phase provided in section 3.6.1, after measuring the duration of stance and swing phases, the average ration between them is reported.

J. *Double Support Time (DST)*

Based on the definition, DST happens when both feet are in touch with the ground at the same time, and the double support time is the total of the moments elapsed throughout the gait cycle's two periods of double support.

K. *Shank Center of Mass Vertical Velocity*

Based on the definition of center of mass[56], after finding the center of a shank, we calculate its vertical velocity.

L. *Thigh Center of Mass Vertical Velocity*

Based on the definition of center of mass[56], after finding the center of a thigh, we calculate its vertical velocity.

M. *Heel Vertical Velocity*

After measuring vertical position of a heel, the velocity of vertical position change of the heel is reported.

N. *Toe Vertical Velocity*

After measuring vertical position of a toe, the velocity of vertical position change of the heel is reported.

O. *Knee Vertical Velocity*

After measuring vertical position of a knee, the velocity of vertical position change of the heel is reported.

P. *Thigh Angular Velocity*

After calculating the angle between a thigh and Z axis of our coordinate system, the velocity of change is reported.

Q. *Leg Angular Velocity*

After calculating the angle between a leg and Z axis of our coordinate system, the velocity of angle change is reported.

3.7 **Method**

The goal is to recognize the parts of the body of the subject in each frame of the video, so that you can understand what each body part is doing in order to do gait analysis. The first step is to process each video camera stream to get a simple raw data 2D model, and that's done by using OpenPose and HyperPose frameworks which are based on The Common Objects in Context (COCO) Models and Max Planck Institut Informatik (MPII) Dataset. These mentioned model specs will be able to offer full-body detection with feet key-points set detection, high accuracy model, and fast and efficient processing speed.

3.7.1 Ground truth

The following approach has been followed to interpret the results:

1. First a ground truth is established based on manual and systematic measurement.
    a. Manual measurement of body limbs of subject.
    b. Manually Heel Strike and and Toe Off events are labelled from 2-D images in the recorded videos.
2. Accuracy of the outputs from the system is compared to the ground truth.
3. Accuracy of the output is compared to existing gait analysis methods.

3.7.2 2D Image Modeling

A. *COCO Data Model*

The Common Objects in Context (COCO))[57] coco is a large-scale object identification, segmentation, and captioning dataset for computer vision. The data model was created in response to a Keypoint detection challenge, which necessitates the localisation of individual keypoints under adverse, uncontrolled conditions.

B. *MPII Data Model*

The MPII Human Pose dataset [46]is a benchmark for assessing the estimate of articulated human poses. The collection contains around 25K photos of over 40K individuals with annotated body joints. The photos were collected in a methodical manner, using a well-established taxonomy of everyday human activity. The collection contains images of 410 human activities and each image is labelled with an activity. Each picture was pulled from a YouTube movie and accompanied with its unannotated previous and succeeding frames.

C. *Body-25 Model*

This is an experimental modem developed by the developer of OpenPose which uses labeled data from both of the above models, accompanied with annotated feet data which is essential for the research objectives[2].

3.7.3 Models Comparison

The main difference between these two data models goes back to the accuracy vs speed. COCO while having a more complex and precise model, is costly in processing, however MPII provides a faster and less demanding detection.

3.7.4 Deep-Learning Frameworks

A. *OpenPose*

OpenPose [2] is a real-time multi-person keypoint detection and multi-threading library created in C++ and based on OpenCV and Caffe. It is written in Caffe, although the code is easily portable to other frameworks (e.g., Tensorflow or Torch). OpenPose is the first real-time system capable of detecting joint key points on the human body, foot, hand, and face (a total of 130 key points) in single photos. Additionally, the computational efficiency of the system for estimating body key points is independent of the number of identified humans in the image.

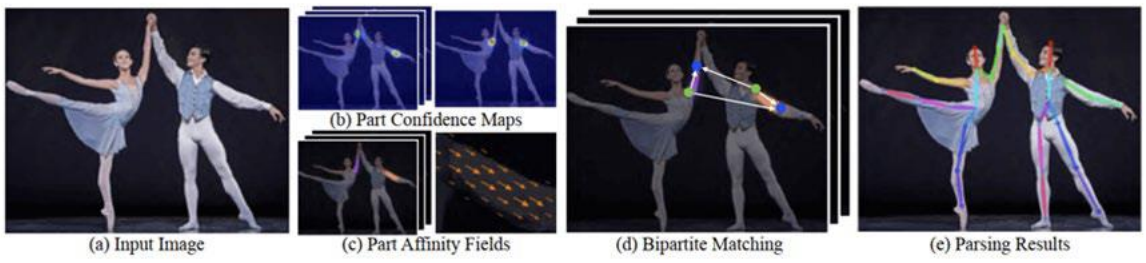

Figure 6 OpenPose Processing Pipeline [2]

B. *HyperPose*

HyperPose is developed as an open-source implementation of the TensorLayer project[58]. It is a library for developing efficient human posture estimate algorithms for use in the wild. HyperPose provides a versatile Python API that enables several applicable posture estimate models (e.g., OpenPose and PoseProposalNetwork). Users may personalize data augmentation, train on parallel GPUs, and swap out deep neural networks (e.g., from ResNet to MobileNet) in HyperPose, resulting in models tailored to their real-world circumstances. Additionally, HyperPose provides real-time posture estimates using a powerful posture estimation engine. Numerous system improvements are included in this engine, including pipeline parallelism, model inference using TensorRT, and CPU/GPU hybrid scheduling. This enables HyperPose to operate at a far quicker rate than OpenPose.

3.8 Key points Detection with Deep-Learning

In the traditional marker-based system, a physical marker (e.g. a reflective marker) used to be attached to the subject in order to track the points. In our case, the frameworks estimate the possible location of a joint using special deep-learning techniques, and then track they track the points extract the gait parameters. Each framework and dataset use their own key point referencing methodology. This section is explained based on the process adapted in implementation of OpenPose framework [2].

3.8.1 Simultaneous Detection and Association

The approach begins by analysing each frame using a Convolutional Neural Network (CNN) [59] (initialised and fine-tuned with the first ten layers of VGG-19[60]), yielding a collection of feature mappings F for input to the first step. The network generates a collection of part

affinity fields (PAF) $L^1 = \varphi^1(F)$, at this step, where φ^1 refers to the CNNs used for inference at Stage 1. Each succeeding step concatenates the predictions from the previous stage with the original picture characteristics F and uses them to generate enhanced predictions.

$$\mathbf{L}^t = \phi^t(\mathbf{F}, \mathbf{L}^{t-1}), \forall 2 \leq t \leq T_P$$

where ϕ^t is the CNNs used for inference at Stage t, and T_P to the number of total PAF stages. Following the T_P iterations, the method is repeated for detection of confidence maps, beginning with in the most recently updated PAF prediction,

$$\mathbf{S}^{T_P} = \rho^t(\mathbf{F}, \mathbf{L}^{T_P}), \forall t = T_P$$

$$\mathbf{S}^t \& = \rho^t(\mathbf{F}, \mathbf{L}^{T_P}, \mathbf{S}^{t-1}), \forall T_P < t \leq T_P + T_C$$

where ρ^t denotes to the CNNs used in inference at Stage t, and T_C denotes to the number of total confidence map stages.

It has been demonstrated empirically that improved affinity field predictions enhance the outcomes of confidence maps, while the converse is not valid. Intuitively, by examining the PAF channel output, the locations of body parts may be deduced [2]. However, if only a collection of body parts without any further information is perceived, it is impossible to segment them into distinct individuals.

The confidence map predictions are made on top of the most recent and revised PAF predictions, resulting in a hardly discernible change between confidence map stages. The process uses a loss function at the conclusion of each stage to lead the network in repeatedly predicting PAFs of body parts in the first branch and confidence maps in the second branch.

Between the calculated predictions and the ground truth maps and fields, the approach employs L_2 loss. The approach weights the loss functions spatially in this case to solve the practical issue of certain datasets not labelling all individuals entirely. Specifically, the PAF branch's loss function at stage t_i and the confidence map branch's loss function at stage t_k are as follows:

$$f_{\mathbf{L}}^{t_i} = \sum_{c=1}^{C} \sum_{\mathbf{p}} \mathbf{W}(\mathbf{p}) \cdot \left\| \mathbf{L}_c^{t_i}(\mathbf{p}) - \mathbf{L}_c^*(\mathbf{p}) \right\|_2^2,$$

$$f_{\mathbf{S}}^{t_k} = \sum_{j=1}^{J} \sum_{\mathbf{p}} \mathbf{W}(\mathbf{p}) \cdot \left\| \mathbf{S}_j^{t_k}(\mathbf{p}) - \mathbf{S}_j^*(\mathbf{p}) \right\|_2^2$$

where $\mathbf{L}_c^*$ is the ground truth part confidence map, , $\mathbf{S}_j^*$ is the ground truth part confidence map, and W is a binary mask with $W(p) = 0$ when the annotation is absent at pixel p. During training, the mask is employed to prevent penalising accurate positive predictions. At each level, intermediate supervision handles the vanishing gradient problem by regularly refreshing the gradient. The overarching goal is,

$$f = \sum_{t=1}^{T_P} f_{\mathbf{L}}^t + \sum_{t=T_P+1}^{T_P+T_C} f_{\mathbf{S}}^t$$

3.8.2 Part Affinity Fields (PAFs) for Part Association

PAFs carry information on the position and direction of the limb's support area. It is a collection of flow fields that represents the ad hoc pairwise connection between bodily components. Each pair of bodily parts is assigned a unique PAF. PAFs are denoted by the

set $\mathbf{L} = (\mathbf{L}_1, \mathbf{L}_2, \dots, \mathbf{L}_C)$, where $\mathbf{L}_c \in \mathbb{R}^{w \times h \times 2}, c \in \{1 \dots C\}$. C specifies the number of body component pairings, and $w\ X\ h$ specifies the dimensions of the input picture.

Each picture position in $\mathbf{L}c$ encodes a two-dimensional vector; if the site is on the limb c between body parts $j1$ and $j2$, the value of PAF at that position is a unit vector pointing from j1 to j2; otherwise, the vector has no value. For person k, the ground truth PAF $\mathbf{L}^*c$ at a position $\mathbf{p}$ is as follows:

$$\mathbf{L}^*_{c,k}(\mathbf{p}) = \begin{cases} \frac{\mathbf{x}_{j_2,k} - \mathbf{x}_{j_1,k}}{\left\| \mathbf{x}_{j_2,k} - \mathbf{x}_{j_1,k} \right\|_2} & \text{if } p \text{ on limb } c \\ 0 & \text{otherwise} \end{cases}$$

3.8.3 Confidence Maps for Part Detection

Each confidence map is a two-dimensional representation of the idea that a specific body part may be located in any particular pixel. Each body part corresponds to a unique confidence map. Confidence maps are denoted by the $\mathbf{S} = (\mathbf{S}_1, \mathbf{S}_2, \dots \mathbf{S}_J)$, where $\mathbf{S}_j \in \mathbb{R}^{w \times h}$, $j \in \{1 \dots J\}$, and J specifies the number of body parts. Individual confidence maps $\mathbf{S}^*_j$ are defined as follows:

$$\mathbf{S}^*_{j,k}(\mathbf{p}) = \exp\left(-\frac{\left\| \mathbf{p} - \mathbf{x}_{j,k} \right\|_2^2}{\sigma^2} \right)$$

Where $\mathbf{x}_j$ denotes the true position of body part j of individual k. The confidence map of the ground truth is an aggregation of individual confidence maps:

$$\mathbf{S}^*_j(\mathbf{p}) = \max_k \mathbf{S}^*_{j,k}(\mathbf{p})$$

3.8.4 Multi-stage CNN

At stage t = 1, the network computes a set of part affinity fields, $\mathbf{L}^1 = \phi^1(\mathbf{F})$, given the feature mappings F produced from VGG-19.

Stage $2 \leq t \leq T_P$: To refine the prediction, the original feature maps F and the PAF forecast from the previous stage are concatenated.

$$\mathbf{L}^t = \phi^t(\mathbf{F}, \mathbf{L}^{t-1}), \forall 2 \leq t \leq T_P$$

T_P is the number of PAF stages, while ϕ_t denotes the CNN at stage t. Stage $T_P < t \leq T_P + T_C$: Following T_P iterations, the method will be repeated for T_C iterations to refine confidence map detection.

$$\mathbf{S}^{T_P} = \rho^t(\mathbf{F}, \mathbf{L}^{T_P}), \forall t = T_P$$

$$\mathbf{S}^t = \rho^t(\mathbf{F}, \mathbf{L}^{T_P}, \mathbf{S}^{t-1}), \forall T_P < t \leq T_P + T_C$$

T_C is the number of stages in the confidence map, and ρ_t denotes the CNN at stage t.

At the conclusion of each stage, an L_2 loss function is applied; it is carefully weighted to account for the circumstance where individuals in some photos are not completely identified.

At PAF stages t_i, there is a loss of function.

$$f_{\mathbf{L}}^{t_i} = \sum_{c=1}^{C} \sum_{\mathbf{p}} \mathbf{W}(\mathbf{p}) \cdot \left\| \mathbf{L}_c^{t_i}(\mathbf{p}) - \mathbf{L}_c^*(\mathbf{p}) \right\|_2^2$$

Where $\mathbf{L}_c^*$ represents the ground truth PAF and $\mathbf{W}$ represents a binary mask. If pixel $\mathbf{pp}$ is not labelled, $\mathbf{W}(\mathbf{p})$ equals zero.

At confidence map stages t_k, the loss function is,

$$f_{\mathbf{S}}^{t_k} = \sum_{j=1}^{J} \sum_{\mathbf{p}} \mathbf{w}(\mathbf{p}) \cdot \left\| \mathbf{s}_j^{t_k}(\mathbf{p}) - \mathbf{S}_j^*(\mathbf{p}) \right\|_2^2$$

where $\mathbf{s}_j^*$ is the confidence map for the ground truth portion. The ultimate target is to minimise total loss.

$$f = \sum_{t=1}^{T_P} f_{\mathrm{L}}^t + \sum_{t=T_P+1}^{T_P+T_C} f_{\mathrm{S}}^t$$

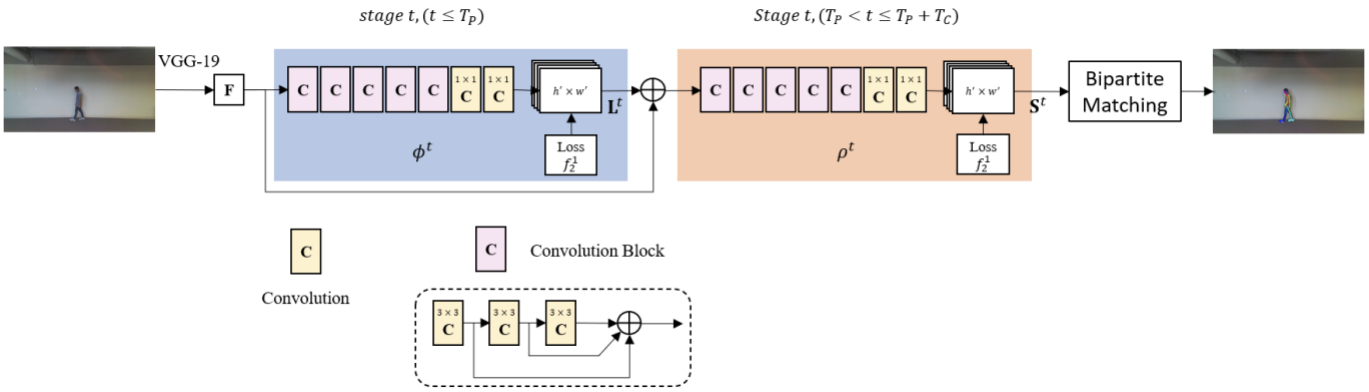

Figure 7 Multi-Stage CNN from [2]

3.8.5 Multi-Person Parsing using PAFs

The following steps describe how to execute Multi-Person Parsing. To begin, the framework generates a list of part potential parts using confidence maps. Then, using PAF, the deep-learning algorithm determines the pairs of body parts that connect limbs. Finally, it arranges identical limbs into full body positions. As illustrated in in the below figure, the OpenPose output is in the BODY-25 format, which consists of a (x, y) coordinate pair and confidence score for each of the 25 joints.

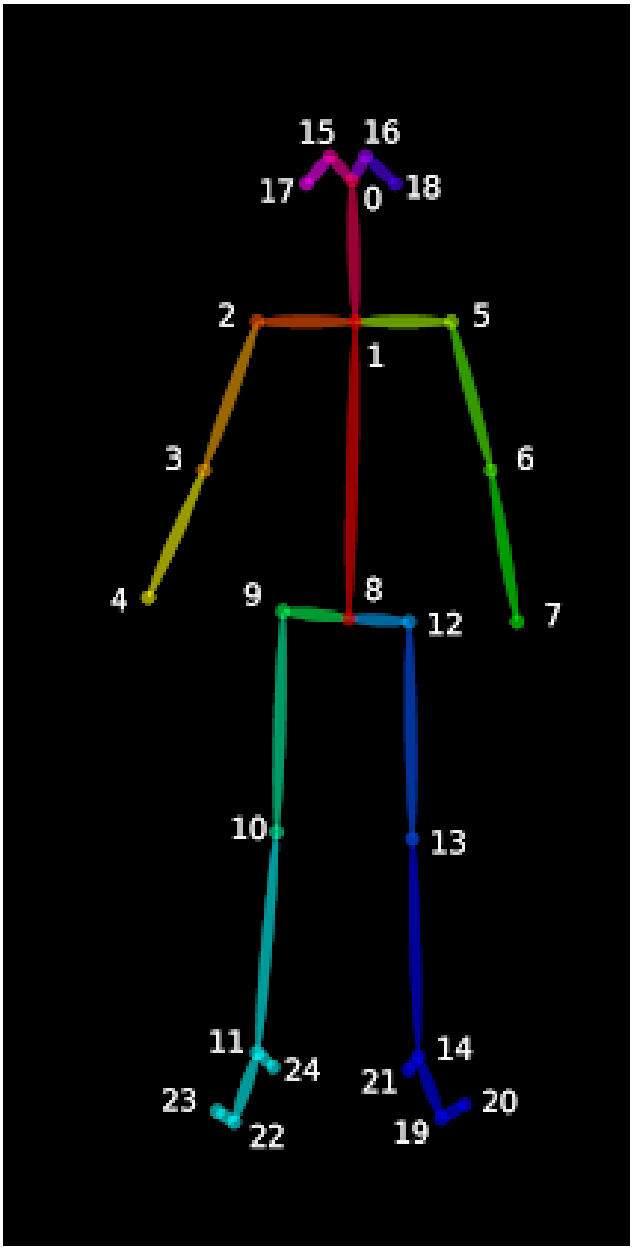

Figure 8 OpenPose Body 25 Model Keypoints [2]

Table 2 Body-25 Key Points

Point ID	Body Segment-Joint
0	Nose
1	Neck
2	Right Shoulder
3	Right Elbow
4	Right Wrist
5	Left Shoulder
6	Left Elbow
7	Left Wrist
8	Mid-Hip
9	Right Hip
10	Right Knee
11	right Ankle
12	Left Hip
13	Left Knee
14	Left Ankle
15	Right Eye
16	Left Eye
17	Right Ear
18	Left Ear
19	Left Big Toe
20	Left Small Toe
21	Left Heel
22	Right Big Toe
23	Right Small Toe
24	Right Heel
25	Background

3.9 **Transforming 2-D to 3-D Data with two Cameras**

The work in this section, was done together with my colleague Connor McGuirk [61] as we both needed the ability to use machine-learning to identify the limb points from a 2D image.

However, after that, our work was different, since Connor was working on a different setup with 4 cameras, and the scope of this research was bounded to two cameras.

Since we record our videos using pin-hole cameras, we loose depth data of the image, or, more precisely, the distance between each point in the image and the camera, as this is a 3D-to-2D conversion. Thus, it is critical to determine whether we can obtain depth information using these cameras. And the answer is to employ more than one camera. Our eyes work similarly in that we employ two cameras (two eyes), a process known as stereo vision.

In order to have the depth information, it is required to triangulate the 2-D outputs from both cameras and go through a process called 3-D Reconstruction. The process starts by calculating the intrinsic parameters of each camera to avoid any lens distortion effect on the result. Next, extrinsic calibration helps in finding the transformation matrix between two cameras. And as the final stage, one of the cameras set as the origin of the 3D world, and then we calculate the 3D coordinates relative to that point, however since the cameras are not located on the ground, we were facing instability in the baseline of the transferred coordinates. In order to overcome the problem, we transferred the origin by x technique to have the origin located in middle of the hallway. The following sections are explained based on the official OpenCV documentation[62], since that is the main library used for our purpose..

3.10 **Calibration and 3-D Reconstruction**

The perspective view of a scene is obtained by projecting the scene's three-dimensional point P_w into the image plane using a perspective transformation that generates the corresponding

pixel p. Both P_w and p are represented in homogeneous coordinates, that is, as a three-dimensional and two-dimensional homogeneous vector, respectively.

$$sp = A[R|t]P_w,$$

Where P_w is a three-dimensional point expressed in terms of the world coordinate system, p is a two-dimensional pixel in the image plane, A is the camera intrinsic matrix, R and tare the rotation and translation parameters that describe the transformation of coordinates from the world to the camera coordinate systems (or camera frame), and s is the projective transformation's arbitrary scaling parameter that is not included in the camera model.

The intrinsic matrix of the camera converts three-dimensional points in the camera coordinate system to two-dimensional pixel coordinates, i.e.

$$p = AP_c.$$

The intrinsic matrix A of the camera is made up of the focal lengths f_x and f_y, which are expressed in pixel units, and the principal point (c_x,c_y), which is typically located near the image centre:

$$A = \begin{bmatrix} f_x & 0 & c_x \\ 0 & f_y & c_y \\ 0 & 0 & 1 \end{bmatrix}$$

Therefore,

$$s\begin{bmatrix} u \\ v \\ 1 \end{bmatrix} = \begin{bmatrix} f_x & 0 & c_x \\ 0 & f_y & c_y \\ 0 & 0 & 1 \end{bmatrix}\begin{bmatrix} X_c \\ Y_c \\ Z_c \end{bmatrix}$$

The matrix of intrinsic parameters is not scene-dependent. Thus, once estimated, it is reusable as long as the focus length remains constant (in case of a zoom lens). Thus, if the image from

the camera is scaled by a factor, all of these parameters must be scaled by the same factor (multiplied/divided, respectively).

The matrix product of a projective and a homogeneous transformation is the joint rotation-translation matrix $[R|t]$. The 3-by-4 projective transformation converts three-dimensional (3D) points in camera coordinates to two-dimensional (2D) points in the picture plane with normalised camera coordinates $x' = X_c/Z_c \; and \; y' = Y_c/Z_c$:

$$Z_c \begin{bmatrix} x' \\ y' \\ 1 \end{bmatrix} = \begin{bmatrix} 1 & 0 & 0 & 0 \\ 0 & 1 & 0 & 0 \\ 0 & 0 & 1 & 0 \end{bmatrix} \begin{bmatrix} X_c \\ Y_c \\ Z_c \\ 1 \end{bmatrix}$$

The extrinsic parameters R and t encode the homogeneous transformation, which reflects the shift in basis from the world coordinate system w to the camera coordinate system c. Thus, given the point P's representation in world coordinates, P_w, we can acquire P's representation in the camera coordinate system, P_c, by following the steps below.

$$P_c = \begin{bmatrix} R & t \\ 0 & 1 \end{bmatrix} P_w$$

This homogeneous transformation is composed of two elements: R, a three-dimensional rotation matrix, and t, a three-by-one dimensional translation vector:

$$\begin{bmatrix} R & t \\ 0 & 1 \end{bmatrix} = \begin{bmatrix} r_{11} & r_{12} & r_{13} & t_x \\ r_{21} & r_{22} & r_{23} & t_y \\ r_{31} & r_{32} & r_{33} & t_z \\ 0 & 0 & 0 & 1 \end{bmatrix}$$

and therefore

$$\begin{bmatrix} X_c \\ Y_c \\ Z_c \\ 1 \end{bmatrix} = \begin{bmatrix} r_{11} & r_{12} & r_{13} & t_x \\ r_{21} & r_{22} & r_{23} & t_y \\ r_{31} & r_{32} & r_{33} & t_z \\ 0 & 0 & 0 & 1 \end{bmatrix} \begin{bmatrix} X_w \\ Y_w \\ Z_w \\ 1 \end{bmatrix}$$

By combining the projective and homogeneous transformations, we obtain the projective transformation that converts three-dimensional points in world coordinates to two-dimensional points in the picture plane and normalised camera coordinates:

$$Z_c \begin{bmatrix} x' \\ y' \\ 1 \end{bmatrix} = [\, R \mid t \,] \begin{bmatrix} X_w \\ Y_w \\ Z_w \\ 1 \end{bmatrix} = \begin{bmatrix} r_{11} & r_{12} & r_{13} & t_x \\ r_{21} & r_{22} & r_{23} & t_y \\ r_{31} & r_{32} & r_{33} & t_z \end{bmatrix} \begin{bmatrix} X_w \\ Y_w \\ Z_w \\ 1 \end{bmatrix}$$

with x' equal to X_c/Z_c and y' equal to Y_c/Z_c. By combining the instrinsic and extrinsic equations, we may write $s\, p = A[R|t]P_w$ as

$$s \begin{bmatrix} u \\ v \\ 1 \end{bmatrix} = \begin{bmatrix} f_x & 0 & c_x \\ 0 & f_y & c_y \\ 0 & 0 & 1 \end{bmatrix} \begin{bmatrix} r_{11} & r_{12} & r_{13} & t_x \\ r_{21} & r_{22} & r_{23} & t_y \\ r_{31} & r_{32} & r_{33} & t_z \end{bmatrix} \begin{bmatrix} X_w \\ Y_w \\ Z_w \\ 1 \end{bmatrix}$$

If $Z_c \neq 0$, the preceding transformation corresponds to the following:

$$\begin{bmatrix} u \\ v \end{bmatrix} = \begin{bmatrix} f_x X_c/Z_c + c_x \\ f_y Y_c/Z_c + c_y \end{bmatrix}$$

with

$$\begin{bmatrix} X_c \\ Y_c \\ Z_c \end{bmatrix} = [\, R \mid t \,] \begin{bmatrix} X_w \\ Y_w \\ Z_w \\ 1 \end{bmatrix}$$

The pinhole camera model is represented in the following figure.

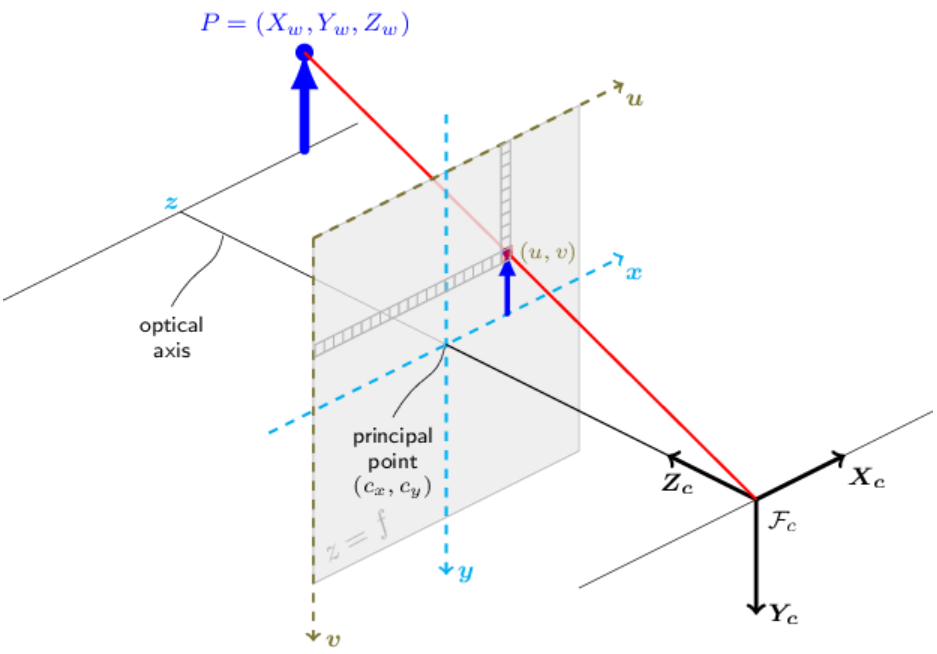

Figure 9 Pinhole camera model from OpenCV online documentation [62]

Camera lenses typically have some distortion, primarily radial distortion and a small amount of tangential distortion. Thus, the preceding model is extended as follows:

$$\begin{bmatrix} u \\ v \end{bmatrix} = \begin{bmatrix} f_x x'' + c_x \\ f_y y'' + c_y \end{bmatrix}$$

where

$$\begin{bmatrix} x'' \\ y'' \end{bmatrix} = \begin{bmatrix} x' \frac{1+k_1 r^2+k_2 r^4+k_3 r^6}{1+k_4 r^2+k_5 r^4+k_6 r^6} + 2p_1 x' y' + p_2(r^2 + 2x'^2) + s_1 r^2 + s_2 r^4 \\ y' \frac{1+k_1 r^2+k_2 r^4+k_3 r^6}{1+k_4 r^2+k_5 r^4+k_6 r^6} + p_1(r^2 + 2y'^2) + 2p_2 x' y' + s_3 r^2 + s_4 r^4 \end{bmatrix}$$

With

$$r^2 = x'^2 + y'^2$$

And

$$\begin{bmatrix} x' \\ y' \end{bmatrix} = \begin{bmatrix} X_c / Z_c \\ Y_c / Z_c \end{bmatrix}$$

if $Z_c \neq 0$.

The distortion parameters are represented by the radial coefficients $k_1, k_2, k_3, k_4, k_5, and\ k_6$, the tangential distortion coefficients $p_1\ and\ p_2$, and the thin prism distortion coefficients and s_1, s_2, s_3, and s_4.

The following pictures illustrate two forms of radial distortion that are frequently encountered: barrel distortion ($1 + k_1r^2 + k_2r^4 + k_3r^6$ monotonically reducing) and pincushion distortion ($1 + k_1r^2 + k_2r^4 + k_3r^6$ monotonically increasing). Radial distortion is always monotonic for genuine lenses, therefore any non-monotonic result produced by the estimator should be regarded as a calibration failure. More broadly, the radial distortion function must be bijective and monotonic. A failed estimation result may appear to be rather good in the image centre but will perform poorly in applications such as AR/SFM. Due to the framework's lack of support for integer programming and polynomial inequalities, the optimization algorithm utilised in OpenCV camera calibration does not incorporate these limitations.

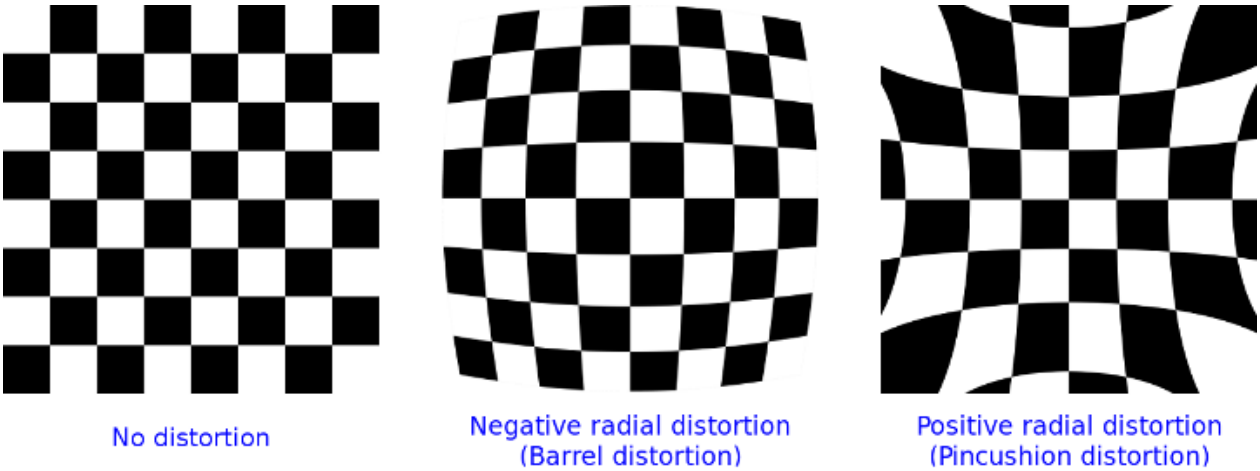

Figure 10 Distortion types - from OpenCV Online Documentation [62]

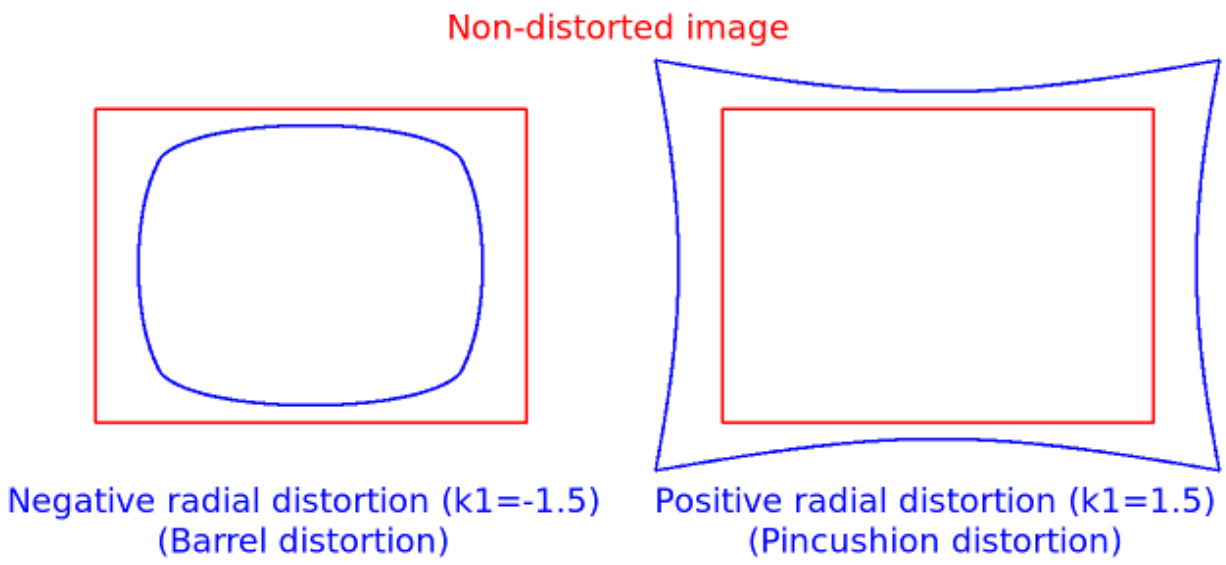

Figure 11 Distortion Fixing - from OpenCV Online Documentation [62]

3.11 Changing Origin of Coordinate System

Connor McGuirk and I both needed to adjust the origin of our coordinate system, and after discussion, we both used the same approach. We both did experiments, but in the end, we decided Connor's approach was the best. By default, both OpenPose and HyperPose, use one of the cameras as the origin of the coordinate system. Still, for our cases, we had to use the pathway's center as the origin of the world to calculate the desired parameters based on that[61].

3.12 Filtering Data

Connor McGuirk and I both needed to explore the approaches to filtering the data[61]. Although there are some differences, we have mostly taken the same approach. We both did experiments but in the end, our similar approach mostly reflected my results. Since the extracted 2-D points from the videos are highly noisy with a high number of outliers, multiple

levels of digital filtering is required to have a useful set of data. The first stage of filtering starts by removing the outliers.

3.12.1 Random sample consensus (RANSAC)

Fischler and Bolles presented the Random Sample Consensus (RANSAC) method [63] as a general parameter estimation methodology capable of dealing with a high proportion of outliers in the input data. Unlike many commonly used robust estimating approaches, such as M-estimators and least-median squares, which were taken by the computer vision community from the statistics literature, RANSAC was invented within the computer vision community. RANSAC is a resampling technique that creates candidate solutions by estimating the underlying model parameters using the fewest possible observations (data points). As Fischler and Bolles [63] note out, unlike conventional sampling techniques, which employ as much data as feasible to obtain an initial solution and subsequently remove outliers, RANSAC starts with the smallest feasible set and gradually expands it with consistent data points.

The fundamental basics of the algorithm are as follows[64]:

1. Randomly select the smallest number of points necessary to establish the model parameters.
2. Solve for the model's parameters.
3. Calculate the number of points in the collection of all points that fit within a particular tolerance.

4. If the ratio of inliers to total points in the set exceeds a predetermined threshold, re-estimate the model parameters using all identified inliers. Alternatively, repeat steps 1–4 (maximum of N times).

The number of iterations, N, is chosen to ensure that at least one of the sets of random samples does not contain an outlier. Let u be the chance that a particular data point is an outlier and $v = 1 - u$ the probability of spotting an inlier. N iterations of the minimum number of points labelled m are necessary, where

$$1 - p = (1 - u^m)^N$$

and hence

$$N = \frac{\log(1-p)}{\log(1-(1-v)^m)}$$

with some manipulation.

3.12.2 Zero-Phase Butterworth Low-Pass Filter

The Butterworth filter [65] provides the optimal trade-off between phase responsiveness and attenuation. Because it has no ripple in either the passband or the stopband, it is also referred to as a maximally flat filter. Butterworth filters are referred to as maximally flat filters because they have the sharpest roll-off possible for a given order without introducing peaking in the Bode plot. The second-order Butterworth filter is a two-pole filter with a damping ratio of 0.707. Butterworth filters are utilised in a wide variety of systems due to their lack of peaking. The requirement that a filter eliminate all peaks is cautious. Allowing for some peaking may be advantageous since it enables similar attenuation at lower frequencies with

less phase lag. Nevertheless, the Butterworth filter is a suitable choice for arranging the numerous poles of higher-order filters employed in control systems[66]

Butterworth filters have a generic formula that is dependent on whether the order is odd or even. For asymmetrical ordering, the formula is

$$T(s) = \left(\frac{\omega_N}{s+\omega_N}\right)\prod_{1}^{(M-1)/2}\left(\frac{\omega_N^2}{s^2+2\cos(\theta_i)\omega_N s+\omega_N^2}\right), \theta_i = i \times 180/N$$

The symbol $\prod$ denotes a sequence of products in the same manner as $\sum$ denotes a total. M denotes the order of the filters. A fifth-order Butterworth filter, for instance, is

$$T(s) = \left(\frac{\omega_N}{s+\omega_N}\right)\left(\frac{\omega_N^2}{s^2+2\cos(36°)\omega_N s+\omega_N^2}\right)\left(\frac{\omega_N^2}{s^2+2\cos(72°)\omega_N s+\omega_N^2}\right)$$

For even orders, the formula is

$$T(s) = \prod_{1}^{M/2}\left(\frac{\omega_N^2}{s^2+2\cos(\theta_i)\omega_N s+\omega_N^2}\right), \theta_i = (i-0.5) \times 180/N$$

For example, a fourth-order Butterworth filter can be written as

$$T(s) = \left(\frac{\omega_N^2}{s^2+2\cos(22.5°)\omega_N s+\omega_N^2}\right)\left(\frac{\omega_N^2}{s^2+2\cos(67.5°)\omega_N s+\omega_N^2}\right)$$

The Butterworth filter introduces a phase shift (delay) onto the filtered data that is often undesirable.

The delay length grows as the cut-off frequency decreases and the order increases. The phase shift becomes non-linear as the frequency (that is, the frequency content of the signal) and filter order increase. This implies that the delay is not constant across all frequencies.

The phase shift can be avoided by travelling forward and backward over the signal.

4 Gait Parameter Results

This chapter reports the results of our research trials whose design was described in chapter 3. Based on the initial project design criteria, the following parameters in table 4.1 were targeted to be measured.

Table 3 Gait Parameters

Gait Parameters	Temporal Parameters	Swing Phase
		Stance Phase
		Stop Phase
	Spatial Parameters	Left Arm Length
		Left Forearm Length
		Right Arm Length
		Right Forearm Length
		Left Thigh Length
		Left Shank Length
		Right Thigh Length
		Right Shank Length
		Left Ankle to Heel Length
		Left Ankle to Big Toe Length
		Left Ankle To Small Toe Length
		Right Ankle to Heel Length
		Right Ankle to Big Toe Length
		Right Ankle to Small Toe Length
		Shoulder Width
		Hip Width
		Chest Height
		Heels Vertical Position
		Toe Vertical Position
		Knee Vertical Position
	Spatial-Temporal Parameters	Stride Length
		Stride Times
		Stride Speeds
		Step Length
		Step Time
		Cadence
		Stance Time
		Swing Time
		Stance to Swing Ratio
		Double Support Time
		Shank Center of Mass Vertical Velocity

		Thigh Center of Mass Vertical Velocity
		Heel Vertical Velocity
		Toe Vertical Velocity
		Knee Vertical Velocity
		Thigh Angular Velocity
		Leg Angular Velocity

First, we show the results for the temporal parameters as that was the order in which we processed the video. These parameters are all about identifying the phases of gait cycle including toe-off and heel-strike events.

Second, we will show the results for the spatial parameters which are mainly on geometric measurements.

And third, we will show the results for spatial-temporal parameters which both time and position play a role in it.

4.1 **Temporal Parameters**

After detecting the 2-D position of each virtual point on body and calculating the 3-D position as described in section 3.8 and 3.9, an algorithm is required to detect gait stance and swing phases while a person is moving. This selection is based on the idea that the technique must detect toe-off and heel-strike timings with the least difference from the ground truth. Moreover, the desired algorithm must show the least sensitivity to signal noise in order to avoid false positives (false toe-off, or false heel-strike) and false negatives (missing toe-off and heel-strike). Finally, the method must require the least number of custom rules and static parameters to produce generalized results.

To extract the related temporal parameters, various methods suggested through the literature has been reviewed and several methods proposed by Zeni and Grimmer were selected and

compared. The first method explored in our research was one suggested by Grimmer based on the concept of using angular velocity of lower limbs, mainly virtual extended legs and shanks. In this method, signal zero crossings on x-axis combined with custom defined rules are used to detect the phases. When the velocity with negative values cross zero considered to be foot-off and when the velocity drops from a positive number to below zero is considered to be a heel-strike.

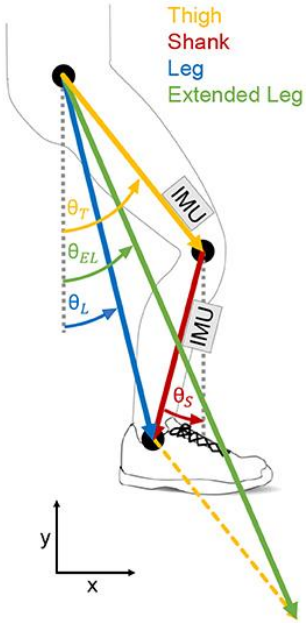

Figure 12 Biological and extended leg model [67]

However, in our case, despite applying 4 Hz, 4th order, dual pass butter worth filter to the data, the concept of using an extended leg showed high sensitivity to noise and needed to be customized per subject to produce valuable results; therefore, it was eliminated at the preliminary stages. In the following figure, a sample output produced by this method is represented. The solid black vertical lines show toe-off timings based on the ground truth, and each dashed green line represents a frame in which a foot-strike happened. However, as it can be observed, due to signal noise, the number of zero crossings is considerably higher than

the actual ground-truth values and cannot be considered as a predictable and reliable method to detect the events.

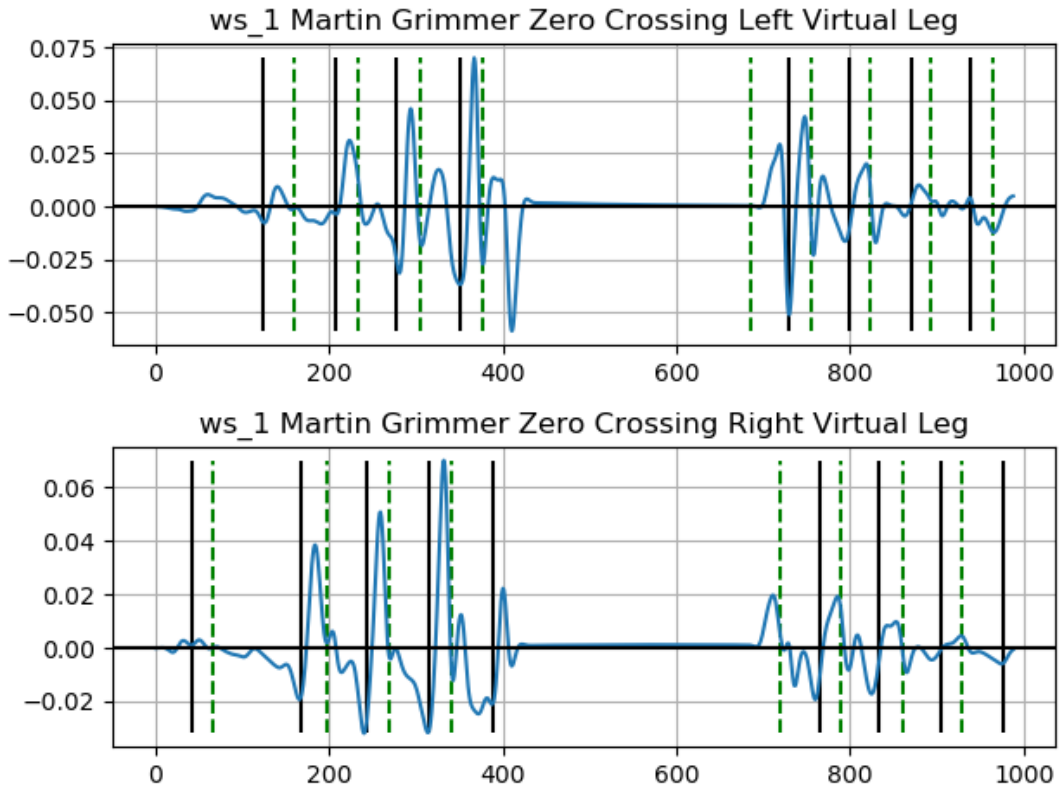

Figure 13 Martin Grimmer Zero Crossing Left and Right Virtual Leg X: Frame, Y; Velocity - Walking Straight Trial 1

The next method explored in our research was one where we use shank angular velocity (also suggested by M. Grimmer [67]. To calculate shank's angular velocity, an imaginary line between Heel and Knee key points are considered, and then the angle between the imaginary line and z axis of the lab coordinate system is measured. Similar to the previous method, after calculating the angular velocity, zero-crossings are used to detect the events. Despite having a cleaner signal after filtering and providing more accurate results, yet the method is prone to false positives, which introduces new challenges to distinguish between a toe-off and heel-

strike. The below figure is the output produced by the method for the right shank of our subject (with comparable results for the left shank).

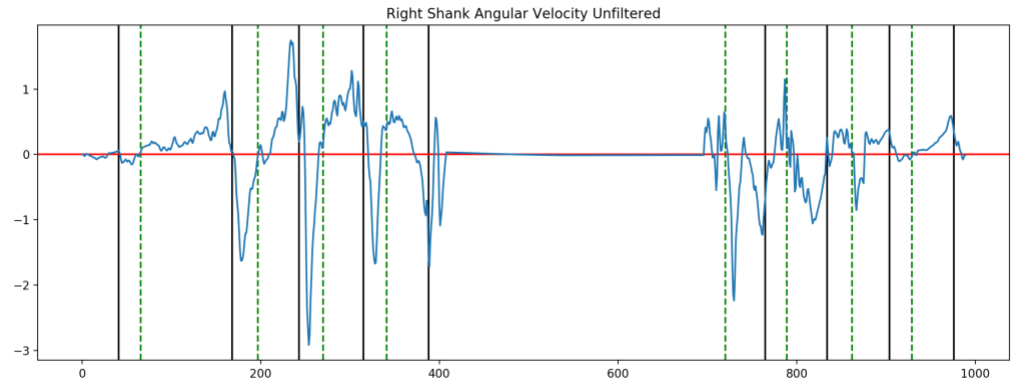

Figure 14 Shank Angular velocity - Right Foot - Walking in a Straight Line- Unfiltered

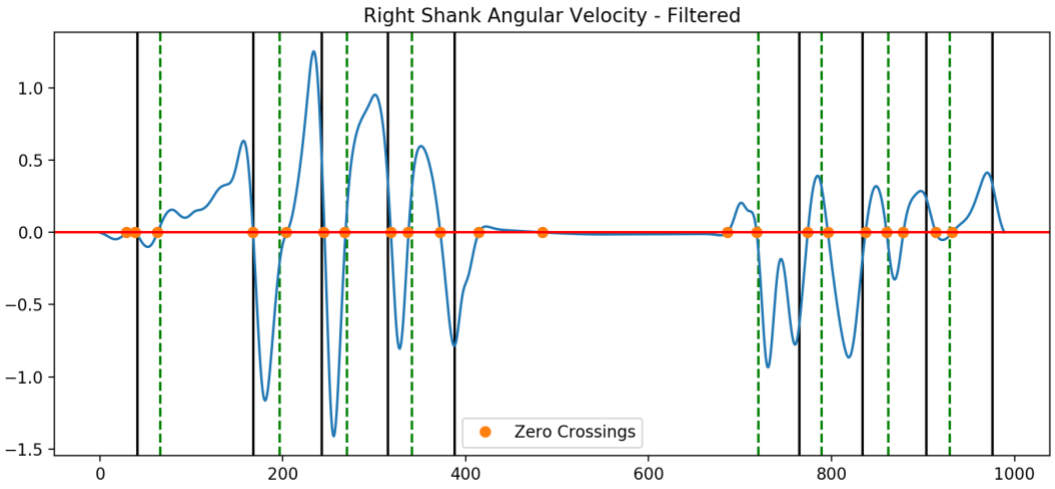

Figure 11 Shank Angular velocity - Right Foot - Walking in a Straight Line- Filtered

Next, a method proposed by Zeni, el. [6] was tested. In this method, heel-strike is identified as the time when the forward distance of the heel marker from the sacral marker is at a maximum. Toe-off was identified as the time when the toe marker is at its furthest posterior

distance from the sacral marker. After applying similar filters as discussed in previous methods, the Zeni method provided the least amount of noise, and the most promising results. However, despite the increased average accuracy in detecting the right toe-off and heel-strike timings, we were facing two main issues. First, we noticed a considerable number of false positives when the subject is not moving, during stops, or when the subject turns. Since two different parameters are used to detect the strikes in this method, it is easy to distinguish between a toe-off and a heel strike.

To detect the stop regions, a solution suggested by our colleague Connor McGuirk [61] is used. Based on his approach, first we calculate torso velocity of the subject throughout the video. If the subject has a constant velocity, it means the subject is in a static situation. Also, if the velocity is constant and drops below zero, we consider the subject to be out of frame. Moreover, to refine the stop regions we defined a manual threshold of 0.5 second, if two consequent stop regions have a duration of 0.5 second or less, they get joined as a single region. In figure 11, the red area shows when the subject is static. Moreover, the blue region indicates that no subject has been detected (moved out of frame).

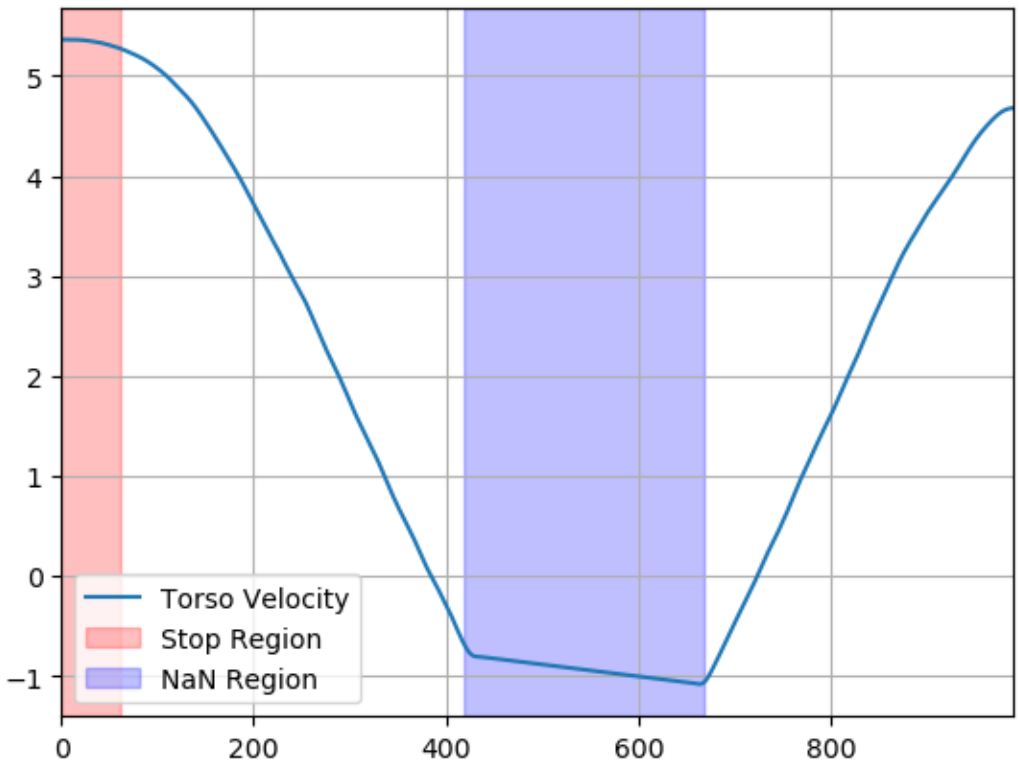

Figure 15 Detected Regions in WS1

After detecting stop and NaN regions, still we were facing two problems due to turns. First, we were noticing true positive (false heel strike or toe-off), and that was mainly when the subject was turning, and next, since the subject turns our values which are dependent on the lab's coordinate system inverts. As a solution for the first problem, we implemented an algorithm to detect the turns by monitoring the distance between left and right hips and two shoulder points. When the distance is changed to negative, the algorithm considers a turn has happened. Since turning is a continuous action, it takes multiple frames to have a complete turn that results in multiple negative points (a range). We estimate the optimum turn point by selecting the mid-point in the range as the optimal point. After detecting the turn, first we

transfer the lab coordinate axis (since direction of the patient changes), and then eliminate first, and last 10 frames before and after turn to reduce false positives. This might cause elimination of a small number of true positives, however studying subject while in turn is not was not within the scope of our research.

The next figure, consists of two plots, the top plot shows right heel position relative to mid hip, the solid green line indicates ground truth for the heel-strike and the dashed red line shows the estimated timing for the heel-strike. The below plot represents right middle toe position relative to mid hip point. The toe-off event, and similarly the solid green lines are the ground truths and dashed lines are calculated via the algorithm.

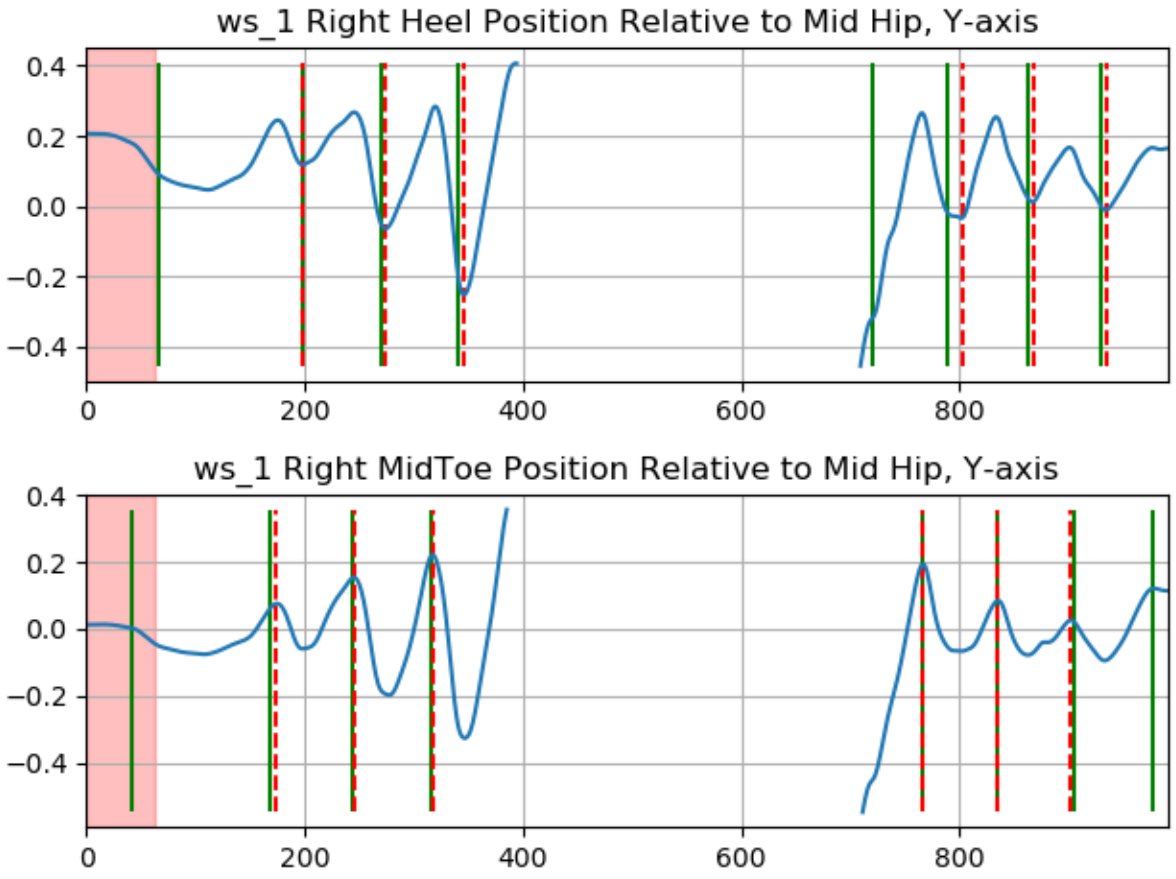

Figure 12 Zeni Method with Detected Regions in WS1

At this stage of research, the goal has been to develop a single method which can provide the best generalization for most of the trials, and as a result, the Zeni method as described in this section is used to measure the temporal parameters. The tables below represents a sample comparison between the three methods described in this section. SAV stands for "Shank Angular Velocity" . Moreover "Missed" means: could not be detected by algorithm or was eliminated in stop or turn regions. "L Off" and "R Off" are the complete reports of temporal parameters results based on comparing Zeni vs SAV is shown in the two tables below: Walking Straight 1- Left and Walking Straight 1- Right Foot.

Table 4 Comparison of Gait Detection Algorithms

Walking Straight 1 - Left Foot									
L Strike Zeni	**SAV L Strike**	**L Strike - Grimmer**	**Delta with Zeni**	**Delta with SAV**	**L Off Zeni**	**SAV L Off**	**L Off - Grimmer**	**Delta with Zeni**	**Delta with SAV**
157	150	159	2	9	Missed	Missed	124	-	-
241	237	233	8	4	211	204	207	4	3
310	307	305	5	2	285	281	278	7	3
Missed	Missed	377	-	-	356	359	351	5	8
OOF	OFF	-1	-	-	OOF	OOF	-1	-	-
Missed	Missed	685	-	-	Missed	Missed	730	-	-
761	760	755	6	5	799	806	800	1	6
830	830	824	6	6	870	876	870	0	6
907	901	893	14	8	Missed	Missed	939	-	-
Missed	Missed	964	-	-	OOF	OOF	-1	-	-
Average			**6.833333**	**5.666667**	**Average**			**3.4**	**5**
Zeni Average	**5.116666667**				**SAV Average**		**5.433333333**		
Zeni False Positives	**0**				**SAV False Positives**	**1**			

Walking Straight 1 - Right Foot									
L Strike Zeni	**SAV L Strike**	**L Strike - Grimmer**	**Delta with Zeni**	**Delta with SAV**	**L Off Zeni**	**SAV L Off**	**L Off - Grimmer**	**Delta with Zeni**	**Delta with SAV**
Missed	Missed	66	-	-	Missed	Missed	41	-	-
198	204	197	1	7	174	167	168	6	1
274	268	270	4	2	245	245	243	2	2
346	337	341	5	4	317	318	315	2	3
OOF	OOF	-1	-	-	Missed	Missed	388	-	-
Missed	Missed	720	-	-	OOF	OOF	-1	-	-
802	796	789	13	7	766	774	765	1	9
867	860	862	5	2	835	837	834	1	3
934	932	929	5	3	902	914	904	2	10
		-1	1	1	Missed	Missed	976	-	-
Average			**4.857143**	**3.714286**	**Average**			**2.333333**	**5**
Zeni Average	**3.595238095**				**SAV Average**		**4.19047619**		
Zeni False Positives	**0**				**SAV False Positives**	**1**			

In the rest of this section, the reports for each trial based on the Zeni method is described. As described in chapter 3, we ran our tests twice per trial type.

4.1.1 Walking with a Cane

In this trial, a subject walks with a cane throughout the hallway, and turns back to the start point. In the following, two figures are included, one for the left and one for the right foot. Furthermore, there are two plots per diagram, each showing heel-strike and foot off events. As explained earlier, in the plot titled “Left heel position relative to mid-hip” the Y-axis shows Y position of heel/toe (based on the 3D lab coordinates) relative to mid-hip, and X-axis indicates the frame number. In this plot, the minima indicates heel-strike.

Similarly in the plot titled “Left Mid-Toe position relative to mid-heap”, plot maxima show toe-off events. Solid green line shows the ground truth, and the dashed lines are values estimated via Zeni algorithm. Similarly for the following figure for the right foot.

The figures are followed with a table, which compares temporal results calculated via Zeni method to the manually detected ground truth (GT), and average difference is reported.

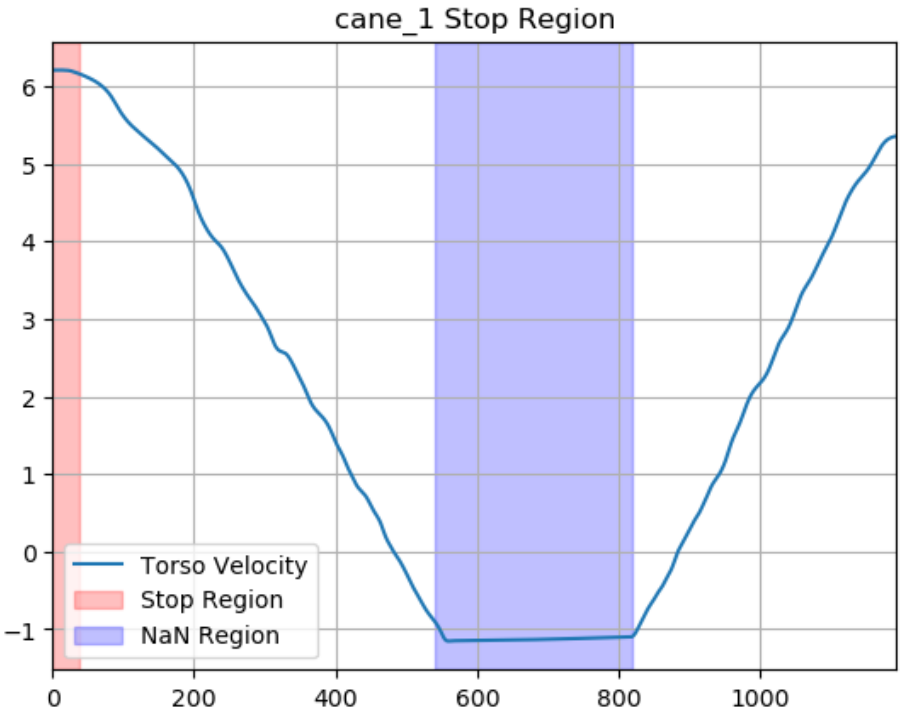

Figure 16 Cane_1 Stop Region

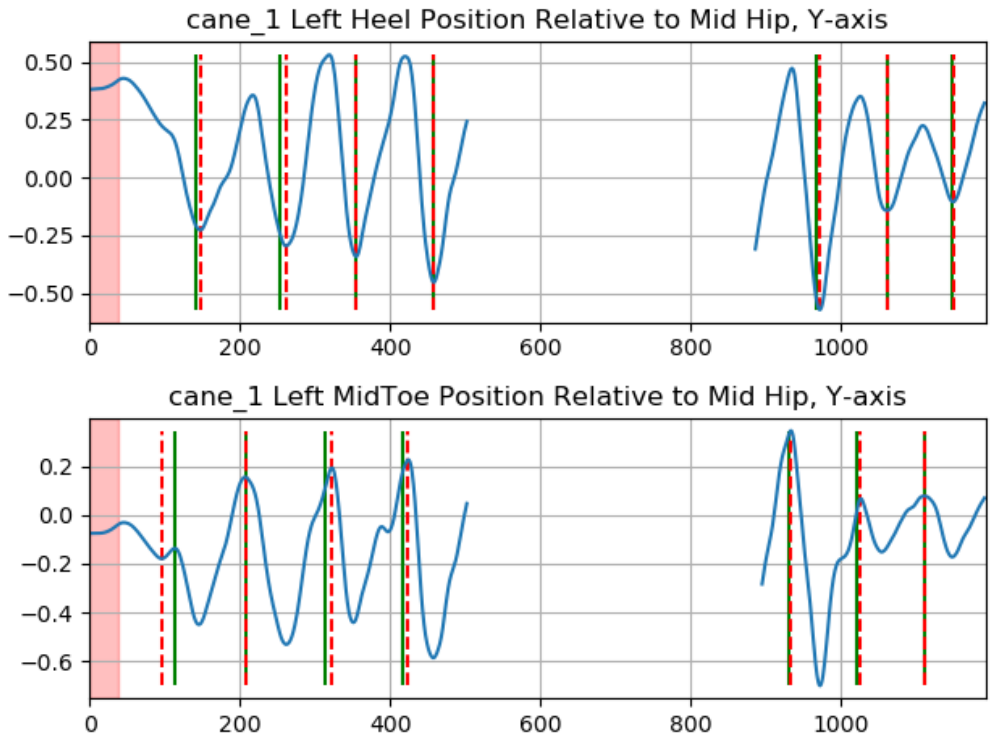

Figure 17 5Cane_1 Right Heel and Right MidToe Positions Relative to Mid Hip, Y-axis

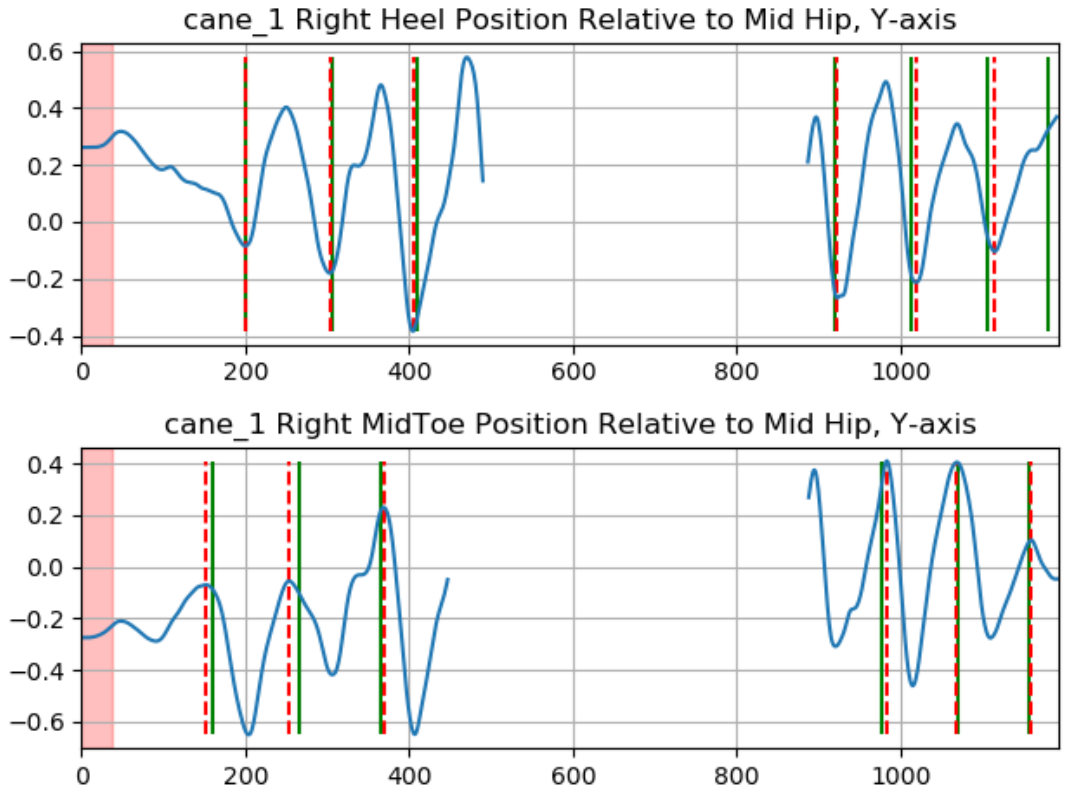

Figure 18 Right Heel and Right MidToe Positions Relative to Mid Hip, Y-axis

Table 5 Cane 1 Zeni Algorithm

Cane 1											
L Strike Zeni	L Strike - GT	Delta	**L Off Zeni**	L Off - GT	Delta	**R Strike Zeni**	R Strike - GT	Delta	**R Off Zeni**	R Off - GT	Delta
147	142	5	96	114	18	200	200	0	152	160	8
261	253	8	207	208	1	303	305	2	253	266	13
355	355	0	322	314	8	405	409	4	369	366	3
458	457	1	424	417	7	923	920	3	983	978	5
972	967	5	933	931	2	1019	1014	5	1069	1070	1
1061	1061	0	1026	1021	5	1115	1106	9	1160	1157	3
1149	1147	2	1111	1112	1	Missed	1181	-			
Average		**3**			**6**			**4**			**6**
W Average	**5**										

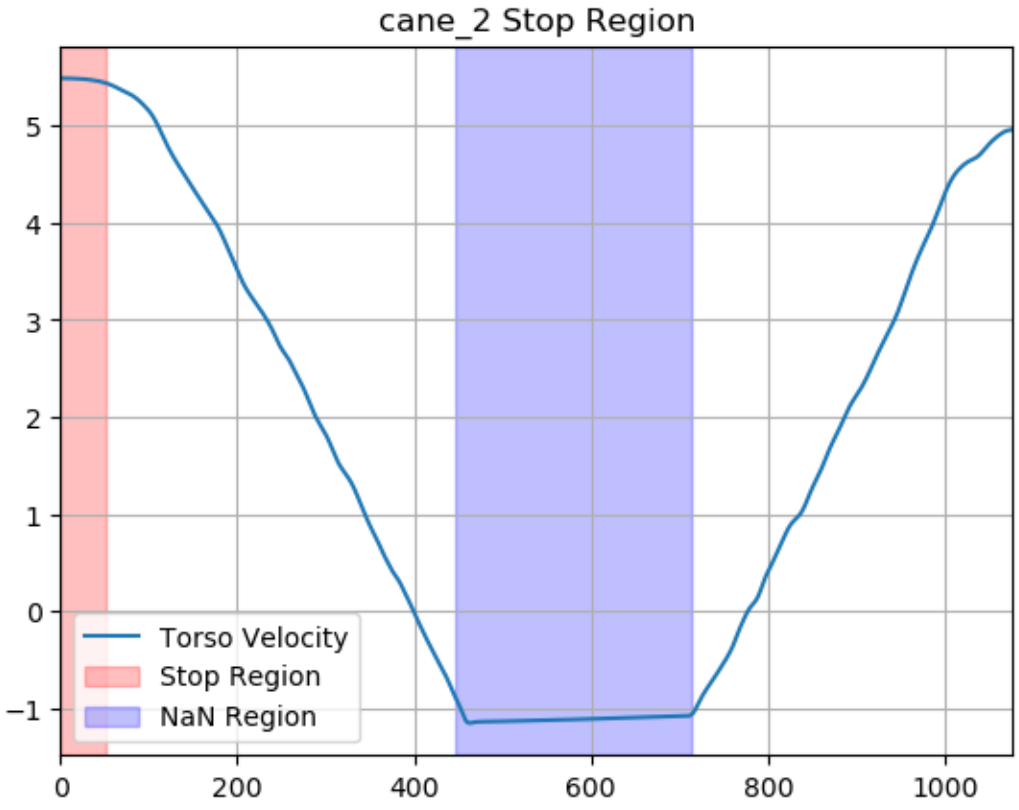

Figure 19 Cane_2 Stop Region

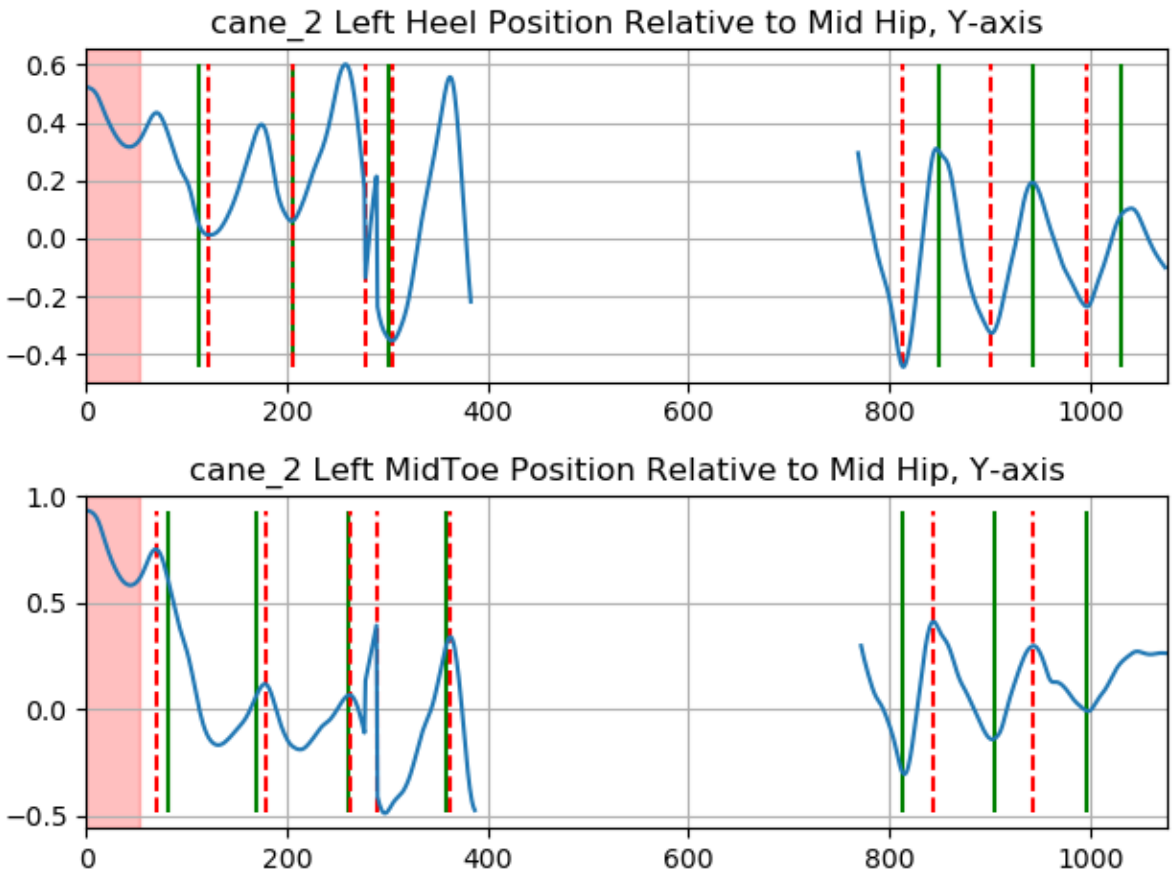

Figure 20 Cane_2 Left Heel and Left MidToe Positions Relative to Mid Hip, Y-axis

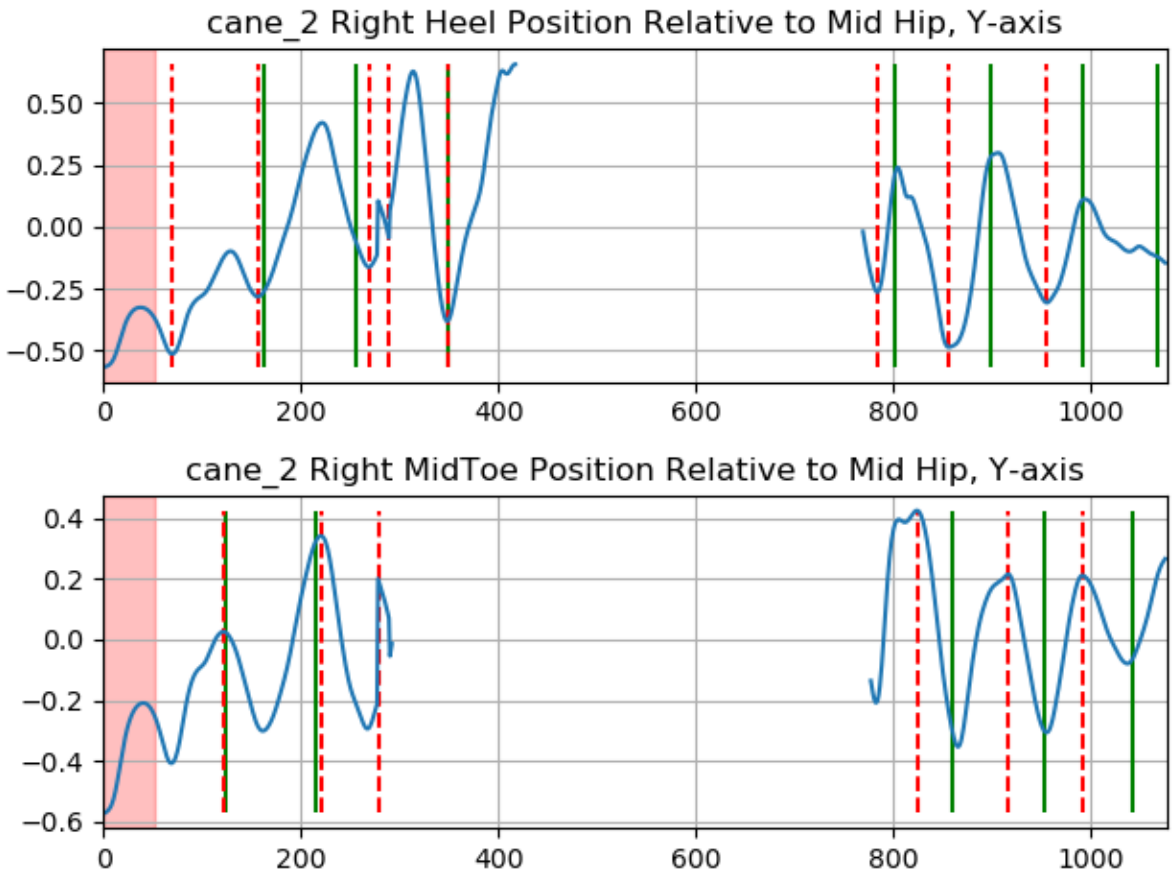

Figure 21 Right Heel vs. Right MidToe Positions Relative to Mid Hip, Y-axis

Table 6 Cane 2 Zeni Algorithm

Cane 2											
L Strike Zeni	L Strike - GT	Delta	**L Off Zeni**	L Off - GT	Delta	**R Strike Zeni**	R Strike - GT	Delta	**R Off Zeni**	R Off - GT	Delta
122	112	10	69	82	13	69	FP	-	121	124	3
205	205	0	178	169	9	156	162	6	220	215	5
278	FP	-	262	261	-	269	255	14	278	FP	-
304	302	2	289	FP	-	289	FP	-	824	860	-
814	849	35	363	358	5	348	349	1	916	953	37
902	943	41	844	814	30	784	802	18	991	1042	51
997	1031	34	944	905	39	856	898	42			
		-	Missed	997	-	955	991	36			
						Missed	1068	-			-
Average		**22.4**			**20.75**			**19.5**			**31**
W Average	**23**										

4.1.2 Walking in a straight path– Turning out of frame

For this trial, the results are reported in the same fashion as the previous trial. In this test. The subject performs a similar activity to the previous test, however this time without a cane. The results are closely related, however in this this we can see more missed strides which can be due to the faster pace of the subject as will be reported in the next chapter section.

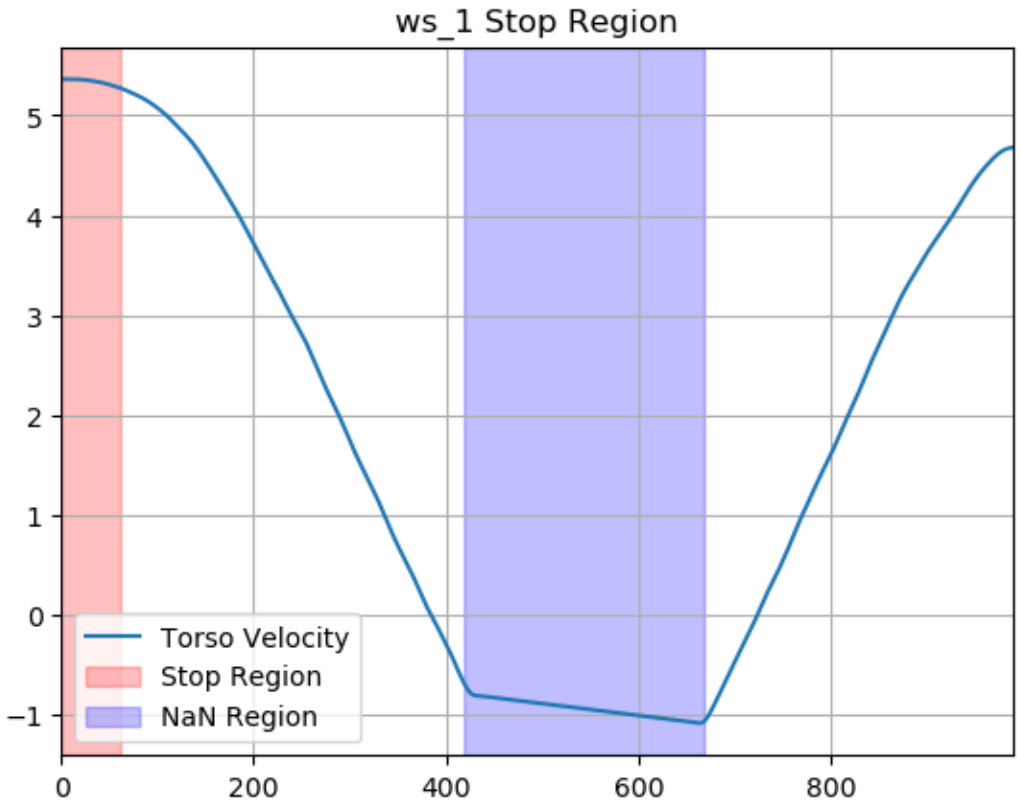

Figure 22 ws_1 Stop Region

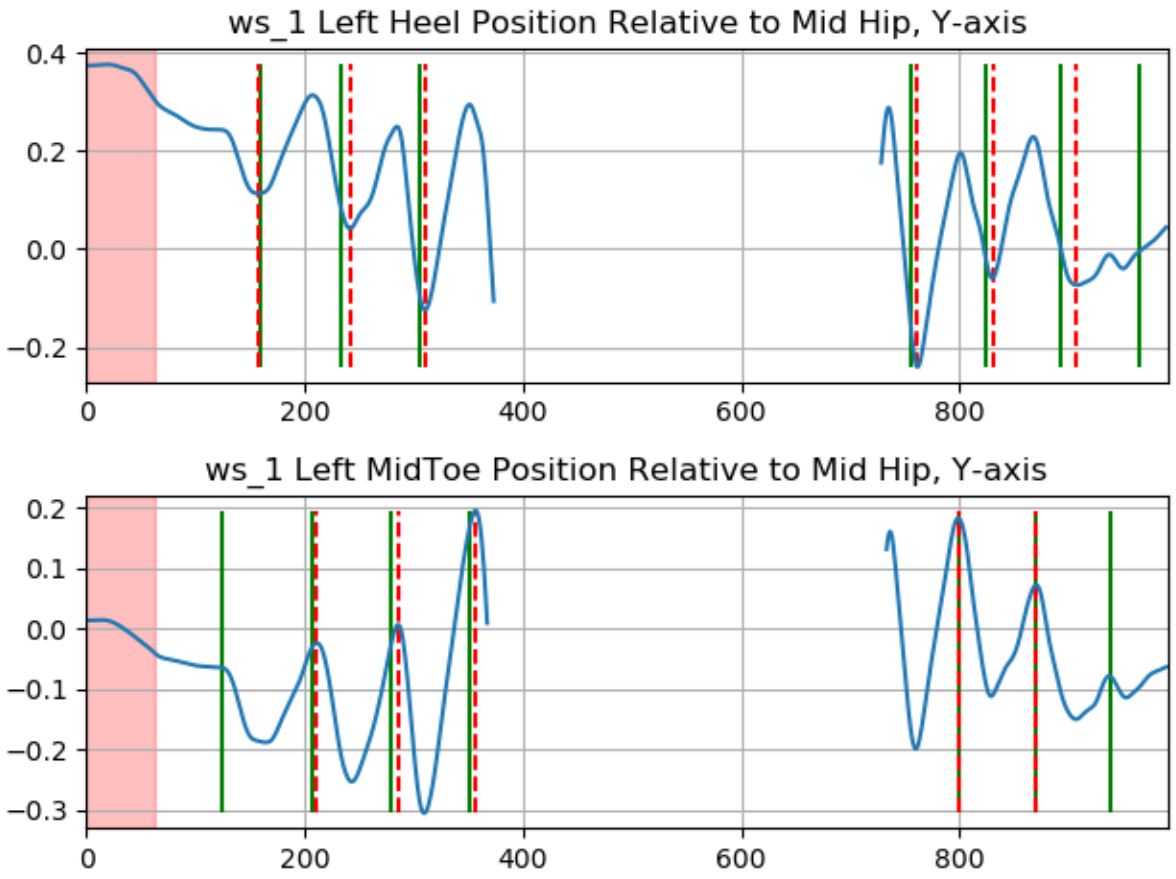

Figure 23 13 ws_1 Left Heel and Left MidToe Positions Relative to Mid Hip, Y-axis

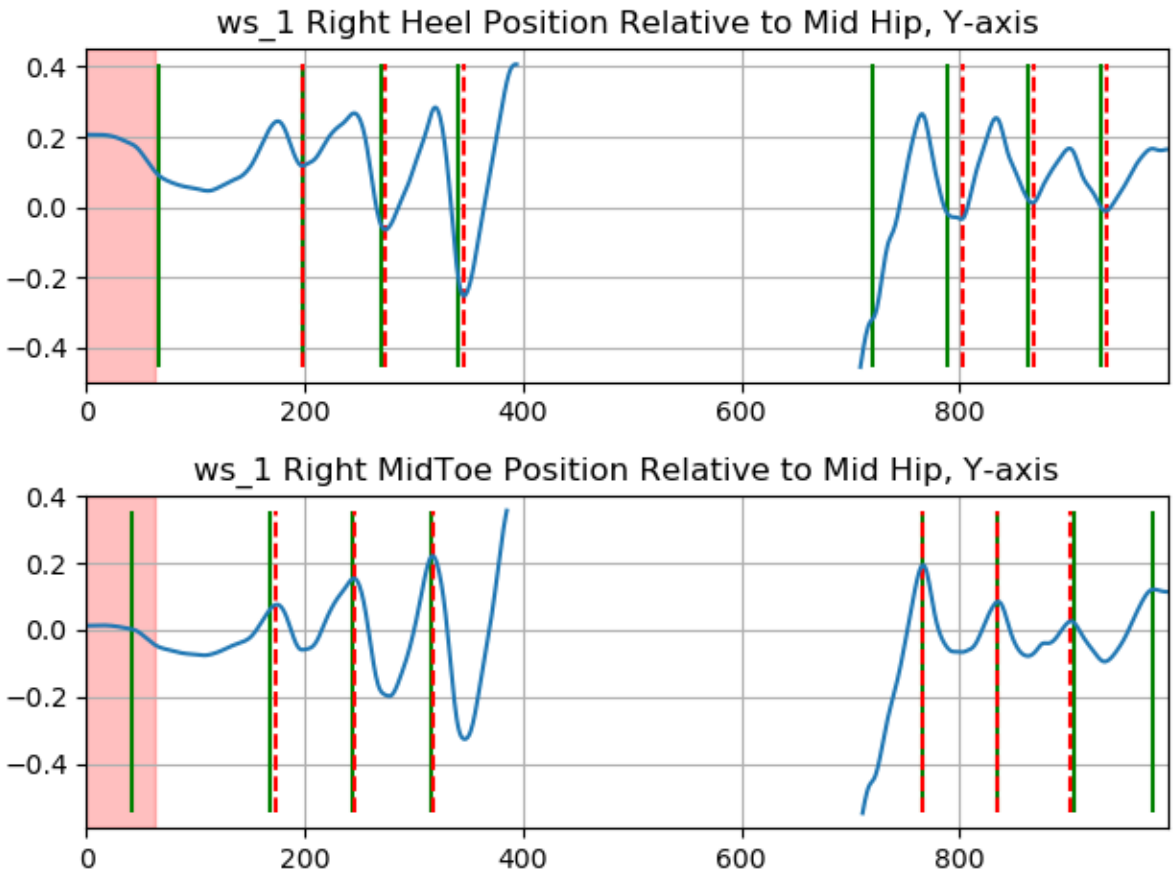

Figure 24 Right Heel and Right MidToe Positions Relative to Mid Hip, Y-axis

Table 7 Walking Straight 1

Walking Straight 1											
L Strike	L Strike - GT	**Delta**	**L Off**	L Off - GT	**Delta**	**R Strike**	R Strike - GT	**Delta**	**R Off**	R Off - GT	**Delta**
157	159	2	Missed	124	-	Missed	66	-	Missed	41	-
241	233	8	211	207	4	198	197	1	174	168	6
310	305	5	285	278	7	274	270	4	245	243	2
Missed	377	-	356	351	5	346	341	5	317	315	2
OOF	-1	-	OOF	-1	-	OOF	-1	-	Missed	388	-
Missed	685	-	Missed	730	-	Missed	720	-	OOF	-1	-
761	755	6	799	800	1	802	789	13	766	765	1
830	824	6	870	870	0	867	862	5	835	834	1
907	893	14	Missed	939	-	934	929	5	902	904	2
Missed	964	-	OOF	-1	-		-1	1	Missed	976	-
Average		**7**	**Average**		**3**	**Average**		**5**	**Average**		**2**
W Average	4										

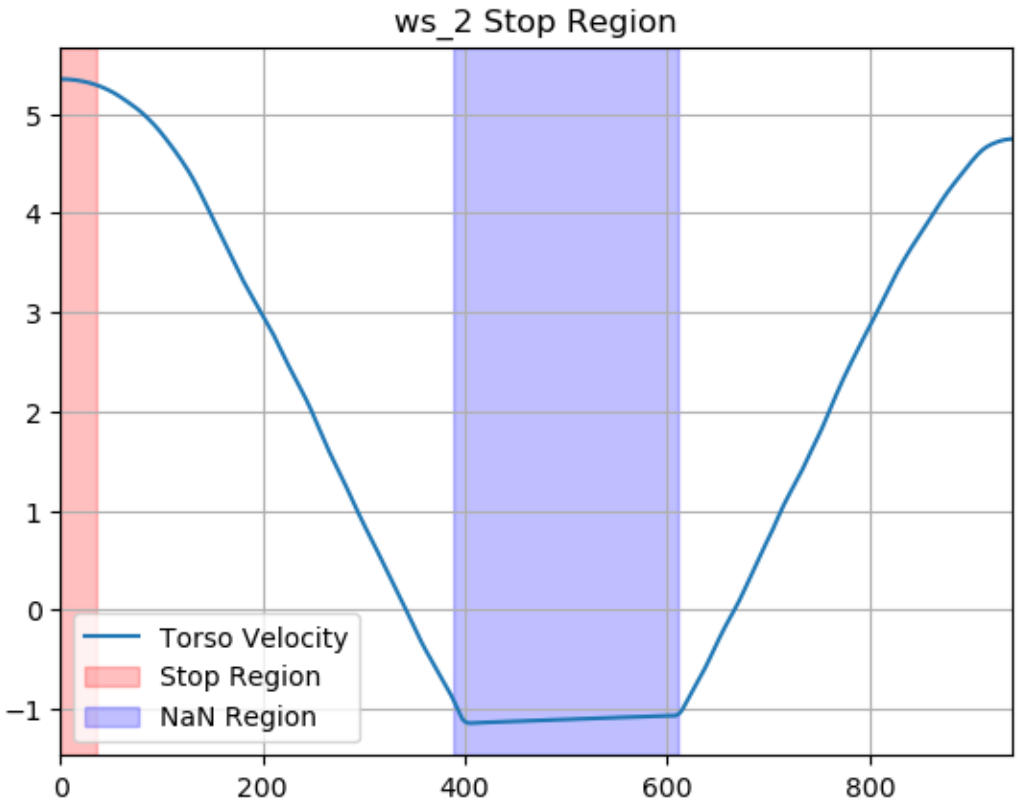

Figure 25 ws_2 Stop Region

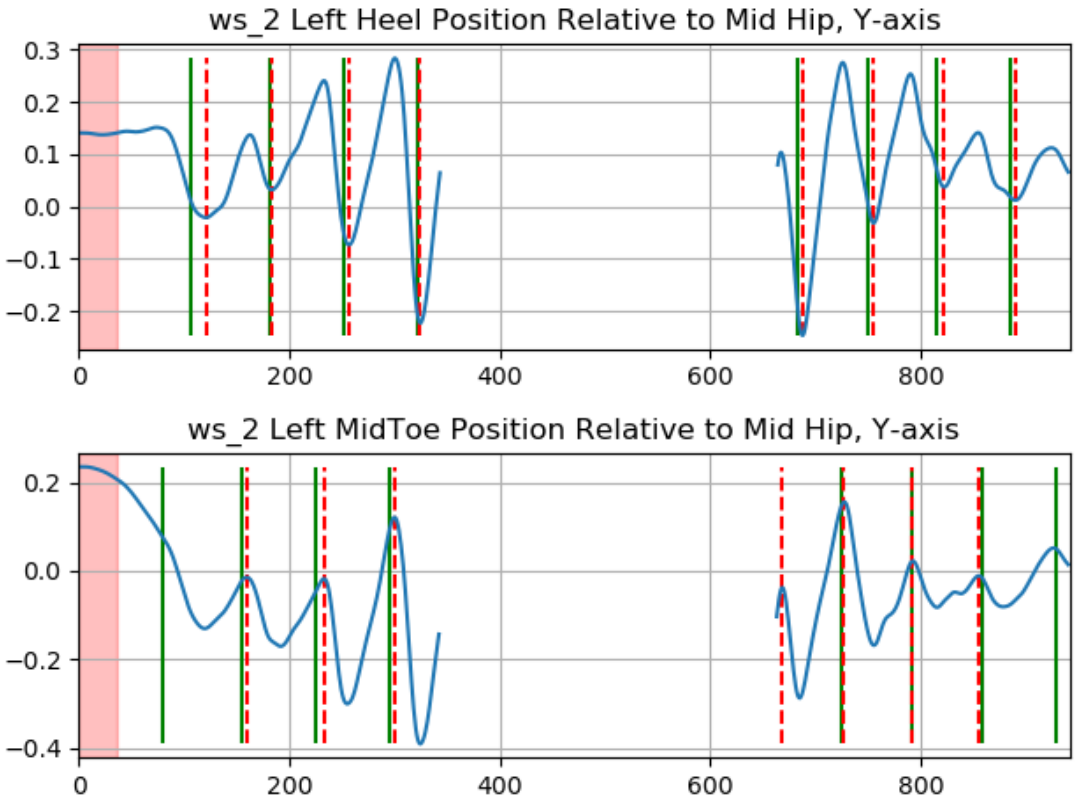

Figure 26 ws_2 Left Heel and Left MidToe Positions Relative to Mid Hip, Y-axis

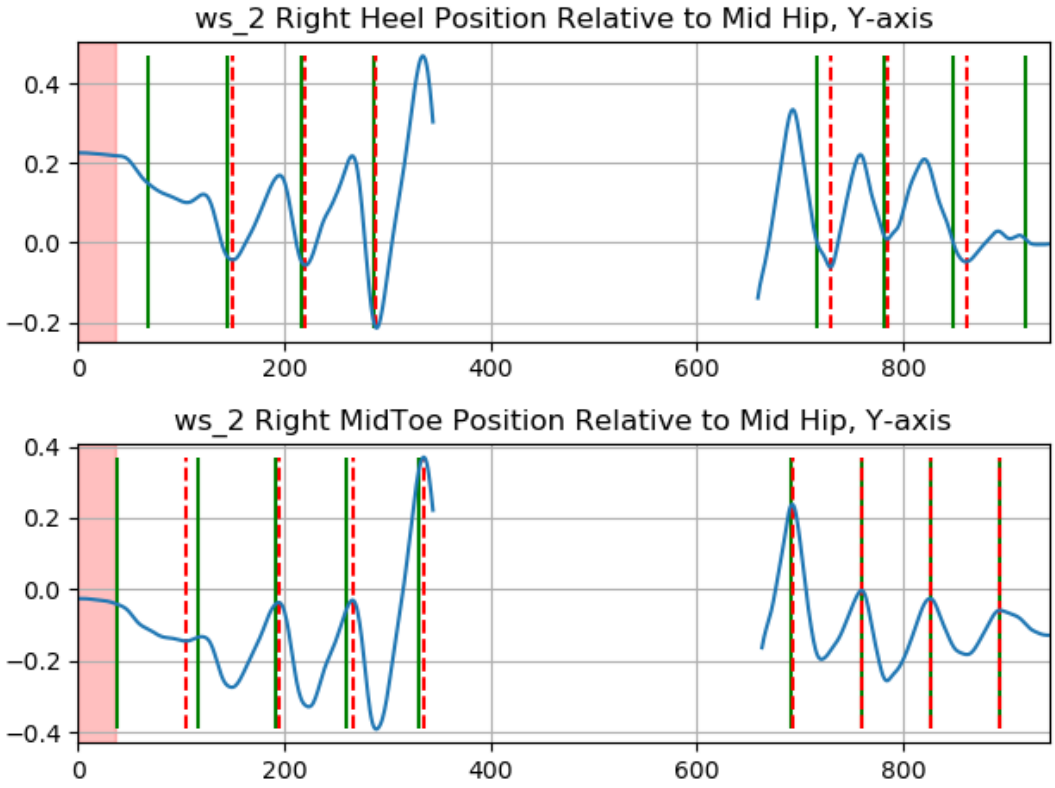

Figure 27 ws_1 Right Heel and Right MidToe Positions Relative to Mid Hip, Y-axis

Table 8 Walking straight 2

Walking Straight 2											
L Strike	L Strike - GT	**Delta**	**L Off**	L Off - GT	**Delta**	**R Strike**	R Strike - GT	**Delta**	**R Off**	R Off - GT	**Delta**
121	106	15	Missed	80	-	Missed	67	-	Missed	38	-
183	181	2	159	154	5	150	144	6	104	116	12
256	251	5	233	225	8	220	216	4	194	191	3
324	321	3	300	295	5	289	286	3	266	260	6
OOF	-1	-	OOF	-1	-	OOF	-1	-	335	330	5
688	682	6	668	655	13	Missed	646	-	692	691	1
755	750	5	727	725	2	729	716	13	760	759	1
822	815	7	792	791	1	784	782	2	826	826	0
890	885	5	855	858	3	861	849	12	894	894	0
OOF	-1	-	Missed	929	-	Missed	919	-	OOF	-1	-
Average		**6**	**Average**		**5**	**Average**		**7**	**Average**		**4**
W Average	5										

4.1.3 Walking Straight – turning in frame

In this trial, the results are reported in the same fashion as the previous trials. The subject performs a similar activity to the previous test, however this time change of direction (a turn) happens in the frame. The results are closely related, however in this this we can see more missed strides which can be due to the faster pace of the subject as will be reported in the next chapter section.

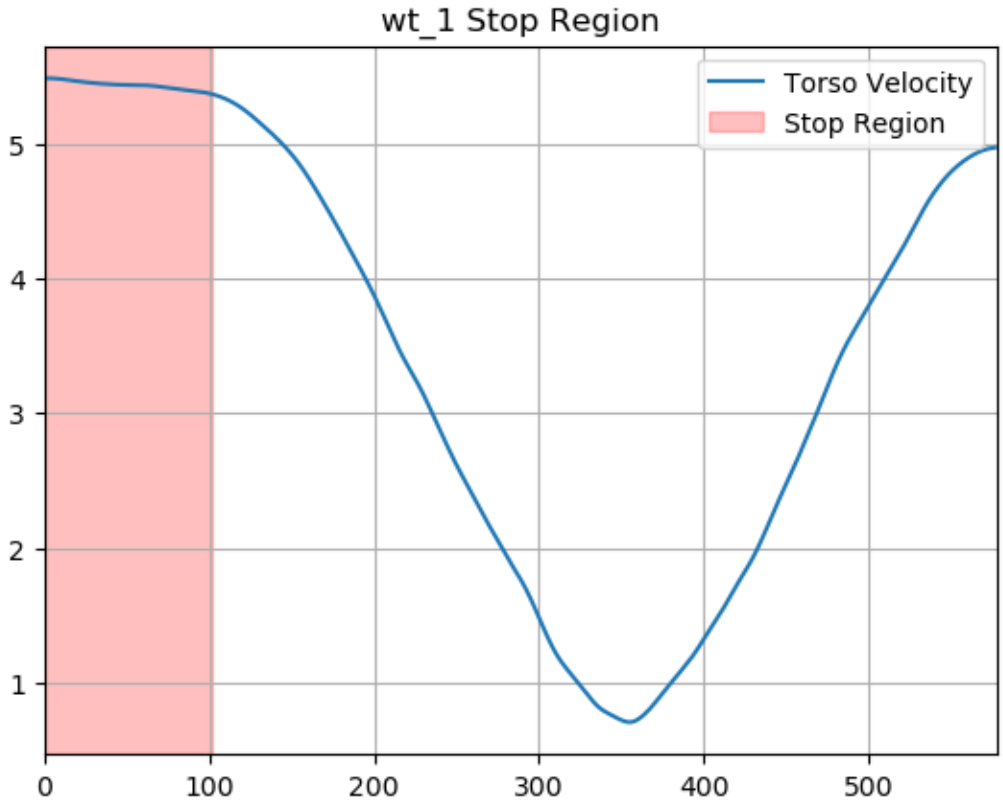

Figure 28 wt_1 Stop Region

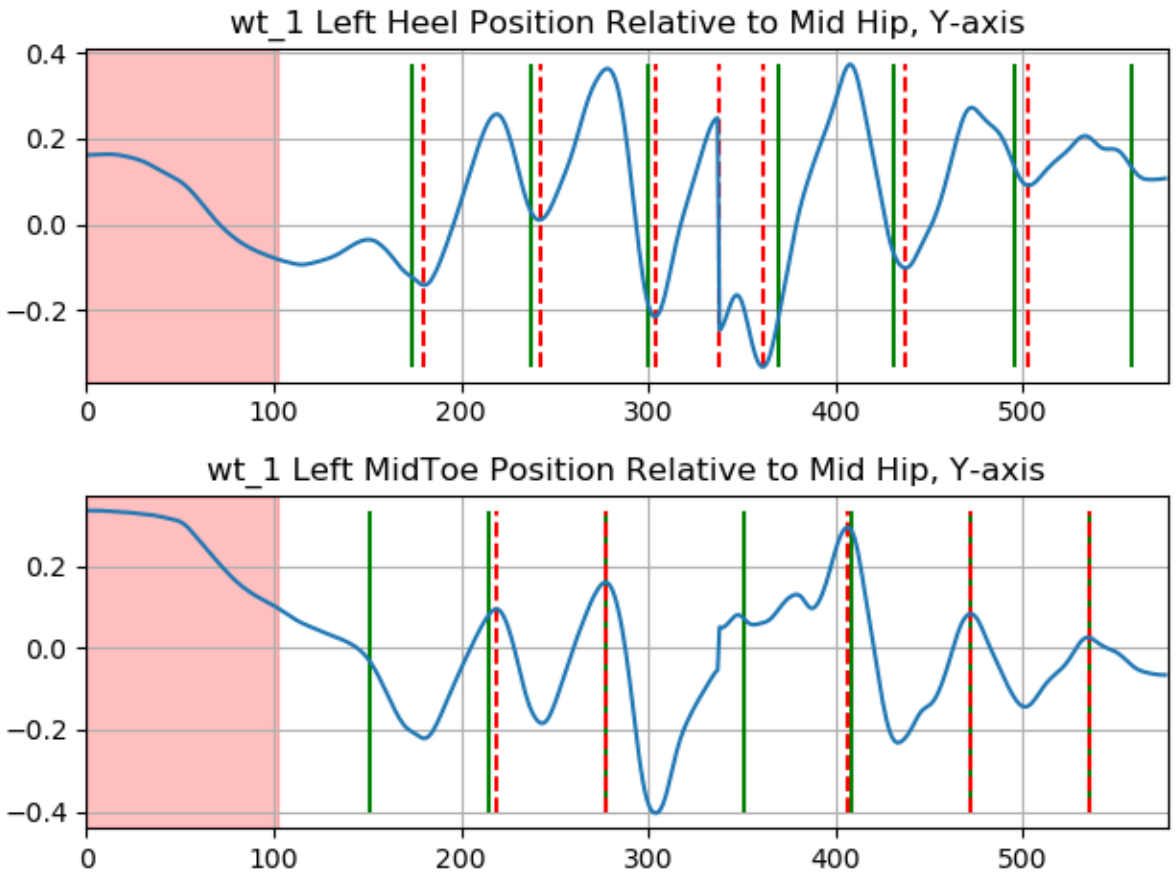

Figure 29 21 wt_1 Left Heel and Left MidToe Positions Relative to Mid Hip, Y-axis

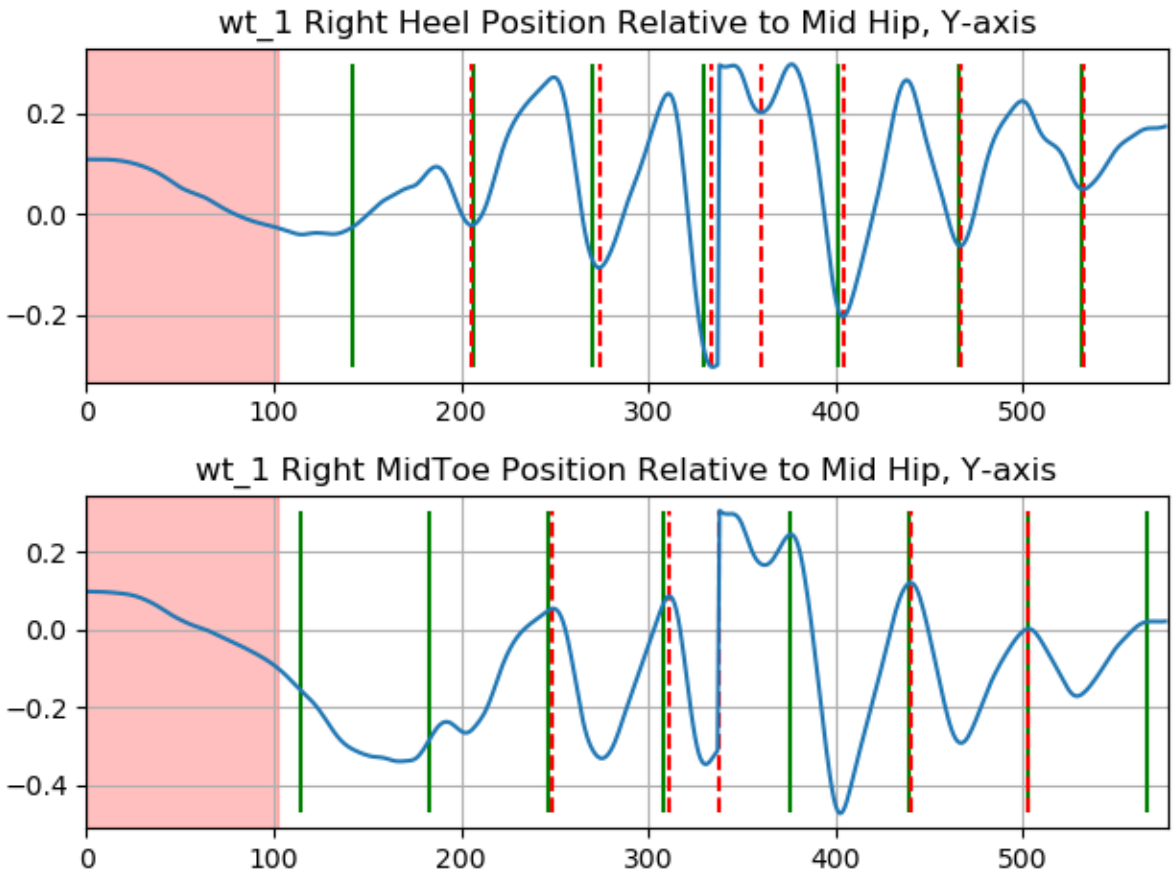

Figure 30 wt_1 Right Heel and Right MidToe Positions Relative to Mid Hip, Y-axis

Table 9 Turn in Frame 1

Turn in Frame 1											
L Strike	L Strike - GT	**Delta**	**L Off**	L Off - GT	**Delta**	**R Strike**	R Strike - GT	**Delta**	**R Off**	R Off - GT	**Delta**
180	174	6	Missed	151	-	Missed	142	-	Missed	114	-
242	237	5	219	215	4	206	207	1	Missed	183	-
304	300	4	277	277	0	274	270	4	249	246	3
338	FP	-	FP	351	-	334	330	4	311	308	3
361	369	8	406	408	2	360	FP	-	338	376	38
437	431	6	472	472	0	404	401	3	440	439	1
503	496	7	535	536	1	467	466	1	503	503	0
	558		Missed				531				
Average		**6**	**Average**		**1**	**Average**		**3**	**Average**		**9**
W Average	5										

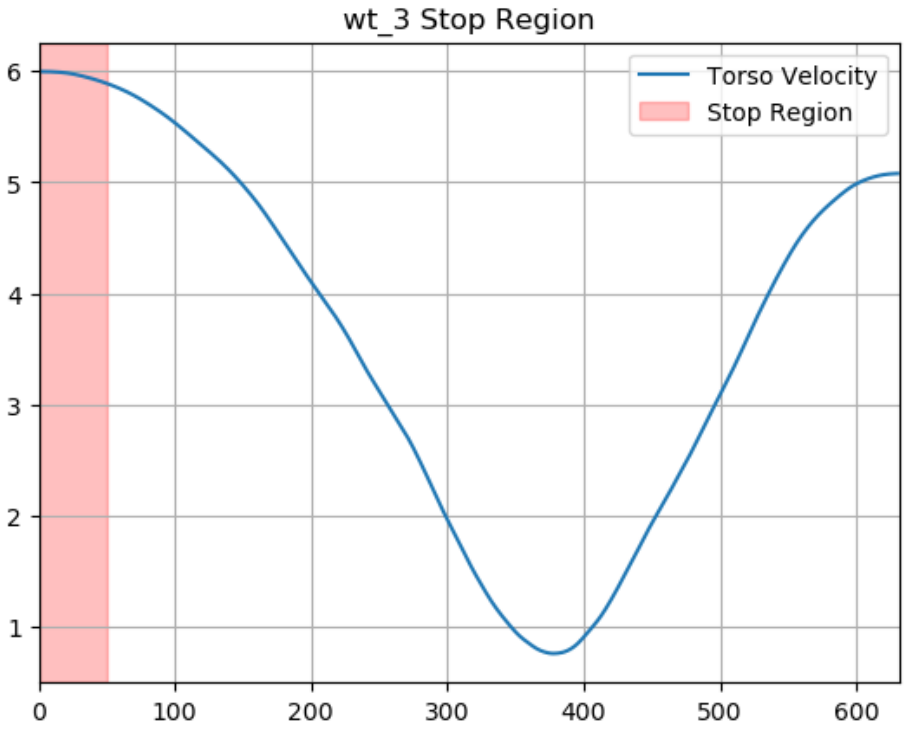

Figure 31 wt_3 Stop Region

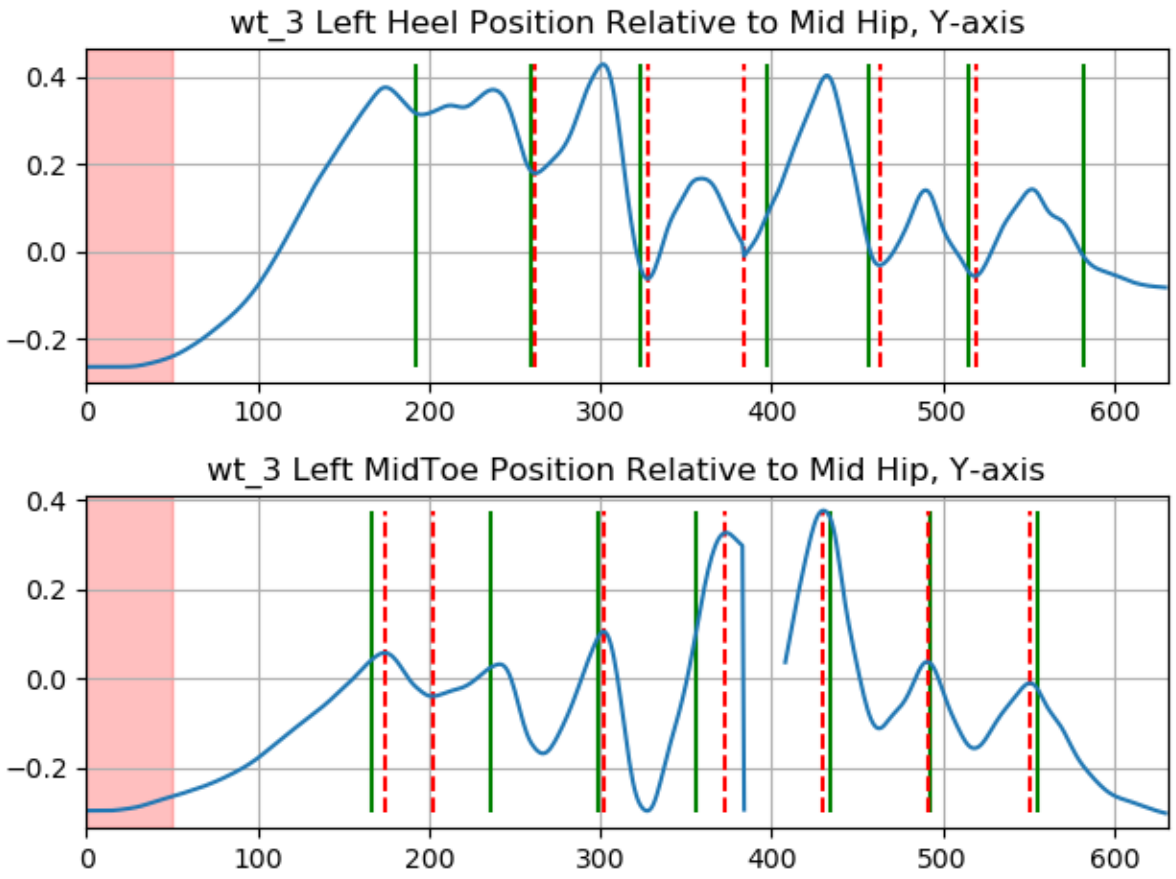

Figure 32 25 wt_3 Left Heel and Left MidToe Positions Relative to Mid Hip, Y-axis

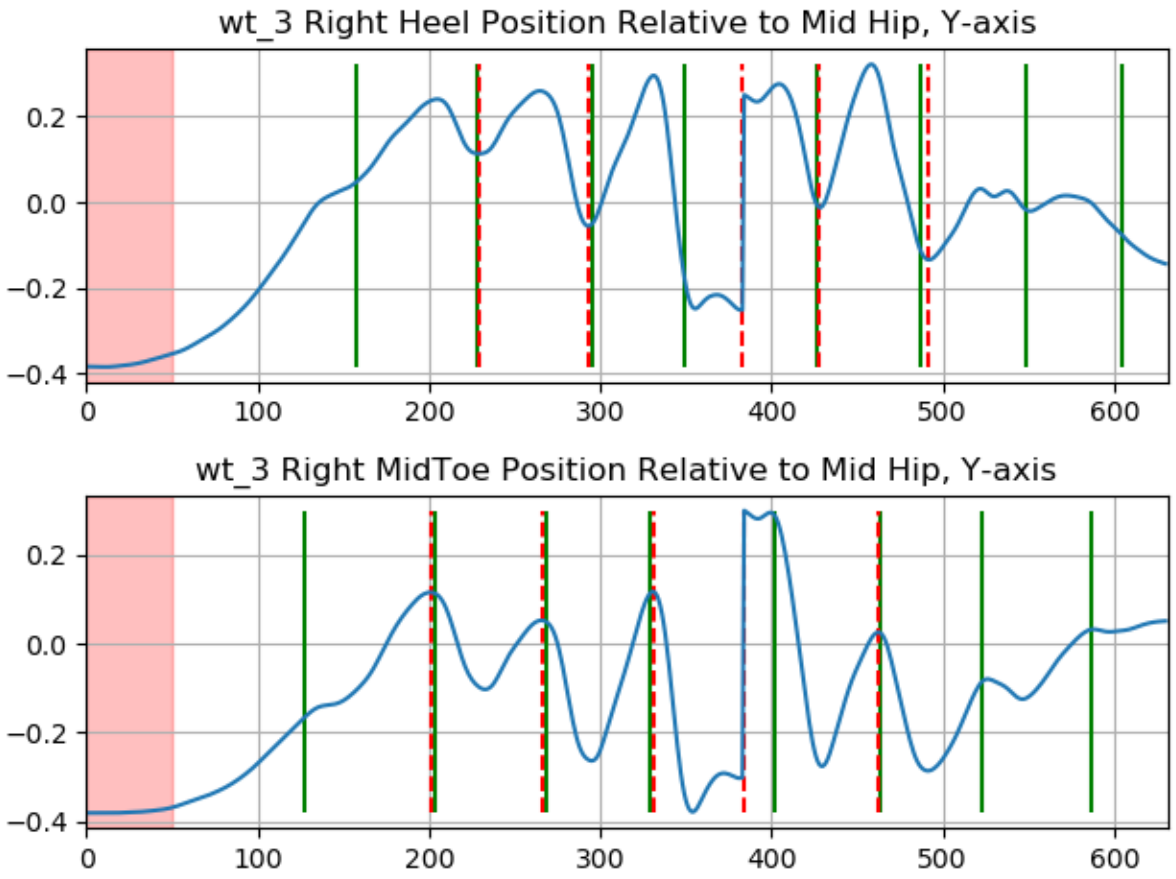

Figure 33 Right Heel and Right MidToe Positions Relative to Mid Hip, Y-axis

Table 10 Turn in Frame 3

Turn in Frame 3											
L Strike	L Strike - GT	**Delta**	**L Off**	L Off - GT	**Delta**	**R Strike**	R Strike - GT	**Delta**	**R Off**	R Off - GT	**Delta**
Missed	192	-	174	166	8	-	157	-	Missed	127	-
262	260	2	202	236	34	229	228	1	201	203	2
328	323	5	302	299	3	293	295	2	266	268	2
384	397	13	373	356	17	383	349	34	331	329	2
463	457	6	430	434	4	428	426	2	384	402	18
519	515	4	491	493	2	492	487	5	462	463	1
Missed	582	-	551	555	4	-	549	-	Missed	523	-
Average		**6**	**Average**		**10**	**Average**		**9**	**Average**		**5**
W Average	8										

4.1.4 Circular (Curve) Walking

In this trial, the results are reported in the same fashion as the previous trials. In this test. The subject walks around the path in a circular manner. Since there is a need to detect when the person is moving toward or away from the cameras, out algorithm selected the middle red region in following figure as the region which the direction changes. The results are closely related the previous test, however for the second try, in ending frames, the deep-learning algorithm could not localize the points on subject's right foot correctly which resulted in a considerable jump in timing error.

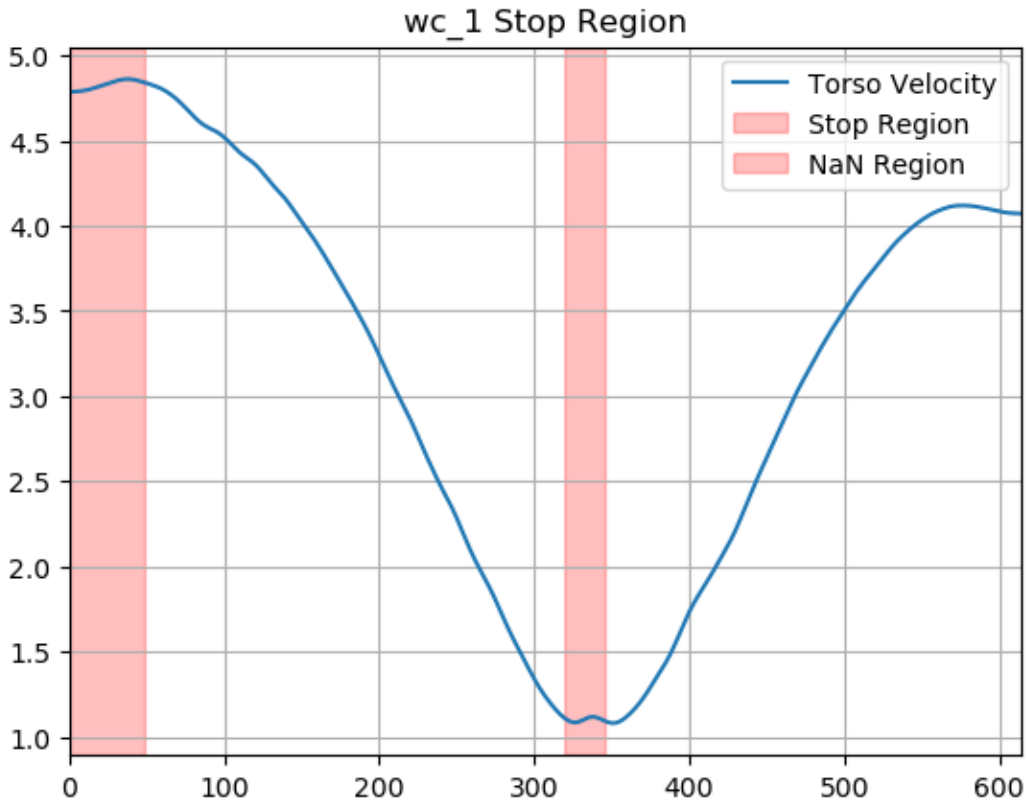

Figure 34 wc_1 Stop Region

Figure 35 Left Heel and Left MidToe Positions Relative to Mid Hip, Y-axis

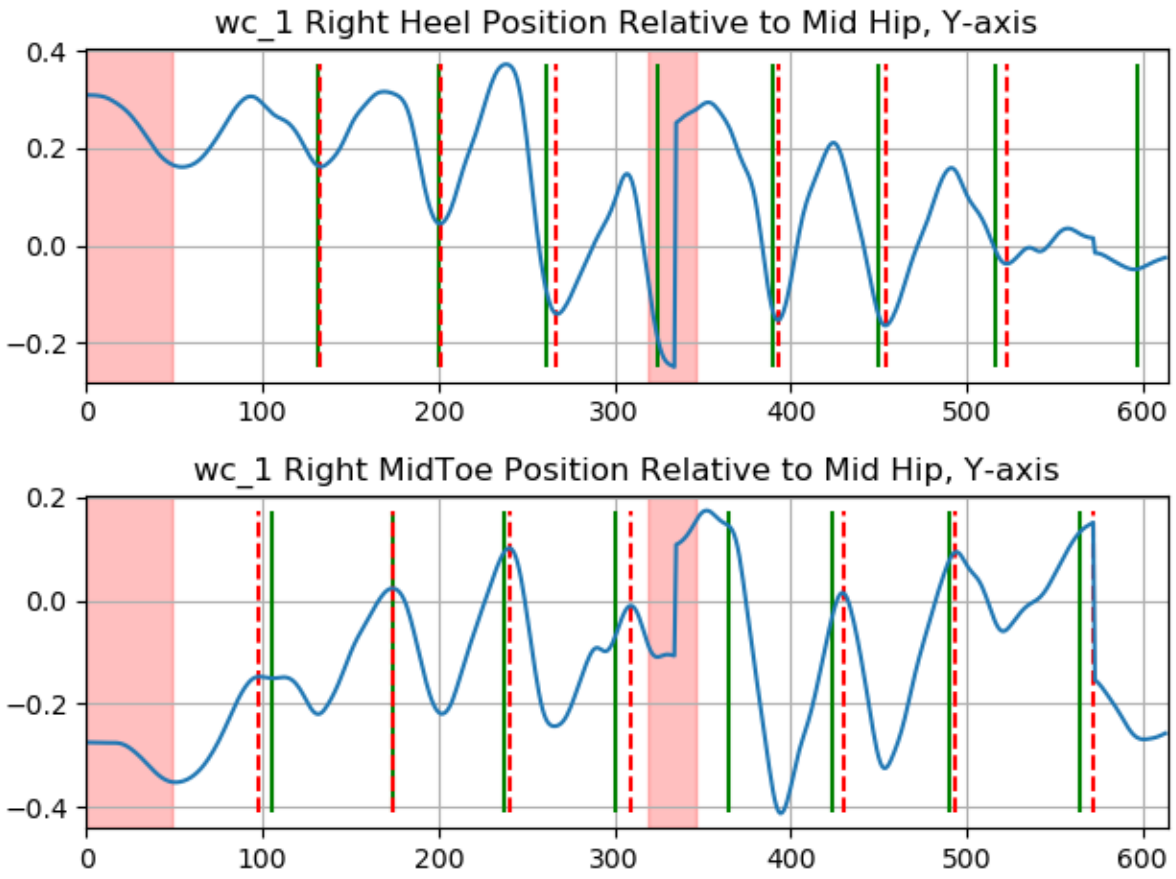

Figure 36 Right Heel and Right MidToe Positions Relative to Mid Hip, Y-axis

Table 11 Curve Walk 1

Curve Walk 1											
L Strike	**L Strike - GT**	**Delta**	**L Off**	**L Off - GT**	**Delta**	**R Strike**	**R Strike - GT**	**Delta**	**R Off**	**R Off - GT**	**Delta**
168	164	4	148	140	8	133	131	2	98	105	7
235	231	4	210	207	3	201	200	1	174	174	0
297	293	4	269	269	0	267	261	6	240	237	3
366	357	9	Missed	332	-	Missed	325	-	309	300	9
422	417	5	399	394	5	393	390	3	Missed	365	-
490	482	8	462	457	5	454	450	4	430	424	6
573	551	22	533	524	9	523	516	7	494	490	4
Average		**8**	**Average**		**5**	**Average**		**4**	**Average**		**5**
W Average	5										

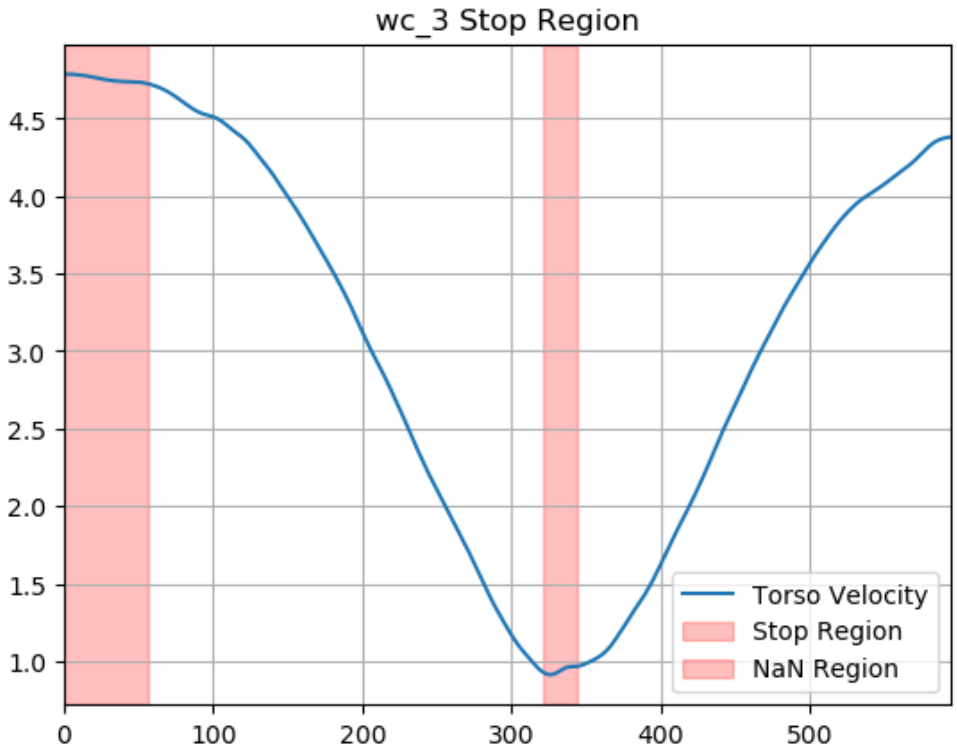

Figure 37 wc_3 Stop Region

Figure 38 Left Heel and Left MidToe Positions Relative to Mid Hip, Y-axis

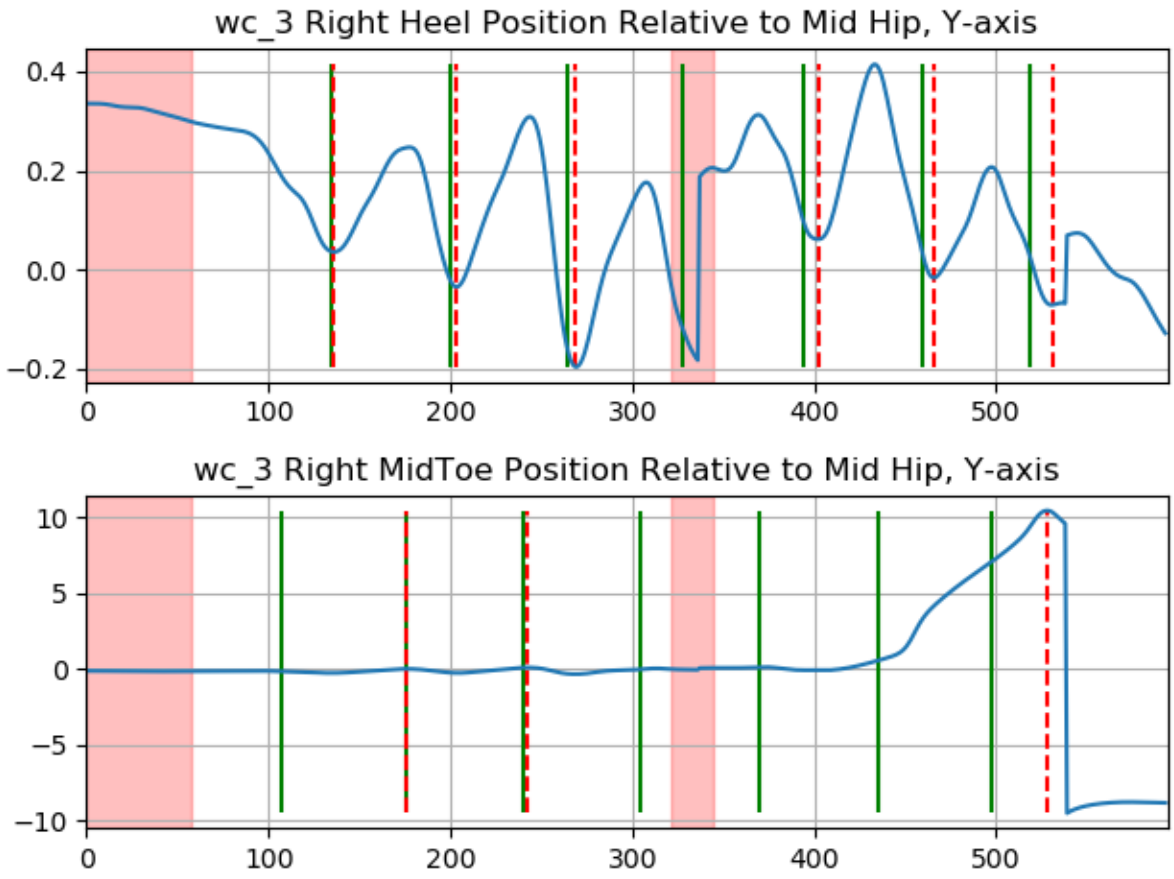

Figure 39 Right Heel and Right MidToe Positions Relative to Mid Hip, Y-axis

Table 12 Curve Walk 3

Curve Walk 3											
L Strike	**L Strike - GT**	**Delta**	**L Off**	**L Off - GT**	**Delta**	**R Strike**	**R Strike - GT**	**Delta**	**R Off**	**R Off - GT**	**Delta**
Missed	107	-	63	143	80	136	135	1	Missed	107	-
169	176	7	211	207	4	203	200	3	176	176	0
235	240	5	276	271	5	269	264	5	242	240	2
315	304	11	Missed	335	-	Missed	328	-	Missed	304	-
368	370	2	405	401	4	402	394	8	Missed	370	-
433	435	2	470	467	3	466	459	7	Missed	435	-
538	497	41	545	526	19	531	519	12	528	497	31
Average		**11**	**Average**		**19**	**Average**		**6**	**Average**		**11**
W Average	**12**										

Curve Walk 3											
L Strike	**L Strike - GT**	**Delta**	**L Off**	**L Off - GT**	**Delta**	**R Strike**	**R Strike - GT**	**Delta**	**R Off**	**R Off - GT**	**Delta**
Missed	107	-	63	143	80	136	135	1	Missed	107	-
169	176	7	211	207	4	203	200	3	176	176	0
235	240	5	276	271	5	269	264	5	242	240	2
315	304	11	Missed	335	-	Missed	328	-	Missed	304	-
368	370	2	405	401	4	402	394	8	Missed	370	-
433	435	2	470	467	3	466	459	7	Missed	435	-
538	497	41	545	526	19	531	519	12	528	497	31
Average		11	Average		19	Average		6	Average		11
W Average	**12**										

4.1.5 Walking with a walker

For this trial, the results are reported in the same fashion as the previous trials. In this test. The subject performs a similar activity to “walking in a straight line – turning out of frame” trial, however he uses a walker to move throughout the path. We see considerably an increased number missed strides which happens since the walker covers the feet in some frames. We also can observe an increase in the average frame timing error in compare to the normal case without a walker.

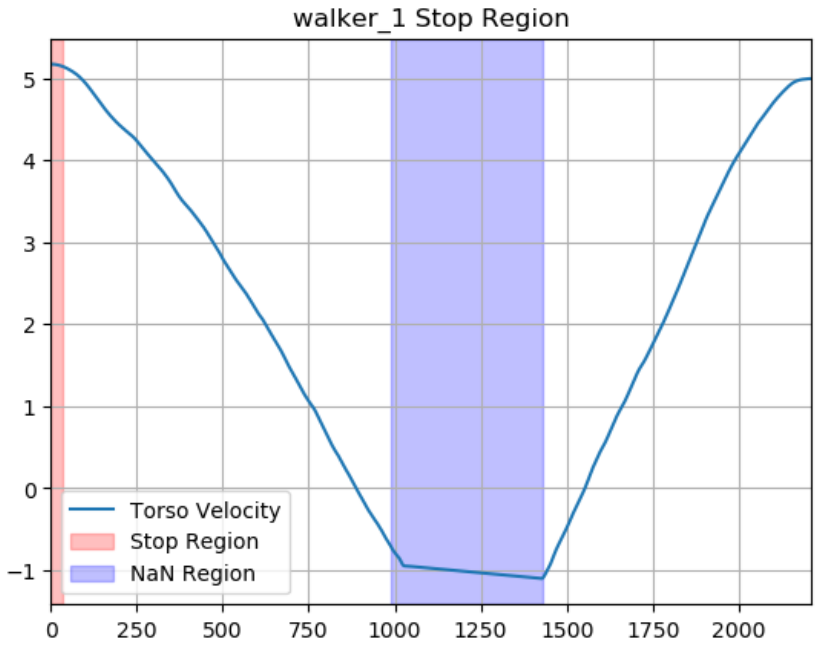

Figure 40 walker_1 Stop Region

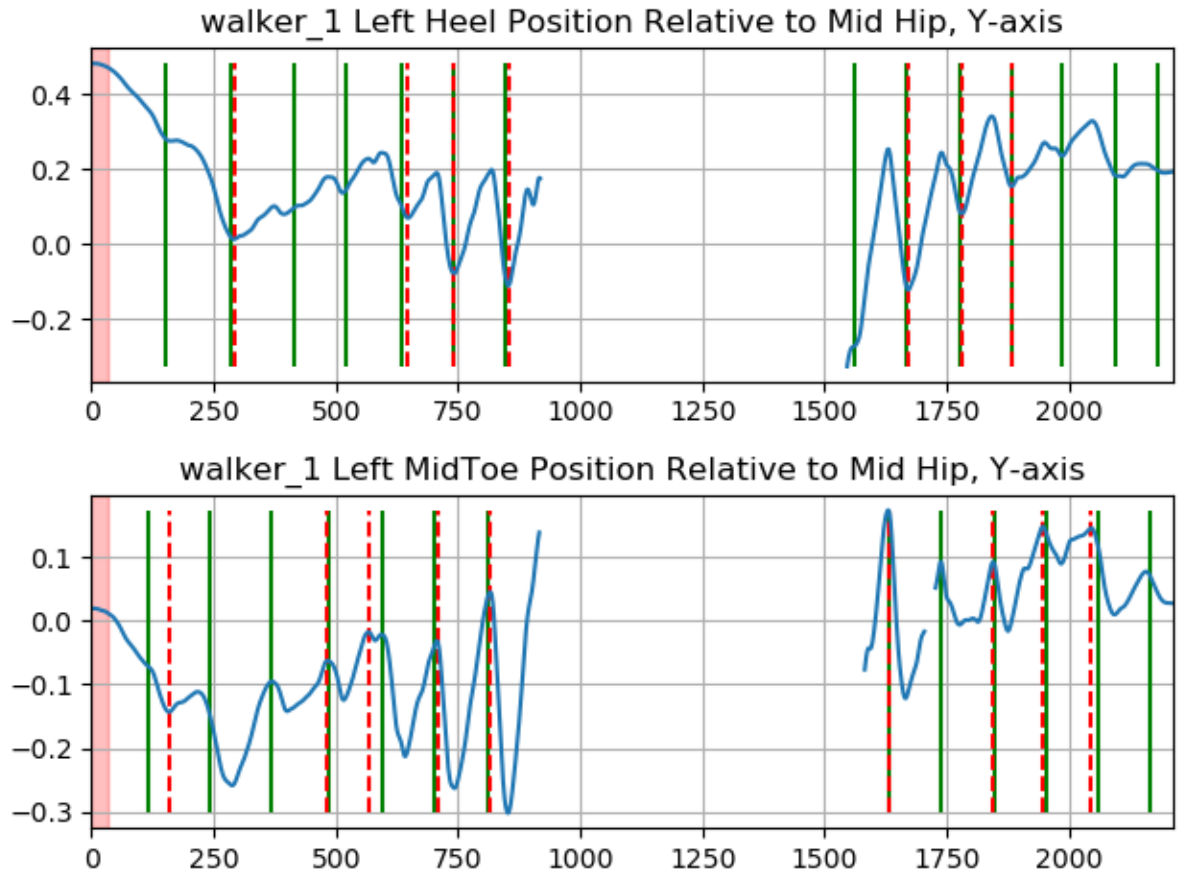

Figure 41 walker_1 Left Heel and Left MidToe Positions Relative to Mid Hip, Y-axis

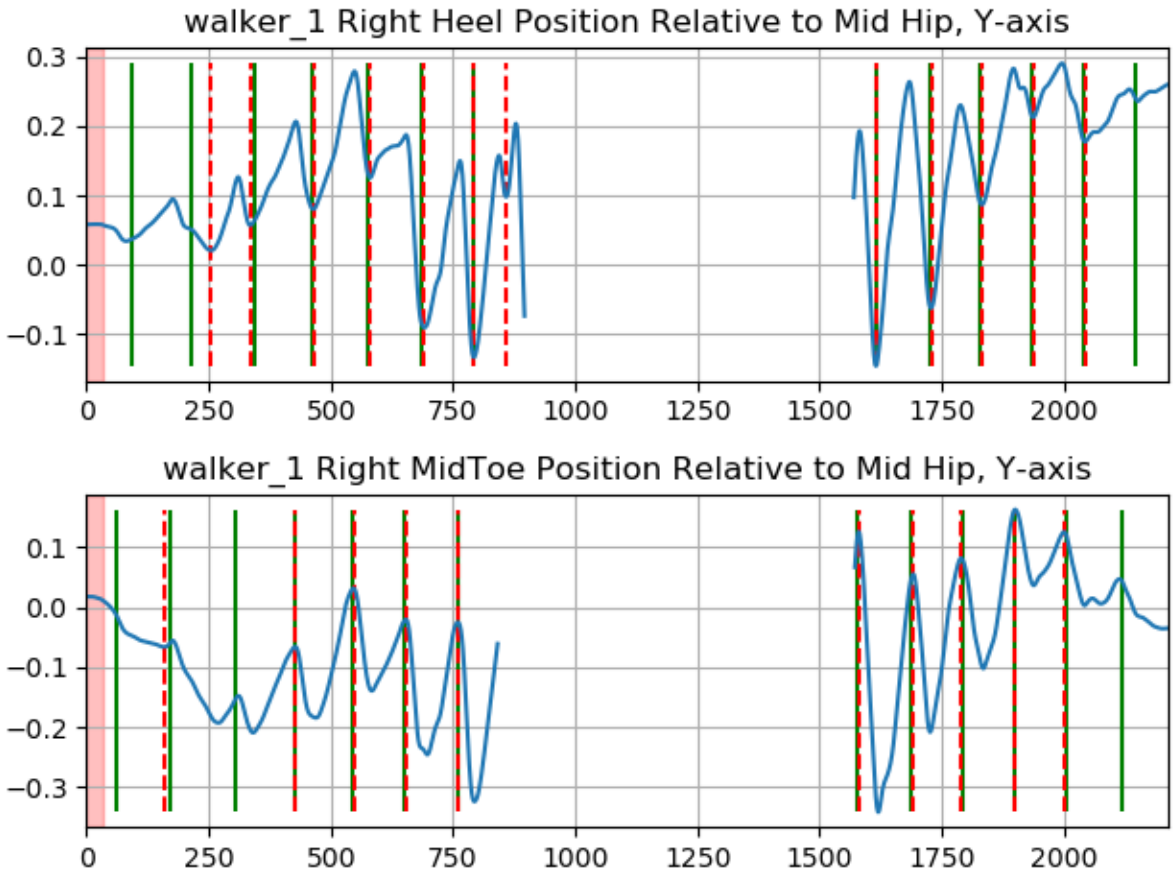

Figure 42 Right Heel and Right MidToe Positions Relative to Mid Hip, Y-axis

Table 13 Walker 1

Walker 1											
L Strike	L Strike - GT	Delta	**L Off**	L Off - GT	Delta	**R Strike**	R Strike - GT	Delta	**R Off**	R Off - GT	Delta
Missed	152	-	158	116	42	Missed	92	-	Missed	60	-
291	283	8	Missed	243	-	255	216	39	158	171	13
Missed	414	-	Missed	368	-	335	342	7	Missed	306	-
Missed	519	-	483	486	3	464	460	4	427	426	1
647	635	12	567	596	29	580	577	3	546	544	2
742	739	3	707	701	6	691	686	5	653	651	2
853	845	8	816	811	5	792	792	0	760	759	1
Missed	1562	-	1630	1631	1	858	FP	-	1580	1576	4
1671	1667	4	Missed	1739	-	1615	1616	1	1692	1688	4
1780	1778	2	1845	1849	4	1728	1725	3	1790	1793	3
1883	1884	1	1947	1954	7	1832	1829	3	1900	1899	1
Missed	1984	-	2046	2061	15	1937	1935	2	2000	2006	6
Missed	2096	-	Missed	2166	-	2043	2041	2	Missed	2117	-
Missed	2183	-				Missed	2145	-			
Average		**5**	**Average**		**12**	**Average**		**6**	**Average**		**4**
W Average	**7**										

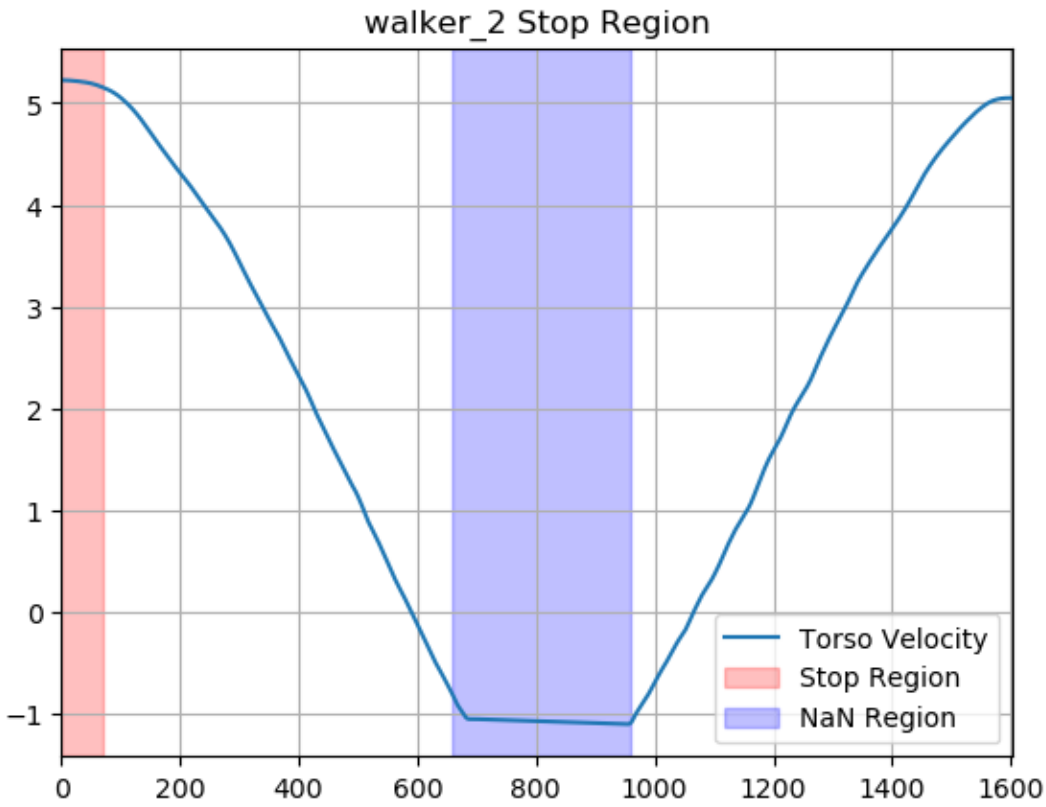

Figure 43 walker_2 Stop Region

Figure 44 walker_2 Left Heel and Left MidToe Positions Relative to Mid Hip, Y-axis

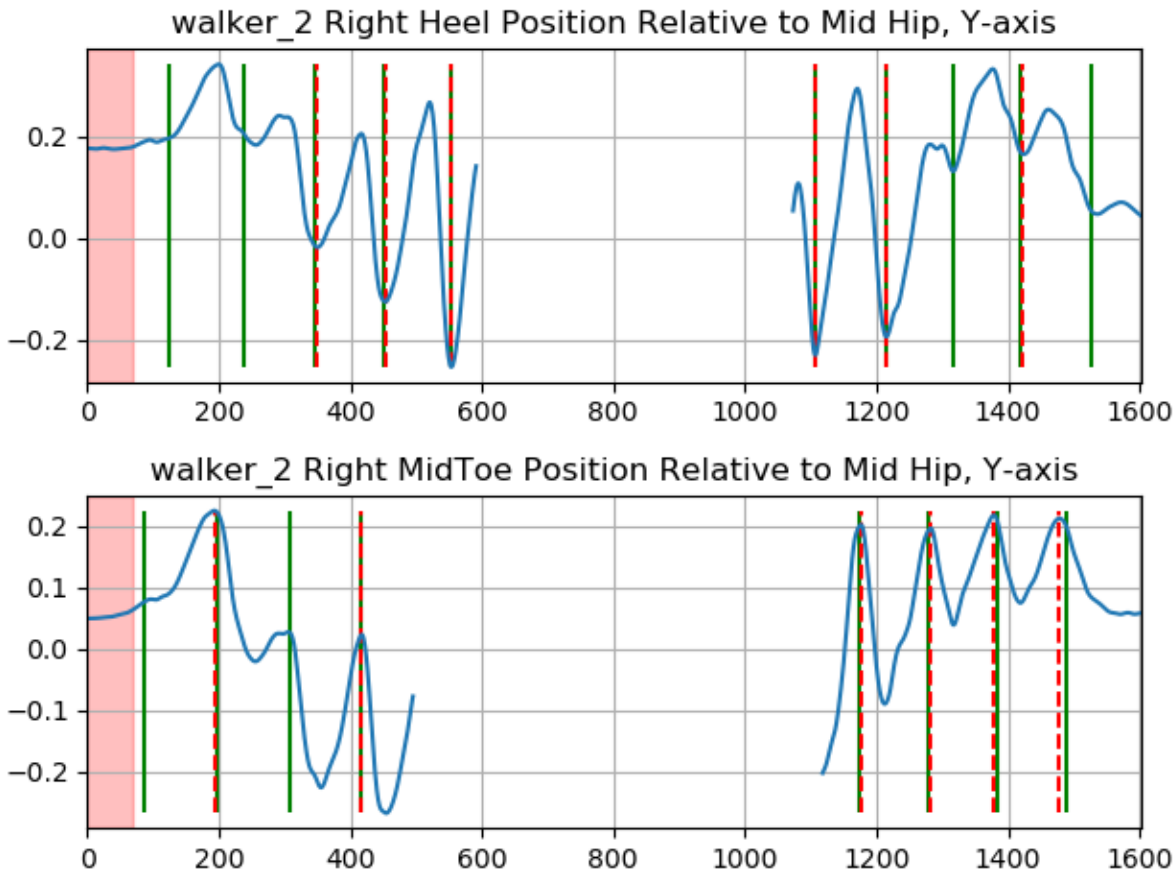

Figure 45 walker_2 Right Heel and Right MidToe Positions Relative to Mid Hip, Y-axis

Walker 2											
L Strike	L Strike - GT	Delta	**L Off**	L Off - GT	Delta	**R Strike**	R Strike - GT	Delta	**R Off**	R Off - GT	Delta
Missed	173	-	Missed	142	-	Missed	124	-	Missed	86	-
304	287	17	196	249	53	Missed	238	-	193	197	4
407	398	9	362	363	1	350	347	3	Missed	307	-
509	504	5	468	465	3	453	452	1	417	415	2
Missed	602	-	557	567	10	553	553	0	Missed	517	-
OOF	-1	-	OOF	-1	-	OOF	-1	-	Missed	614	-
Missed	1049	-	Missed	1121	-	1107	1108	1	Missed	1067	-
1156	1161	5	1225	1226	1	1215	1215	0	1176	1174	2
1269	1267	2	1328	1330	2	Missed	1316	-	1282	1280	2
1367	1367	0	1429	1437	8	1423	1418	5	1379	1384	5
Average		**6**	**Average**		**11**	**Average**		**2**	**Average**		**3**
W Average	**6**										

Figure 46 Walker 2

4.2 Spatial Parameters

To extract spatial parameters, we first used the techniques described in chapter 3 for key-points detections and 2D to 3D transformation to develop the set of points that defined the endpoints of the following limbs (Both left and right): Arms, Forearms, Thighs, Shanks, Ankles to Heels, Ankle to Big Toe, Ankle To Small Toe Length, Ankle to Heel Length, Shoulders Width, Hip Width, and Chest Height. Then, we extract each limb's lengths, an imaginary line between two ends of a limb is considered, and the mean value of the imaginary line through the trial is reported. This allowed us to do standard geometry calculations for the spatial parameters.

4.2.1 Walking with a cane

The table represents four statistical parameters mean, standard deviation, difference between the mean and ground truth (delta) and the difference in percentage of the targeted parameters. As it can be seen the error is around 5% and <2 CM which is in totally in line with our targeted criteria. The highest error rates are related to the points which either has more movement in 3-D or are challenging to be detected by the Deep-Learning technique (e.g. an ankle when the subject is moving toward the cameras).

Table 14 Trial: Cane 1

units: meters			**Trial: Cane 1**	
segment	**mean**	**std**	**delta**	**Percentage**
Left Arm	0.325	0.1	0.05	15%
Left Forearm	0.269	0	0	0%
Right Arm	0.315	0.1	0.04	13%
Right Forearm	0.284	0	0.014	5%
Left Thigh	0.439	0.1	0	0%
Left Shank	0.429	0.1	0.014	3%
Right Thigh	0.43	0.1	-0.02	-3%
Right Shank	0.399	0.1	-0.02	-4%
Left Ankle to Heel	0.079	0.1	0	-1%
Left Ankle to Big Toe	0.153	0.1	-0.04	-27%
Left Ankle To Small Toe	0.172	0.1	0.007	4%
Right Ankle to Heel Length	0.182	0.2	0.102	56%
Right Ankle to Big Toe Length	0.199	0.1	0	-1%
Right Ankle to Small Toe Length	0.151	0.1	-0.01	-9%
Shoulder Width	0.367	0.1	0.027	7%
Hip Width	0.248	0.1	0.038	15%
Chest Height	0.533	0	-0.03	-5%
Average	**0.275**	**0.1**	**0.013**	**5%**

Table 15 Trial: Cane 2

units: meters			**Trial: Cane 2**	
segment	**mean**	**std**	**delta**	**Percentage**
Left Arm	0.323	0.068	0.048	14.86
Left Forearm	0.277	0.028	0.007	2.53
Right Arm	0.301	0.036	0.026	8.64
Right Forearm	0.288	0.056	0.018	6.25
Left Thigh	0.422	0.054	-0.018	-4.27
Left Shank	0.429	0.053	0.014	3.26
Right Thigh	0.420	0.045	-0.025	-5.95
Right Shank	0.417	0.051	0.002	0.48
Left Ankle to Heel	0.084	0.029	0.004	4.76
Left Ankle to Big Toe	0.182	0.058	-0.013	-7.14
Left Ankle To Small Toe	0.218	0.121	0.053	24.31
Right Ankle to Heel Length	0.090	0.050	0.010	11.11
Right Ankle to Big Toe Length	0.227	0.093	0.027	11.89
Right Ankle to Small Toe Length	0.152	0.046	-0.013	-8.55
Shoulder Width	0.420	0.219	0.080	19.05
Hip Width	0.266	0.157	0.056	21.05
Chest Height	0.530	0.023	-0.030	-5.66
Average	**0.277**	**0.070**	**0.016**	**5.78**

4.2.2 Walking in a straight path result (Turn out of Frame)

Similar to the earlier trials, the table represents four statistical parameters mean, standard deviation, difference between the mean and ground truth (delta) and the difference in percentage of the targeted parameters. As it can be seen the error is < 5% and <1 CM with a consistent standard deviation which is in totally in line with our targeted criteria. The highest error rates are related to the points which either has more movement in 3-D or are challenging to be detected by the Deep-Learning technique. The difference from our ground truth values are smaller than the previous trial.

Table 16 Trial: Walking Straight 1

units: meters			**Trial: Walking Straight 1**	
segment	**Mean Length**	**STD**	**GT Difference**	**percentage**
Left Arm	0.286	0.02	0.011	4%
Left Forearm	0.265	0.03	-0.005	-2%
Right Arm	0.306	0.02	0.031	10%
Right Forearm	0.26	0.03	-0.01	-4%
Left Thigh	0.415	0.03	-0.025	-6%
Left Shank	0.417	0.05	0.002	0%
Right Thigh	0.4	0.04	-0.045	-11%
Right Shank	0.408	0.05	-0.007	-2%
Left Ankle to Heel	0.083	0.03	0.003	4%
Left Ankle to Big Toe	0.199	0.11	0.004	2%
Left Ankle To Small Toe	0.203	0.14	0.038	19%
Right Ankle to Heel Length	0.075	0.03	-0.005	-7%
Right Ankle to Big Toe Length	0.141	0.03	-0.059	-42%
Right Ankle to Small Toe Length	0.146	0.04	-0.019	-13%
Shoulder Width	0.331	0.02	-0.009	-3%
Hip Width	0.208	0.02	-0.002	-1%
Chest Height	0.519	0.02	-0.041	-8%
Average	**0.274**	**0.041**	**-0.008**	**-3%**

Table 17 Trial: Walking Straight 2

units: meters			**Trial: Walking Straight 2**	
segment	**mean**	**std**	**delta**	**percentage**
Left Arm	0.302	0.03	0.027	9%
Left Forearm	0.268	0.04	-0.002	-1%
Right Arm	0.294	0.03	0.019	6%
Right Forearm	0.259	0.03	-0.011	-4%
Left Thigh	0.419	0.03	-0.021	-5%
Left Shank	0.394	0.06	-0.021	-5%
Right Thigh	0.425	0.04	-0.02	-5%
Right Shank	0.388	0.06	-0.027	-7%
Left Ankle to Heel	0.06	0.03	-0.02	-33%
Left Ankle to Big Toe	0.16	0.06	-0.035	-22%
Left Ankle To Small Toe	0.135	0.06	-0.03	-22%
Right Ankle to Heel Length	0.09	0.04	0.01	11%
Right Ankle to Big Toe Length	0.181	0.06	-0.019	-10%
Right Ankle to Small Toe Length	0.135	0.04	-0.03	-22%
Shoulder Width	0.33	0.01	-0.01	-3%
Hip Width	0.216	0.04	0.006	3%
Chest Height	0.523	0.02	-0.037	-7%
Average	**0.249**	**0.04**	**-0.012**	**-5%**

4.2.3 Walking in a straight path result (Turn in Frame)

Similar to the earlier trials, the table represents four statistical parameters mean, standard deviation, difference between the mean and ground truth (delta) and the difference in percentage of the targeted parameters. As it can be seen the error is < 5% and <1 CM with a consistent standard deviation which is in totally in line with our targeted criteria. The highest error rates are related to the points which either has more movement in 3-D or are challenging to be detected by the Deep-Learning technique. The difference from our ground truth values is smaller than the previous trial.

Table 18 Trial: Turn in Frame 1

units: meters			**Trial: Turn in Frame 1**	
segment	**mean**	**std**	**delta**	**percentage**
Left Arm	0.312	0.02	0.037	12%
Left Forearm	0.256	0.03	-0.014	-5%
Right Arm	0.297	0.01	0.022	7%
Right Forearm	0.247	0.04	-0.023	-9%
Left Thigh	0.407	0.04	-0.033	-8%
Left Shank	0.393	0.05	-0.022	-6%
Right Thigh	0.426	0.07	-0.019	-4%
Right Shank	0.412	0.05	-0.003	-1%
Left Ankle to Heel	0.106	0.05	0.026	25%
Left Ankle to Big Toe	0.152	0.04	-0.043	-28%
Left Ankle To Small Toe	0.246	0.15	0.081	33%
Right Ankle to Heel Length	0.091	0.05	0.011	12%
Right Ankle to Big Toe Length	0.222	0.07	0.022	10%
Right Ankle to Small Toe Length	0.269	0.09	0.104	39%
Shoulder Width	0.331	0.02	-0.009	-3%
Hip Width	0.208	0.02	-0.002	-1%
Chest Height	0.526	0.02	-0.034	-6%
Average	**0.277**	**0.06**	**0.015**	**5%**

Table 19 Trial: Turn in Frame 2

units: meters			**Trial: Turn in Frame 3**	
segment	**mean**	**std**	**delta**	**percentage**
Left Arm	0.287	0.03	0.012	4%
Left Forearm	0.255	0.03	-0.015	-6%
Right Arm	0.302	0.05	0.027	9%
Right Forearm	0.253	0.03	-0.017	-7%
Left Thigh	0.425	0.07	-0.015	-4%
Left Shank	0.434	0.05	0.019	4%
Right Thigh	0.416	0.04	-0.029	-7%
Right Shank	0.411	0.06	-0.004	-1%
Left Ankle to Heel	0.145	0.12	0.065	45%
Left Ankle to Big Toe	0.243	0.08	0.048	20%
Left Ankle To Small Toe	0.325	0.26	0.16	49%
Right Ankle to Heel Length	0.068	0.02	-0.012	-18%
Right Ankle to Big Toe Length	0.168	0.06	-0.032	-19%
Right Ankle to Small Toe Length	0.134	0.03	-0.031	-23%
Shoulder Width	0.334	0.02	-0.006	-2%
Hip Width	0.239	0.04	0.029	12%
Chest Height	0.521	0.02	-0.039	-7%
Average	**0.276**	**0.06**	**0.014**	**5%**

4.2.4 Circular (Curve) walking

Similar to the previous trials the table represents four statistical parameters mean, standard deviation, difference between the mean and ground truth(delta) and the difference in percentage of the targeted parameters. As it can be seen the error rate is higher than the other trials, and in some manners unpredictable. This result is mainly due so the movement type of the subject which in some frames becomes parallel to the two cameras. As a result only the side view of the subject is visible and the deep-learning algorithm tries to have a rough estimation of the point's location in space.

Table 20 Trial: Curve Walk 1

units: meters			**Trial: Curve Walk 1**	
segment	**mean**	**std**	**delta**	**percentage**
Left Arm	0.296	0.02	0.021	7%
Left Forearm	0.432	0.42	0.162	38%
Right Arm	0.291	0.02	0.016	5%
Right Forearm	0.251	0.01	-0.019	-8%
Left Thigh	0.395	0.02	-0.045	-11%
Left Shank	0.431	0.03	0.016	4%
Right Thigh	0.396	0.02	-0.049	-12%
Right Shank	0.46	0.09	0.045	10%
Left Ankle to Heel	0.067	0.03	-0.013	-19%
Left Ankle to Big Toe	0.287	0.15	0.092	32%
Left Ankle To Small Toe	0.18	0.04	0.015	8%
Right Ankle to Heel Length	0.092	0.03	0.012	13%
Right Ankle to Big Toe Length	0.251	0.12	0.051	20%
Right Ankle to Small Toe Length	0.195	0.05	0.03	15%
Shoulder Width	0.33	0.05	-0.01	-3%
Hip Width	0.215	0.06	0.005	2%
Chest Height	0.543	0.02	-0.017	-3%
Average	**0.282**	**0.07**	**0.02**	**7%**

Table 21 Trial: Curve Walk 3

units: meters			**Trial: Curve Walk 3**	
segment	**mean**	**std**	**delta**	**percentage**
Left Arm	0.303	0.038	0.028	9%
Left Forearm	0.264	0.021	-0.006	-2%
Right Arm	0.296	0.039	0.021	7%
Right Forearm	0.26	0.024	-0.01	-4%
Left Thigh	0.405	0.019	-0.035	-9%
Left Shank	0.4	0.046	-0.015	-4%
Right Thigh	0.396	0.023	-0.049	-12%
Right Shank	0.438	0.048	0.023	5%
Left Ankle to Heel	0.111	0.051	0.031	28%
Left Ankle to Big Toe	0.186	0.042	-0.009	-5%
Left Ankle To Small Toe	0.181	0.051	0.016	9%
Right Ankle to Heel Length	0.154	0.109	0.074	48%
Right Ankle to Big Toe Length	0.343	0.431	0.143	42%
Right Ankle to Small Toe Length	2.109	4.621	1.944	92%
Shoulder Width	0.334	0.055	-0.006	-2%
Hip Width	0.218	0.065	0.008	4%
Chest Height	0.532	0.019	-0.028	-5%
Average	**0.484**	**0.531**	**0.222**	**46%**

4.2.5 Walking with a walker

Similar to the earlier trial, the table represents four statistical parameters mean, standard deviation, difference between the mean and ground truth (delta) and the difference in percentage. Surprisingly, this trial have the best results in term of spatial parameters among the other tests. As it can be seen the error is < 2% and <0.5 CM which is in totally in line with our targeted criteria. A reason for the enhanced result is slower pace of the subject while walking throughout the pathway. The highest error rates are related to the points which either has more movement in 3-D or are challenging to be detected by the Deep-Learning technique. The difference from our ground truth values are smaller than the previous trial.

Table 22 Trial: Walker 1

units: meters			**Trial: Walker 1**	
segment	**mean**	**std**	**delta**	**percentage**
Left Arm	0.3	0	0.025	8%
Left Forearm	0.286	0	0.016	6%
Right Arm	0.298	0	0.023	8%
Right Forearm	0.298	0.1	0.028	9%
Left Thigh	0.397	0	-0.04	-10%
Left Shank	0.442	0	0.027	6%
Right Thigh	0.395	0	-0.05	-13%
Right Shank	0.4	0.1	-0.02	-5%
Left Ankle to Heel	0.078	0	0	0%
Left Ankle to Big Toe	0.181	0.1	-0.01	-6%
Left Ankle To Small Toe	0.195	0.1	0.03	15%
Right Ankle to Heel Length	0.087	0	0.007	8%
Right Ankle to Big Toe Length	0.208	0.1	0.008	4%
Right Ankle to Small Toe Length	0.206	0.1	0.041	20%
Shoulder Width	0.334	0	-0.01	-3%
Hip Width	0.211	0	0.001	0%
Chest Height	0.558	0	0	0%
Average	**0.265**	**0**	**0.003**	**1%**

Table 23 Trial: Walker 2

units: meters			**Trial: Walker 2**	
segment	**mean**	**std**	**delta**	**percentage**
Left Arm	0.338	0.07	0.063	19%
Left Forearm	0.284	0.06	0.014	5%
Right Arm	0.308	0.03	0.033	11%
Right Forearm	0.306	0.08	0.036	12%
Left Thigh	0.409	0.03	-0.03	-8%
Left Shank	0.41	0.03	-0.01	-1%
Right Thigh	0.413	0.04	-0.03	-8%
Right Shank	0.417	0.04	0.002	0%
Left Ankle to Heel	0.079	0.04	-0	-1%
Left Ankle to Big Toe	0.185	0.07	-0.01	-5%
Left Ankle To Small Toe	0.187	0.06	0.022	12%
Right Ankle to Heel Length	0.081	0.04	0.001	1%
Right Ankle to Big Toe Length	0.179	0.08	-0.02	-12%
Right Ankle to Small Toe Length	0.211	0.09	0.046	22%
Shoulder Width	0.33	0.01	-0.01	-3%
Hip Width	0.221	0.02	0.011	5%
Chest Height	0.545	0.03	-0.02	-3%
Average	**0.267**	**0.05**	**0.005**	2%

4.3 Spatial-temporal Parameters

In this section, we have organized tables differently, since for the below parameters our main target is to evaluate consistency of the outcome to see what a parameter looks like across all five trials. For these parameters we are simply measuring how consistent the result is in our simulated hallway.

4.3.1 Stride Length

In this section, we are not comparing the accuracy of our stride length with the stride length of the ground truth. We are simply measuring how much variation there is. There is no ground truth to compare, and therefore no measure of error. Through our trials, walking in a straight line with a turn in frame and walking with a cane had the highest stride lengths and walking with a walker had the lowest length. The calculation is based on the stride definition in chapter 3, which a stride is the distance of both the right and the left step.

Table 24 Stride Length in meter

Parameter	**Stride Length in meter**									
Trial	**Cane 1 Left**	**Cane 1 Right**	**Cane 2 Left**	**Cane 2 Right**	**Walker 1 Left**	**Walker 1 Right**	**Walker 2 Left**	**Walker 2 Right**	**Curve Walk 1 Left**	**Curve Walk 1 Right**
Values	1.557	1.819	1.660	1.645	0.830	0.493	1.241	0.852	1.506	1.159
	1.798	1.780	2.041	1.866	0.690	0.600	1.256	1.284	1.389	1.395
	1.762	1.624	1.621	1.611	0.664	0.653	1.401	1.349	1.193	1.085
	1.530	1.637	1.582	0.902	0.813	0.782	1.168	0.888	1.341	0.600
	1.405	0.912			0.935	0.958	1.089	1.045	1.243	1.205
					0.818	0.846	1.008	1.046	0.426	1.011
					0.965	0.809				0.514
					0.845	0.939				
					0.840	0.888				
					0.419	0.588				
Average	**1.611**	**1.554**	**1.726**	**1.506**	**0.782**	**0.756**	**1.194**	**1.077**	**1.183**	**0.996**
STD	**0.166**	**0.369**	**0.212**	**0.418**	**0.157**	**0.162**	**0.138**	**0.202**	**0.387**	**0.323**
Median	**1.557**	**1.637**	**1.641**	**1.628**	**0.824**	**0.795**	**1.205**	**1.045**	**1.292**	**1.085**
MaxValue	**1.798**	**1.819**	**2.041**	**1.866**	**0.965**	**0.958**	**1.401**	**1.349**	**1.506**	**1.395**
LowValue	**1.405**	**0.912**	**1.582**	**0.902**	**0.419**	**0.493**	**1.008**	**0.852**	**0.426**	**0.514**

Table 25 Stride Length in meter

Parameter	Stride Length in meter									
Trial	Curve Walk 3 Left	Curve Walk 3 Right	Walking Straight 1 Left	Walking Straight 1 Right	Walking Straight 2 Left	Walking Straight 2 Right	Turn in Frame 1 Left	Turn in Frame 1 Right	Turn in Frame 3 Left	Turn in Frame 3 Right
Values	1.603	1.143	1.351	1.390	1.291	1.103	1.485	1.316	1.458	1.171
	1.433	1.501	1.623	1.561	1.466	1.419	1.729	1.694	1.700	1.633
	1.258	0.885	1.345	1.633	1.705	1.622	0.452	1.533	0.767	1.335
	1.387	0.544	1.426	1.155	1.286	1.386	1.022	0.723	1.207	1.493
	1.131	1.411	1.096	1.528	1.321	1.366	1.509	1.485	1.446	1.431
		1.070		1.210	1.253	0.970	1.214	1.417	1.374	0.845
Average	**1.363**	**1.093**	**1.368**	**1.413**	**1.387**	**1.311**	**1.235**	**1.361**	**1.325**	**1.318**
STD	**0.179**	**0.351**	**0.189**	**0.196**	**0.173**	**0.235**	**0.456**	**0.337**	**0.316**	**0.279**
Median	**1.387**	**1.107**	**1.351**	**1.459**	**1.306**	**1.376**	**1.349**	**1.451**	**1.410**	**1.383**
Highest Value	**1.603**	**1.501**	**1.623**	**1.633**	**1.705**	**1.622**	**1.729**	**1.694**	**1.700**	**1.633**
Lowest Value	**1.131**	**0.544**	**1.096**	**1.155**	**1.253**	**0.970**	**0.452**	**0.723**	**0.767**	**0.845**

4.3.2 Stride times

Similar to the previous results, in this section, we are not comparing the accuracy of our stride time with the stride time of the ground truth. We are simply measuring how much variation there is. There is no ground truth to compare, and therefore no measure of error. Through our trials, walking in a straight and walking with a cane had the smallest stride time and walking with a walker had the highest values. Based on the definition provided in chapter 3, the time difference between start of the right step and the end of left step was calculated.

Table 26 Stride Times in Seconds

Parameter	Stride Times in Seconds									
Trial	Cane 1 Left	Cane 1 Right	Cane 2 Left	Cane 2 Right	Walker 1 Left	Walker 1 Right	Walker 2 Left	Walker 2 Right	Curve Walk 1 Left	Curve Walk 1 Right
Values	1.85	1.75	1.55	1.55	2.18	2.07	1.90	1.90	1.12	1.15
	1.70	1.73	1.62	1.60	2.18	2.10	1.85	1.82	1.03	1.02
	1.70	1.57	1.57	1.55	1.75	1.97	1.77	1.75	1.00	1.07
	1.57	1.53	1.47	1.28	1.93	1.95	1.77	1.68	1.08	1.08
	1.43	1.25			1.73	1.82	1.67	1.70	1.15	1.00
					1.77	1.77	1.73	1.83	0.92	1.10
					1.77	1.73				1.35
					1.67	1.77				
					1.87	1.77				
					1.45	1.73				
Average	**1.65**	**1.57**	**1.55**	**1.50**	**1.83**	**1.87**	**1.78**	**1.78**	**1.05**	**1.11**
STD	**0.16**	**0.20**	**0.06**	**0.14**	**0.23**	**0.14**	**0.08**	**0.08**	**0.08**	**0.12**
Median	**1.70**	**1.57**	**1.56**	**1.55**	**1.77**	**1.79**	**1.77**	**1.78**	**1.06**	**1.08**
High	**1.85**	**1.75**	**1.62**	**1.60**	**2.18**	**2.10**	**1.90**	**1.90**	**1.15**	**1.35**
Low	**1.43**	**1.25**	**1.47**	**1.28**	**1.45**	**1.73**	**1.67**	**1.68**	**0.92**	**1.00**

Table 27 Stride Times in Seconds

Parameter	Stride Times in Seconds									
Trial	Curve Walk 3 Left	Curve Walk 3 Right	Walking Straight 1 Left	Walking Straight 1 Right	Walking Straight 2 Left	Walking Straight 2 Right	Turn in Frame 1 Left	Turn in Frame 1 Right	Turn in Frame 3 Left	Turn in Frame 3 Right
Values	1.07	1.08	1.23	2.18	1.25	1.28	1.05	1.08	1.13	1.18
	1.08	1.07	1.20	1.22	1.17	1.20	1.05	1.05	1.05	1.12
	1.10	1.07	1.15	1.18	1.17	1.17	1.15	1.00	1.23	0.90
	1.05	1.10	1.15	1.15	1.13	1.10	1.03	1.18	1.00	1.02
	1.00	1.08	1.18	1.22	1.08	1.12	1.08	1.08	0.97	1.03
		1.00		1.12	1.17	1.17	1.03	1.08	1.12	0.93
Average	**1.06**	**1.07**	**1.18**	**1.34**	**1.16**	**1.17**	**1.07**	**1.08**	**1.08**	**1.03**
STD	**0.04**	**0.03**	**0.04**	**0.41**	**0.05**	**0.07**	**0.04**	**0.06**	**0.10**	**0.11**
Median	**1.07**	**1.08**	**1.18**	**1.20**	**1.17**	**1.17**	**1.05**	**1.08**	**1.08**	**1.03**
High	**1.10**	**1.10**	**1.23**	**2.18**	**1.25**	**1.28**	**1.15**	**1.18**	**1.23**	**1.18**
Low	**1.00**	**1.00**	**1.15**	**1.12**	**1.08**	**1.10**	**1.03**	**1.00**	**0.97**	**0.90**

4.3.3 Stride Speeds

Again, in this section, we are not comparing the accuracy of our stride speed with the stride speed of the ground truth. We are simply measuring how much variation there is. there is no ground truth to compare, and therefore no measure of error. Through our trials, walking in a straight line with a turn in frame and curve walk had the highest stride speeds and walking with a walker had the lowest value. Similar to the previous two results, the calculation was based on the definition provided in chapter 3. After getting the distance and time, we calculated the stride speed.

Table 28 Stride Speeds in Meter

Parameter	**Stride Speeds in Meter/ Second**									
Trial	**Cane 1 Left**	**Cane 1 Right**	**Cane 2 Left**	**Cane 2 Right**	**Walker 1 Left**	**Walker 1 Right**	**Walker 2 Left**	**Walker 2 Right**	**Curve Walk 1 Left**	**Curve Walk 1 Right**
Values	0.841	0.842	1.071	1.003	0.380	0.318	0.653	0.494	1.349	1.094
	1.058	0.945	1.262	1.085	0.316	0.379	0.679	0.666	1.344	1.407
	1.037	1.080	1.035	1.213	0.380	0.309	0.793	0.679	1.193	1.210
	0.977	1.205	1.079	0.999	0.421	0.387	0.661	0.761	1.238	1.246
	0.980	1.022			0.540	0.442	0.653	0.645	1.081	1.459
					0.463	0.467	0.582	0.548	0.465	1.103
					0.546	0.477				0.988
					0.507	0.647				
					0.450	0.433				
					0.289	0.443				
Average	**0.979**	**1.019**	**1.112**	**1.075**	**0.429**	**0.430**	**0.670**	**0.632**	**1.112**	**1.215**
STD	**0.084**	**0.137**	**0.102**	**0.100**	**0.089**	**0.096**	**0.069**	**0.096**	**0.332**	**0.171**
Median	**0.980**	**1.022**	**1.075**	**1.044**	**0.435**	**0.438**	**0.657**	**0.655**	**1.215**	**1.210**
High	**1.058**	**1.205**	**1.262**	**1.213**	**0.546**	**0.647**	**0.793**	**0.761**	**1.349**	**1.459**
Low	**0.841**	**0.842**	**1.035**	**0.999**	**0.289**	**0.309**	**0.582**	**0.494**	**0.465**	**0.988**

Table 29 Stride Speeds in Meter

Parameter	Stride Speeds in Meter									
Trial	Curve Walk 3 Left	Curve Walk 3 Right	Walking Straight 1 Left	Walking Straight 1 Right	Walking Straight 2 Left	Walking Straight 2 Right	Turn in Frame 1 Left	Turn in Frame 1 Right	Turn in Frame 3 Left	Turn in Frame 3 Right
Values	1.503	1.238	1.096	0.656	1.033	0.801	1.414	1.035	1.286	1.005
	1.323	1.422	1.352	1.231	1.257	1.080	1.646	1.393	1.619	1.273
	1.144	1.326	1.169	1.209	1.461	1.261	0.393	1.479	0.622	1.645
	1.321	1.237	1.240	1.187	1.135	1.256	0.989	0.191	1.207	1.587
	1.131	1.442	0.926	1.201	1.219	1.273	1.393	1.564	1.496	1.472
		1.267		1.287	1.074	0.861	1.174	1.431	1.230	1.056
Average	**1.284**	**1.322**	**1.157**	**1.129**	**1.196**	**1.089**	**1.168**	**1.182**	**1.243**	**1.340**
STD	**0.153**	**0.091**	**0.160**	**0.234**	**0.155**	**0.213**	**0.441**	**0.518**	**0.345**	**0.272**
Median	**1.321**	**1.297**	**1.169**	**1.205**	**1.177**	**1.168**	**1.284**	**1.412**	**1.258**	**1.372**
High	**1.503**	**1.442**	**1.352**	**1.287**	**1.461**	**1.273**	**1.646**	**1.564**	**1.619**	**1.645**
Low	**1.131**	**1.237**	**0.926**	**0.656**	**1.033**	**0.801**	**0.393**	**0.191**	**0.622**	**1.005**

4.3.4 Step Length

As mentioned earlier, we are not comparing the accuracy of our stride speed with the stride length of the ground truth. We are simply measuring how much variation there is. There is no ground truth to compare, and therefore no measure of error. Through our trials, walking in a straight line with a turn in frame and walking with a cane had the highest step length and walking with a walker had the lowest value. The step length is based on the definition of a "step" provided in chapter 3, which is the distance from a subject picks up one foot (Toe Off) and put it back down on the ground (Heel Strike).

Table 30 Step Lengths in Meter

Parameter	Step Lengths in Meter									
Trial	Cane 1 Left	Cane 1 Right	Cane 2 Left	Cane 2 Right	Walker 1 Left	Walker 1 Right	Walker 2 Left	Walker 2 Right	Curve Walk 1 Left	Curve Walk 1 Right
Values	0.34	0.29	0.25	0.55	0.21	0.36	0.03	0.16	0.24	0.02
	0.64	0.64	0.22	0.64	0.04	0.20	0.26	0.08	0.44	0.15
	0.69	0.78	0.77	0.46	0.08	0.01	0.19	0.16	0.24	0.19
	0.77	0.54	0.72	0.59	0.06	0.06	0.33	0.32	0.05	0.09
	0.90	0.48	0.42	0.32	0.07	0.09	0.33	0.49	0.11	0.09
	0.43	0.27	0.16	0.06	0.14	0.25	0.15	0.10	0.11	0.47
	0.28	0.10			0.23	0.27	0.20	0.05	0.05	0.32
					0.12	0.23	0.09	0.09	0.13	0.13
					0.09	0.22				0.13
					0.04	0.02				
					0.04	0.15				
					0.05	0.03				
Average	**0.579**	**0.441**	**0.423**	**0.438**	**0.099**	**0.156**	**0.197**	**0.182**	**0.172**	**0.178**
STD	**0.231**	**0.237**	**0.263**	**0.218**	**0.066**	**0.115**	**0.106**	**0.151**	**0.133**	**0.138**
Median	**0.636**	**0.476**	**0.333**	**0.506**	**0.077**	**0.173**	**0.195**	**0.129**	**0.119**	**0.134**
High	**0.901**	**0.781**	**0.767**	**0.644**	**0.234**	**0.359**	**0.328**	**0.492**	**0.443**	**0.473**
Low	**0.282**	**0.096**	**0.164**	**0.057**	**0.036**	**0.006**	**0.033**	**0.051**	**0.048**	**0.019**

Table 31 Step Lengths in Meter

Parameter	Step Lengths in Meter									
Trial	Curve Walk 3 Left	Curve Walk 3 Right	Walking Straight 1 Left	Walking Straight 1 Right	Walking Straight 2 Left	Walking Straight 2 Right	Turn in Frame 1 Left	Turn in Frame 1 Right	Turn in Frame 3 Left	Turn in Frame 3 Right
Values	0.07	0.27	0.06	0.20	0.09	0.00	0.18	0.02	0.11	0.25
	0.35	0.28	0.15	0.17	0.07	0.07	0.20	0.17	0.07	0.23
	0.30	0.30	0.25	0.23	0.17	0.20	0.33	0.41	0.27	0.44
	0.18	0.14	0.32	0.44	0.48	0.36	0.48	0.46	0.17	0.30
	0.24	0.14	0.21	0.32	0.38	0.19	0.26	0.49	0.17	0.36
	0.16	0.23	0.15	0.12	0.16	0.19	0.09	0.28	0.31	0.24
	0.06	0.14	0.14	0.18	0.12	0.14	0.02	0.15	0.05	0.15
		0.01		0.04	0.00	0.10			0.02	0.02
Average	**0.194**	**0.188**	**0.181**	**0.212**	**0.185**	**0.156**	**0.221**	**0.284**	**0.146**	**0.250**
STD	**0.110**	**0.097**	**0.086**	**0.123**	**0.163**	**0.106**	**0.152**	**0.176**	**0.104**	**0.130**
Median	**0.178**	**0.186**	**0.150**	**0.193**	**0.142**	**0.161**	**0.196**	**0.282**	**0.140**	**0.246**
High	**0.353**	**0.295**	**0.318**	**0.437**	**0.484**	**0.356**	**0.476**	**0.488**	**0.313**	**0.445**
Low	**0.057**	**0.012**	**0.055**	**0.038**	**0.002**	**0.003**	**0.020**	**0.023**	**0.020**	**0.015**

4.3.5 Step Width

As mentioned earlier, we are not comparing the accuracy of our step width with the step width of the ground truth. We are simply measuring how much variation there is. There is no ground truth to compare, and therefore no measure of error. Through our trials, curve walk had the highest step width and walking with a walker had the lowest value. The step length is based on the definition of a "step" provided in chapter 3, which is the distance from a subject picks up one foot (Toe Off) and put it back down on the ground (Heel Strike). Width of a step is considered to be horizontal change in position of the feet, before and after the step is taken.

Table 32 Step Widths in Meter

Parameter	**Step Widths in Meter**									
Trial	**Cane 1 Left**	**Cane 1 Right**	**Cane 2 Left**	**Cane 2 Right**	**Walker 1 Left**	**Walker 1 Right**	**Walker 2 Left**	**Walker 2 Right**	**Curve Walk 1 Left**	**Curve Walk 1 Right**
Values	0.09	0.09	0.04	0.07	0.03	0.11	0.06	0.11	0.36	0.20
	0.07	0.07	0.05	0.11	0.04	0.11	0.03	0.12	0.18	0.28
	0.05	0.00	0.01	0.09	0.01	0.11	0.00	0.10	0.23	0.02
	0.05	0.12	0.04	0.06	0.05	0.13	0.03	0.11	0.53	0.49
	0.06	0.07	0.02	0.09	0.00	0.12	0.02	0.08	0.12	0.49
	0.10	0.08	0.14	0.13	0.04	0.12	0.08	0.11	0.11	0.17
	0.13	0.14			0.06	0.08	0.05	0.11	0.32	0.08
					0.11	0.18	0.11	0.14	0.08	0.46
					0.04	0.14				0.07
					0.11	0.11				
					0.09	0.16				
					0.13	0.11				
Avarage	**0.080**	**0.082**	**0.050**	**0.092**	**0.061**	**0.124**	**0.047**	**0.110**	**0.241**	**0.249**
STD	**0.030**	**0.044**	**0.045**	**0.026**	**0.042**	**0.026**	**0.034**	**0.016**	**0.152**	**0.187**
Median	**0.067**	**0.082**	**0.037**	**0.091**	**0.047**	**0.116**	**0.042**	**0.110**	**0.204**	**0.197**
High	**0.132**	**0.140**	**0.139**	**0.129**	**0.132**	**0.185**	**0.109**	**0.139**	**0.528**	**0.487**
Low	**0.053**	**0.002**	**0.013**	**0.057**	**0.004**	**0.085**	**0.001**	**0.084**	**0.080**	**0.016**

Table 33 Step Widths in Meter

Parameter	Step Widths in Meter									
Trial	Curve Walk 3 Left	Curve Walk 3 Right	Walking Straight 1 Left	Walking Straight 1 Right	Walking Straight 2 Left	Walking Straight 2 Right	Turn in Frame 1 Left	Turn in Frame 1 Right	Turn in Frame 3 Left	Turn in Frame 3 Right
Values	0.31	0.28	0.00	1.55	0.10	0.13	0.08	0.13	0.06	0.13
	0.13	0.21	0.03	0.60	0.17	0.12	0.07	0.16	0.04	0.07
	0.19	0.04	0.01	0.58	0.13	0.03	0.09	0.14	0.06	0.16
	0.46	0.50	0.09	0.58	0.10	0.04	0.01	0.08	0.07	0.03
	0.09	0.50	0.09	0.58	0.18	0.08	0.08	0.20	0.07	0.18
	0.16	0.00	0.14	0.52	0.06	0.08	0.04	0.18	0.08	0.15
	0.15	0.16	0.10	0.58	0.02	0.08	0.13	0.10	0.11	0.10
		0.36			0.11	0.13			0.13	0.15
Avarage	**0.214**	**0.256**	**0.066**	**0.714**	**0.109**	**0.087**	**0.070**	**0.140**	**0.077**	**0.121**
STD	**0.128**	**0.189**	**0.052**	**0.369**	**0.052**	**0.039**	**0.037**	**0.042**	**0.028**	**0.050**
Median	**0.163**	**0.247**	**0.085**	**0.583**	**0.105**	**0.083**	**0.077**	**0.135**	**0.073**	**0.141**
High	**0.458**	**0.495**	**0.141**	**1.550**	**0.178**	**0.134**	**0.127**	**0.195**	**0.126**	**0.177**
Low	**0.091**	**0.000**	**0.005**	**0.517**	**0.025**	**0.034**	**0.010**	**0.078**	**0.036**	**0.029**

4.3.6 Step Time

As mentioned earlier, we are not comparing the accuracy of our step time with the step time of the ground truth. We are simply measuring how much variation there is. There is no ground truth to compare, and therefore no measure of error. Through our trials, walking with a cane had the highest step time and curve walk and turning in frame the lowest values. The step length is based on the definition of a "step" provided in chapter 3, which is the distance from a subject picks up one foot (Toe Off) and put it back down on the ground (Heel Strike). The duration taken from starting the action and ending is reported.

Table 34 Step Times in Seconds

Parameter	Step Times in Seconds									
Trial	Cane 1 Left	Cane 1 Right	Cane 2 Left	Cane 2 Right	Walker 1 Left	Walker 1 Right	Walker 2 Left	Walker 2 Right	Curve Walk 1 Left	Curve Walk 1 Right
Values	2.25	0.97	1.50	0.83	1.00	1.47	0.82	1.42	0.55	1.87
	0.88	0.87	0.72	0.83	1.12	1.07	0.82	1.08	0.52	0.60
	0.83	0.90	0.78	0.93	1.20	0.98	0.85	1.00	0.53	0.50
	0.80	0.93	0.78	0.82	0.98	0.77	0.87	0.90	0.53	0.53
	0.78	0.78	0.75	0.80	0.97	0.97	0.38	0.90	0.45	0.15
	0.78	0.75	0.67	0.62	0.88	0.85	0.87	0.82	0.53	0.55
	0.68	0.57			0.88	0.88	0.85	0.85	0.58	0.55
					0.88	0.48	0.88	0.95	0.15	0.57
					0.92	0.85				0.77
					0.82	0.85				
					0.92	0.95				
					0.63	0.82				
Average	**1.00**	**0.82**	**0.87**	**0.81**	**0.93**	**0.91**	**0.79**	**0.99**	**0.48**	**0.68**
STD	**0.55**	**0.14**	**0.31**	**0.10**	**0.14**	**0.23**	**0.17**	**0.19**	**0.14**	**0.47**
Median	**0.80**	**0.87**	**0.77**	**0.83**	**0.92**	**0.87**	**0.85**	**0.93**	**0.53**	**0.55**
High	**2.25**	**0.97**	**1.50**	**0.93**	**1.20**	**1.47**	**0.88**	**1.42**	**0.58**	**1.87**
Low	**0.68**	**0.57**	**0.67**	**0.62**	**0.63**	**0.48**	**0.38**	**0.82**	**0.15**	**0.15**

Table 35 Step Times in Seconds

Parameter	Step Times in Seconds									
Trial	Curve Walk 3 Left	Curve Walk 3 Right	Walking Straight 1 Left	Walking Straight 1 Right	Walking Straight 2 Left	Walking Straight 2 Right	Turn in Frame 1 Left	Turn in Frame 1 Right	Turn in Frame 3 Left	Turn in Frame 3 Right
Values	0.53	1.80	1.55	0.57	0.65	1.02	0.53	1.17	0.58	2.28
	0.52	0.55	0.60	0.63	0.62	0.63	0.50	0.55	0.53	0.60
	0.53	0.55	0.58	0.62	0.58	0.58	0.50	0.55	0.47	0.58
	0.55	0.53	0.58	0.60	0.58	0.58	0.65	0.50	0.80	0.43
	0.55	0.23	0.58	0.30	0.82	0.57	0.50	0.53	0.33	0.48
	0.52	0.55	0.52	0.57	0.57	0.53	0.50	0.58	0.52	0.50
	0.52	0.53	0.58	0.63	0.55	0.57	0.45	0.58	0.47	0.57
		0.48		0.60	0.60	0.57			0.55	0.38
Average	**0.53**	**0.65**	**0.71**	**0.56**	**0.62**	**0.63**	**0.52**	**0.64**	**0.53**	**0.73**
STD	**0.01**	**0.48**	**0.37**	**0.11**	**0.08**	**0.16**	**0.06**	**0.23**	**0.13**	**0.63**
Median	**0.53**	**0.54**	**0.58**	**0.60**	**0.59**	**0.58**	**0.50**	**0.55**	**0.53**	**0.53**
High	**0.55**	**1.80**	**1.55**	**0.63**	**0.82**	**1.02**	**0.65**	**1.17**	**0.80**	**2.28**
Low	**0.52**	**0.23**	**0.52**	**0.30**	**0.55**	**0.53**	**0.45**	**0.50**	**0.33**	**0.38**

4.3.7 Cadence

As mentioned earlier, we are not comparing the accuracy of the Cadence ratio the ground truth. We are simply measuring how much variation there is. There is no ground truth to compare, and therefore no measure of error. Through our trials, circular (curve) walking had the highest value and walking with a cane had the lowest value. Cadence value is calculated based on the definition provided in chapter 3, which is number steps or cycles per minute.

Table 36 Cadence

Parameter	Cadence									
Trial	Cane 1 Left	Cane 1 Right	Cane 2 Left	Cane 2 Right	Walker 1 Left	Walker 1 Right	Walker 2 Left	Walker 2 Right	Curve Walk 1 Left	Curve Walk 1 Right
Walking Toward	50.35	65.85	60.00	72.00	59.72	60.14	71.64	54.55	112.50	68.57
Walking Away	80.00	79.12	81.82	75.79	72.00	75.95	80.45	68.25	133.33	116.13
Average	**65.17**	**72.49**	**70.91**	**73.89**	**65.86**	**68.05**	**76.04**	**61.40**	**122.92**	**92.35**
STD	**20.97**	**9.38**	**15.43**	**2.68**	**8.69**	**11.18**	**6.23**	**9.69**	**14.73**	**33.63**
Median	**65.17**	**72.49**	**70.91**	**73.89**	**65.86**	**68.05**	**76.04**	**61.40**	**122.92**	**92.35**
High	**80.00**	**79.12**	**81.82**	**75.79**	**72.00**	**75.95**	**80.45**	**68.25**	**133.33**	**116.13**
Low	**50.35**	**65.85**	**60.00**	**72.00**	**59.72**	**60.14**	**71.64**	**54.55**	**112.50**	**68.57**

Table 37 Cadence

Parameter	Cadence									
Trial	Curve Walk 3 Left	Curve Walk 3 Right	Walking Straight 1 Left	Walking Straight 1 Right	Walking Straight 2 Left	Walking Straight 2 Right	Turn in Frame 1 Left	Turn in Frame 1 Right	Turn in Frame 3 Left	Turn in Frame 3 Right
Walking Toward	113.68	69.90	65.85	99.31	98.63	85.21	115.60	94.03	100.70	61.54
Walking Away	112.50	133.33	105.88	114.29	94.74	107.46			128.57	124.14
Average	**113.09**	**101.62**	**85.87**	**106.80**	**96.68**	**96.33**	**115.60**	**94.03**	**114.64**	**92.84**
STD	**0.84**	**44.85**	**28.30**	**10.59**	**2.75**	**15.74**	115.60	94.03	**19.71**	**44.26**
Median	**113.09**	**101.62**	**85.87**	**106.80**	**96.68**	**96.33**	**115.60**	**94.03**	**114.64**	**92.84**
High	**113.68**	**133.33**	**105.88**	**114.29**	**98.63**	**107.46**	**115.60**	**94.03**	**128.57**	**124.14**
Low	**112.50**	**69.90**	**65.85**	**99.31**	**94.74**	**85.21**	**115.60**	**94.03**	**100.70**	**61.54**

4.3.8 Stance Time

As mentioned earlier, we are not comparing the accuracy of the Stance Times the ground truth. We are simply measuring how much variation there is. There is no ground truth to compare, and therefore no measure of error. Through our trials, walking with a walker had the highest value and circular walking the lowest value. The value is reported based on the definition of a stance in the chapter 3. The table shows the average duration taken from start to end in the stance phase.

Table 38 Stance Times

Parameter	**Stance Times**									
Trial	**Cane 1 Left**	**Cane 1 Right**	**Cane 2 Left**	**Cane 2 Right**	**Walker 1 Left**	**Walker 1 Right**	**Walker 2 Left**	**Walker 2 Right**	**Curve Walk 1 Left**	**Curve Walk 1 Right**
Values	1.100	1.100	0.950	0.883	1.517	1.317	1.267	1.217	0.717	0.717
	1.017	1.017	0.933	0.967	1.417	1.500	1.267	1.150	0.633	0.617
	1.033	0.967	0.933	0.917	1.200	1.400	1.117	1.133	0.650	0.650
	0.900	0.933	0.900	0.850	1.283	1.400	1.083	1.083	0.617	0.667
	0.850	0.850			1.100	1.233	1.050	1.133	0.667	0.567
					1.200	1.217	1.167	1.183	0.700	0.667
					1.183	1.133	1.667	1.217	0.767	0.800
					1.167	1.167		1.150		
					1.283	1.183		1.133		
					1.167	1.267		1.083		
								1.133		
								1.183		
Average	**0.98**	**0.97**	**0.93**	**0.90**	**1.25**	**1.28**	**1.23**	**1.15**	**0.68**	**0.67**
STD	**0.10**	**0.09**	**0.02**	**0.05**	**0.13**	**0.12**	**0.21**	**0.04**	**0.05**	**0.07**
Median	**1.02**	**0.97**	**0.93**	**0.90**	**1.20**	**1.25**	**1.17**	**1.14**	**0.67**	**0.67**
High	**1.10**	**1.10**	**0.95**	**0.97**	**1.52**	**1.50**	**1.67**	**1.22**	**0.77**	**0.80**
Low	**0.85**	**0.85**	**0.90**	**0.85**	**1.10**	**1.13**	**1.05**	**1.08**	**0.62**	**0.57**

Table 39 Stance Times

Parameter	Stance Times									
Trial	**Curve Walk 3 Left**	**Curve Walk 3 Right**	**Walking Straight 1 Left**	**Walking Straight 1 Right**	**Walking Straight 2 Left**	**Walking Straight 2 Right**	**Turn in Frame 1 Left**	**Turn in Frame 1 Right**	**Turn in Frame 3 Left**	**Turn in Frame 3 Right**
Values	0.667	0.683	0.800	1.700	0.800	0.817	0.683	0.683	0.733	0.767
	0.667	0.667	0.750	0.767	0.733	0.783	0.667	0.650	0.650	0.667
	0.650	0.667	0.767	0.750	0.733	0.733	0.850	0.633	0.550	0.567
	0.667	0.700	0.750	0.750	0.717	0.733	0.650	0.767	0.617	0.883
	0.667	0.683	0.767	0.750	0.683	0.717	0.683	0.633	0.600	0.617
	0.600	0.633	0.767	0.700	0.717	0.733	0.667	0.617	0.667	0.600
				0.783	0.733	0.750		0.583		0.633
Average	**0.65**	**0.67**	**0.77**	**0.89**	**0.73**	**0.75**	**0.70**	**0.65**	**0.64**	**0.68**
STD	**0.03**	**0.02**	**0.02**	**0.36**	**0.04**	**0.04**	**0.07**	**0.06**	**0.06**	**0.11**
Median	**0.67**	**0.68**	**0.77**	**0.75**	**0.73**	**0.73**	**0.68**	**0.63**	**0.63**	**0.63**
High	**0.67**	**0.70**	**0.80**	**1.70**	**0.80**	**0.82**	**0.85**	**0.77**	**0.73**	**0.88**
Low	**0.60**	**0.63**	**0.75**	**0.70**	**0.68**	**0.72**	**0.65**	**0.58**	**0.55**	**0.57**

4.3.9 Swing Time

As mentioned, we are not comparing the accuracy of the Swing Times the ground truth. We are simply measuring how much variation there is. There is no ground truth to compare, and therefore no measure of error. Through our trials, walking with a cane had the highest value and circular walking the lowest value. The value is reported based on the definition of a swing in the chapter 3. The table shows the average duration taken from start to end for a swing phase.

Table 40 Swing Times

Parameter	Swing Times									
Trial	**Cane 1 Left**	**Cane 1 Right**	**Cane 2 Left**	**Cane 2 Right**	**Walker 1 Left**	**Walker 1 Right**	**Walker 2 Left**	**Walker 2 Right**	**Curve Walk 1 Left**	**Curve Walk 1 Right**
Values	0.47	0.67	0.50	0.63	0.60	0.53	0.52	0.63	0.40	0.43
	0.75	0.65	0.60	0.67	0.67	0.75	0.63	0.68	0.40	0.43
	0.68	0.72	0.68	0.63	0.77	0.60	0.58	0.67	0.40	0.40
	0.67	0.60	0.58	0.63	0.55	0.57	0.65	0.62	0.42	0.42
	0.60	0.60	0.63	0.43	0.65	0.55	0.68	0.68	0.38	0.42
	0.67	0.40	0.57		0.63	0.58	0.62	0.60	0.42	0.43
	0.58				0.57	0.55	0.57	0.57	0.45	0.43
					0.65	0.60		0.65	0.15	0.55
					0.58	0.60				
					0.50	0.58				
					0.58	0.47				
					0.28					
Average	**0.63**	**0.61**	**0.59**	**0.60**	**0.59**	**0.58**	**0.61**	**0.64**	**0.38**	**0.44**
STD	**0.09**	**0.11**	**0.06**	**0.09**	**0.12**	**0.07**	**0.06**	**0.04**	**0.09**	**0.05**
Median	**0.67**	**0.63**	**0.59**	**0.63**	**0.59**	**0.58**	**0.62**	**0.64**	**0.40**	**0.43**
High	**0.75**	**0.72**	**0.68**	**0.67**	**0.77**	**0.75**	**0.68**	**0.68**	**0.45**	**0.55**
Low	**0.47**	**0.40**	**0.50**	**0.43**	**0.28**	**0.47**	**0.52**	**0.57**	**0.15**	**0.40**

Table 41 Swing Times

Parameter	Swing Times									
Trial	**Curve Walk 3 Left**	**Curve Walk 3 Right**	**Walking Straight 1 Left**	**Walking Straight 1 Right**	**Walking Straight 2 Left**	**Walking Straight 2 Right**	**Turn in Frame 1 Left**	**Turn in Frame 1 Right**	**Turn in Frame 3 Left**	**Turn in Frame 3 Right**
Values	0.40	0.47	0.58	0.42	0.43	0.48	0.38	0.47	0.43	0.50
	0.40	0.40	0.43	0.48	0.45	0.47	0.37	0.40	0.40	0.42
	0.42	0.40	0.45	0.45	0.43	0.42	0.38	0.40	0.40	0.45
	0.43	0.40	0.40	0.43	0.43	0.43	0.30	0.37	0.68	0.33
	0.43	0.40	0.38	0.40	0.42	0.42	0.38	0.42	0.38	0.40
	0.38	0.40	0.42	0.47	0.40	0.38	0.40	0.45	0.37	0.40
	0.40	0.37		0.42	0.45	0.38	0.37	0.47	0.45	0.43
						0.42				0.30
Average	**0.41**	**0.40**	**0.44**	**0.44**	**0.43**	**0.43**	**0.37**	**0.42**	**0.45**	**0.40**
STD	**0.02**	**0.03**	**0.07**	**0.03**	**0.02**	**0.04**	**0.03**	**0.04**	**0.11**	**0.06**
Median	**0.40**	**0.40**	**0.43**	**0.43**	**0.43**	**0.42**	**0.38**	**0.42**	**0.40**	**0.41**
High	**0.43**	**0.47**	**0.58**	**0.48**	**0.45**	**0.48**	**0.40**	**0.47**	**0.68**	**0.50**
Low	**0.38**	**0.37**	**0.38**	**0.40**	**0.40**	**0.38**	**0.30**	**0.37**	**0.37**	**0.30**

4.3.10 Stance to Swing Ratio

Again, we are not comparing the accuracy of the Stance to Swing rations the ground truth. We are simply measuring how much variation there is. There is no ground truth to compare, and therefore no measure of error. Through our trials, walking in a straight line (turning out of frame) had the highest value and circular walking the lowest value. The importance of this value is highlighted by M Iosa [10] in The Golden Ratio of Gait Harmony: Repetitive Proportions of Repetitive Gait Phases.

Table 42 Stance Swing Rations

Parameter	**Stance Swing Rations**									
Trial	**Cane 1 Left**	**Cane 1 Right**	**Cane 2 Left**	**Cane 2 Right**	**Walker 1 Left**	**Walker 1 Right**	**Walker 2 Left**	**Walker 2 Right**	**Curve Walk 1 Left**	**Curve Walk 1 Right**
Values	2.36	1.65	1.90	1.39	2.53	2.47	2.45	1.92	1.79	1.65
	1.36	1.56	1.56	1.53	2.13	2.00	2.00	1.68	1.58	1.42
	1.51	1.61	1.60	1.45	1.57	2.33	1.91	1.70	1.63	1.63
	1.50	1.56	1.42	1.96	2.33	2.47	1.59	1.59	1.48	1.60
	1.28	2.13			1.69	2.24	1.70	1.89	1.74	1.31
					1.89	2.09	2.06	2.09	1.68	1.54
					1.82	1.89			1.70	1.45
					2.00	1.94				
					2.57	2.03				
					2.00	2.71				
Average	**1.60**	**1.70**	**1.62**	**1.58**	**2.05**	**2.22**	**1.95**	**1.81**	**1.66**	**1.51**
STD	**0.43**	**0.24**	**0.20**	**0.26**	**0.34**	**0.27**	**0.30**	**0.19**	**0.10**	**0.13**
Median	**1.50**	**1.61**	**1.58**	**1.49**	**2.00**	**2.16**	**1.96**	**1.79**	**1.68**	**1.54**
High	**2.36**	**2.13**	**1.90**	**1.96**	**2.57**	**2.71**	**2.45**	**2.09**	**1.79**	**1.65**
Low	**1.28**	**1.56**	**1.42**	**1.39**	**1.57**	**1.89**	**1.59**	**1.59**	**1.48**	**1.31**

Table 43 Stance Swing Rations

Parameter	Stance Swing Rations									
Trial	**Curve Walk 3 Left**	**Curve Walk 3 Right**	**Walking Straight 1 Left**	**Walking Straight 1 Right**	**Walking Straight 2 Left**	**Walking Straight 2 Right**	**Turn in Frame 1 Left**	**Turn in Frame 1 Right**	**Turn in Frame 3 Left**	**Turn in Frame 3 Right**
Values	1.67	1.46	1.37	4.08	1.85	1.69	1.78	1.46	1.69	1.53
	1.67	1.67	1.73	1.59	1.63	1.68	1.82	1.63	1.63	1.60
	1.56	1.67	1.70	1.67	1.69	1.76	2.22	1.58	1.38	1.26
	1.54	1.75	1.88	1.88	1.72	1.69	2.17	2.09	1.61	2.65
	1.54	1.71	2.00	1.61	1.71	1.72	1.78	1.52	1.64	1.54
	1.57	1.73	1.84	1.68	1.59	1.91	1.67	1.37	1.48	1.50
						1.96		1.25		1.46
Average	**1.59**	**1.66**	**1.75**	**2.08**	**1.70**	**1.77**	**1.91**	**1.56**	**1.57**	**1.65**
STD	**0.06**	**0.10**	**0.22**	**0.98**	**0.09**	**0.11**	**0.23**	**0.27**	**0.12**	**0.45**
Median	**1.56**	**1.69**	**1.79**	**1.67**	**1.70**	**1.72**	**1.80**	**1.52**	**1.62**	**1.53**
High	**1.67**	**1.75**	**2.00**	**4.08**	**1.85**	**1.96**	**2.22**	**2.09**	**1.69**	**2.65**
Low	**1.54**	**1.46**	**1.37**	**1.59**	**1.59**	**1.68**	**1.67**	**1.25**	**1.38**	**1.26**

4.3.11 Double Support Time

Double support occurs when both feet are in contact with the ground at the same time. Again, we are not comparing the accuracy of the double support times the ground truth. We are simply measuring how much variation there is. There is no ground truth to compare, and therefore no measure of error. Through our trials, with a walker had the highest value and circular walking the lowest value. The calculation is based on the definition provided earlier in chapter 3.

Table 44 Double Support Times

Parameter	Double Support Times									
Trial	**Cane 1 Left**	**Cane 1 Right**	**Cane 2 Left**	**Cane 2 Right**	**Walker 1 Left**	**Walker 1 Right**	**Walker 2 Left**	**Walker 2 Right**	**Curve Walk 1 Left**	**Curve Walk 1 Right**
Values	0.30	0.13	0.20	0.12	0.32	0.40	0.40	0.30	0.17	0.15
	0.22	0.15	0.17	0.10	0.38	0.45	0.33	0.18	0.10	0.12
	0.18	0.13	0.18	0.20	0.20	0.43	0.28	0.27	0.12	0.13
	0.18	0.18	0.17	0.12	0.42	0.43	1.48	0.22	0.13	0.12
	0.15	0.12	0.18	0.10	0.27	0.32	0.22	0.18	0.12	0.12
	0.17	0.10			0.33	0.25	0.22	0.23	0.13	0.07
					1.43	0.32	0.28	0.32	0.22	0.12
					0.25	0.23	0.30	0.72		0.13
					0.25	0.33				0.00
					0.37	0.32				
					0.35	0.33				
						0.35				
Average	**0.20**	**0.14**	**0.18**	**0.13**	**0.42**	**0.35**	**0.44**	**0.30**	**0.14**	**0.11**
STD	**0.05**	**0.03**	**0.01**	**0.04**	**0.34**	**0.07**	**0.43**	**0.17**	**0.04**	**0.05**
Median	**0.18**	**0.13**	**0.18**	**0.12**	**0.33**	**0.33**	**0.29**	**0.25**	**0.13**	**0.12**
High	**0.30**	**0.18**	**0.20**	**0.20**	**1.43**	**0.45**	**1.48**	**0.72**	**0.22**	**0.15**
Low	**0.15**	**0.10**	**0.17**	**0.10**	**0.20**	**0.23**	**0.22**	**0.18**	**0.10**	**0.00**

Table 45 Double Support Times

Parameter	Double Support Times									
Trial	**Curve Walk 3 Left**	**Curve Walk 3 Right**	**Walking Straight 1 Left**	**Walking Straight 1 Right**	**Walking Straight 2 Left**	**Walking Straight 2 Right**	**Turn in Frame 1 Left**	**Turn in Frame 1 Right**	**Turn in Frame 3 Left**	**Turn in Frame 3 Right**
Values	0.15	0.13	0.15	0.97	0.17	0.22	0.15	0.15	0.18	0.15
	0.15	0.12	0.17	0.17	0.17	0.17	0.15	0.13	0.13	0.13
	0.13	0.12	0.17	0.13	0.15	0.15	0.13	0.12	0.10	0.07
	0.15	0.12	0.17	0.17	0.15	0.15	0.12	0.35	0.08	0.12
	0.13	0.12	0.17	0.18	0.15	0.15	0.13	0.12	0.08	0.13
	0.12	0.12	0.18	0.13	0.15	0.15	0.12	0.10	0.10	0.10
		0.13	0.20	0.17	0.18	0.15	0.13	0.08	0.13	0.10
		0.12			0.15	0.17			0.08	
Average	**0.1**	**0.1**	**0.2**	**0.3**	**0.2**	**0.2**	**0.1**	**0.2**	**0.1**	**0.1**
STD	**0.0**	**0.0**	**0.0**	**0.3**	**0.0**	**0.0**	**0.0**	**0.1**	**0.0**	**0.0**
Median	**0.1**	**0.1**	**0.2**	**0.2**	**0.2**	**0.2**	**0.1**	**0.1**	**0.1**	**0.1**
High	**0.2**	**0.1**	**0.2**	**1.0**	**0.2**	**0.2**	**0.2**	**0.4**	**0.2**	**0.2**
Low	**0.1**	**0.1**	**0.2**	**0.1**	**0.2**	**0.2**	**0.1**	**0.1**	**0.1**	**0.1**

4.4 Unreliable Gait Parameters and methods

In addition to the above-mentioned results, we have tried several other methods and parameters to extract our desired outputs. However not all of them were usable in term of accuracy and reliability and the below sections lists some of them.

Table 46 Unreliable Spatial-temporal parameters

Spatial-Temporal Parameters	Vertical Velocity	Heel Vertical Velocity
		Toe Vertical Velocity
		Knee Vertical Velocity
	Angular Velocity	Thigh Angular Velocity
		Foot Angular Velocity
	Sagittal Velocity	Salim Ghoussayni Algorithm

4.4.1 Vertical Velocity of Keypoints

Using vertical velocity of feet keypoints specially heels, toes, and knees where one of the early methods that we considered. However, despite applying and testing various combination of digital filters to the output data we could not have a consistent and reliable result. There are many reasons engaged in this situation including high-level of estimation in the deep-learning model (due to missing points), and complex movement of the points in 3-D coordinates. The below figure shows an example of heel vertical velocity on the right foot, the green vertical lines represent foot-off event and the red ones correspond to heal strike. As it can be observed there is no consistent pattern to detect the gait phases and FO and HS can happen at any point of the signal. The results for other considered points followed the same or worse level of reliability

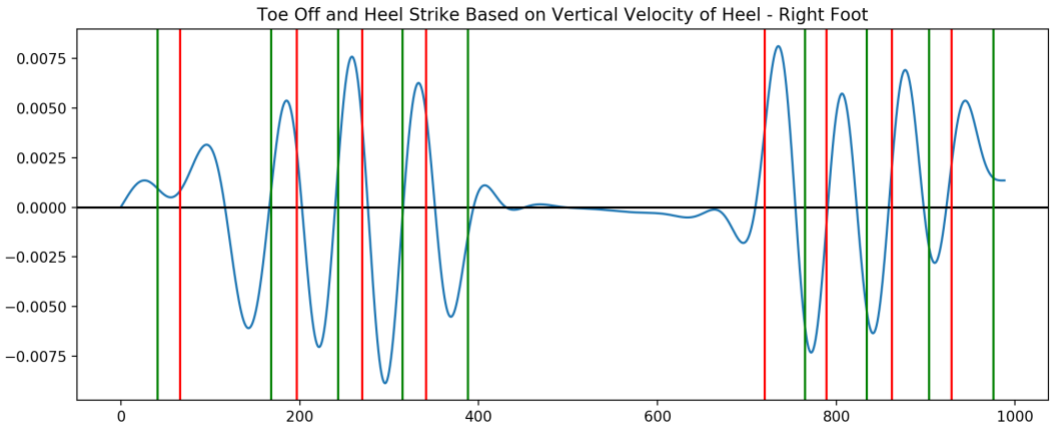

Figure 47 Toe Off and Heel Strike Based on Vertical Velocity of Heel - Right Foot - WS1

4.4.2 Angular velocity

In addition to the reported shank angular velocity results in the first section of chapter 4, calculating angular velocity of other body segments, including thighs and full legs the results were not usable. Moreover, despite applying and testing various combination of digital filters to the output data was showing high sensitivity to noise. There are many reasons engaged in this situation including high-level of estimation in the deep-learning model (due to missing points per frame), and complex movement of the points in 3-D coordinates. The following figure represents signal generated from right thigh's Vertical angular velocity in WS1.

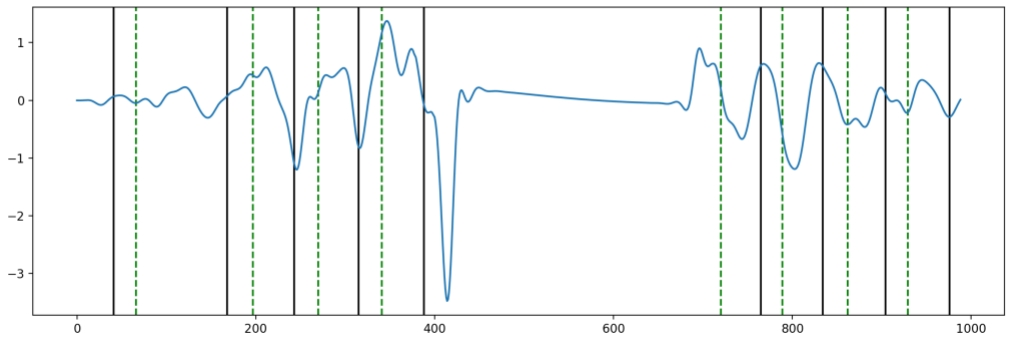

Figure 48 Right Thigh Vertical Angular Velocity in WS1

4.4.3 Sagittal Velocity

This method is proposed by Salim Ghoussayni in “Assessment and validation of a simple automated method for the detection of gait events and intervals” [68]. The method is based on sagittal velocity of heels and toes and uses priori model with average walking speed to optimize the outcome. The results of this method were highly variable based on the walking type, therefore could not be generalized for a diverse situation like an institutional hallway. Implementation of this algorithm was done by Mr. Connor[61], with small modifications done by the author.

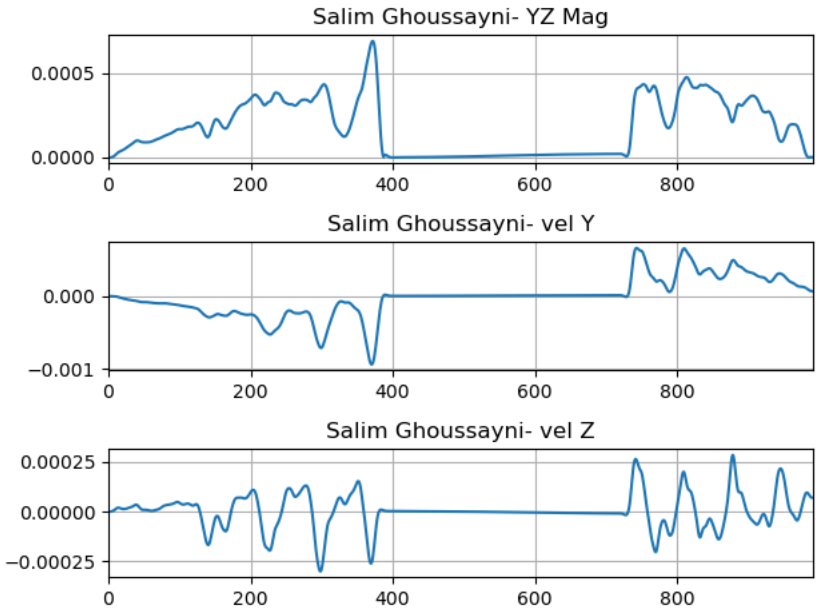

Figure 49 WS1 Signal - Salim Ghoussayni Algorithm

5 Analysis and Discussion

The following approach has been followed to interpret the results:

1. First a ground truth is established based on manual and systematic measurement.
    a) Manual measurement of body limbs of subject.
    b) Manually Heel Strike and and Toe Off events are labelled from 2-D images in the recorded videos.
2. Accuracy of the outputs from the system is compared to the ground truth.
3. Accuracy of the output is compared to existing gait analysis methods .

5.1 Analysis of Gait Results

The table below characterizes the results obtained for each of the different gait parameters that we investigated. Dark green cells mean accuracy compared to ground truth was consistent and within the defined threshold. Light green defines good results but with occasional inconsistent behavior. Cells with no colors are parameters that were not compared with a ground truth but can be relied on based on known size of the lab setup and calculations performed. Orange and red cells indicate unreliable gait parameters for which we were unable to obtain usable results.

Table 47 Rated Gait Parameters

Gait Parameters	Temporal Parameters	Swing Phase
		Stance Phase
		Stop Phase
	Spatial Parameters	Left Arm Length
		Left Forearm Length
		Right Arm Length
		Right Forearm Length
		Left Thigh Length
		Left Shank Length
		Right Thigh Length
		Right Shank Length
		Left Ankle to Heel Length
		Left Ankle to Big Toe Length
		Left Ankle To Small Toe Length
		Right Ankle to Heel Length
		Right Ankle to Big Toe Length
		Right Ankle to Small Toe Length
		Shoulder Width
		Hip Width
		Chest Height
		Heels Vertical Position
		Toe Vertical Position
		Knee Vertical Position
	Spatial-Temporal Parameters	Stride Length
		Stride Times
		Stride Speeds
		Step Length

		Step Time
		Cadence
		Stance Time
		Swing Time
		Stance to Swing Ratio
		Double Support Time
		Shank Center of Mass Vertical Velocity
		Thigh Center of Mass Vertical Velocity
		Heel Vertical Velocity
		Toe Vertical Velocity
		Knee Vertical Velocity
		Thigh Angular Velocity
		Leg Angular Velocity

5.1.1 Temporal Parameters

We used temporal parameters to extract toe-off and heel strike timings from the data using the method proposed by Zeni, et. El [6] Based on the results, we have noticed by average +-4 frames difference among the trials while the subject is walking in a straight line without any other complexity added to the situation. There are, however, factors that affect the outcome. We noticed that the increased stride speed, direction change of the subject, and distance from the cameras play an important role in the accuracy of the system. For example, it can be noticed that when the subject turns in the frame, the average error can raise up to 8 frames. Moreover, surprisingly walking with a walker had one of the lowest error rates. First due to nature of walking style, and an extra equipment in the scene, we were expecting a high number missed key points per frame, but with the average error of +-5 frames the results

were promising. It worth mentioning that slower pace of the subject played an important role in reducing the missed frames.

Walking with a cane and circular walking showed some level of inconsistency; however, repeating the trials multiple times with a cautious interpretation of results could provide helpful insight.

Moreover, it worth mentioning that turning and circular walking could increase the chance of false positives for toe-off and heel strike, which could result in lousy swing and stance detection. Therefore, we highly recommend using this system only for cases that include walking back and forth in a straight line.

The current gold standard methods allow up to 4 frames difference for both of the gait phases; and walking in a straight line, especially toward camera is well within the range.

5.1.2 Spatial Parameters

Detecting a single point position on a specific time in 3-D showed its complications in our method. Mainly due to small size of the points in a frame (in term of pixels area), or the point not being visible to cameras, while walking away from them. In general, walking toward camera showed better results for all of the points. Yet, the inconsistency tends to be high. This mainly goes back to the detection algorithm of OpenPose which tries to estimate the location of a points via PAF where a point is not detectable. The estimation might be useful for some other applications, but for our type of intended use, it seems to be beyond the defined threshold. However, the average segment lengths reported over a time interval we could measure with <2 CM accuracy and constant standard deviation, by applying digital filters.

Feet key points position, for neither the localization, nor timing could be extracted, since the data were highly affected by signal noise, especially for points located on the lower feet portion including toes and heels. A main reason for this problem is the dataset size being used for it is made of roughly 14k images, in comparison to other points images which are made of over 2 million annotated samples [2].

Finally, due to unavailability of a reference system, such as Vicon, the reported Step and Stride length were not compared to the ground truth, and we only assessed their consistency while walking in an institutional hallway. However the results tend to be within the standard range which are calculated by other studies [69]. Also, since the length of the hallway is known to the researchers, we could roughly verify the values.

5.1.3 Spatial-Temporal Parameters

Spatial-temporal parameters are mainly extracted around the features related to step and stride events. Again, since this parameter was collected and extracted over a time period, by applying digital filters, we could have constant results for the trials. Stride Times, Stride Speeds, Step Times in Seconds, Stance Swing Rations, Cadence, Stance Times, Swing Times Stance Swing Ration, and Double Support Times values were reported in the previous chapter. Our main target was to evaluate consistency of the outcome to see what a parameter looks like across all five trials. Despite not having a ground truth for the parameters, the results are within the measured numbers by other researchers [69]. Heel Vertical Velocity, and Toe Vertical Velocity results were not useful since the original Heel and Toe position data were noisy with noticeable inconsistency, and therefore their velocities are also affected. Knee Vertical Velocity, Thigh Angular Velocity and Leg Angular Velocity due to their continuous micro three axial movement in 3-D space, our system with two RGB cameras

faced challenges since estimating the depth data was not possible in many frames. Finally, while using Salim Ghoussayni's Algorithm [68] it showed poor performance in generalizing and the results were not consistent. More precisely, detecting the phases needed manual customization of the parameters per trial and subjects to get results that match our initial considered threshold.

5.2 **Comparison to Related Work**

In related works, the defined threshold for an acceptable method varies depending on the application, as was described in chapter 2. Most approaches use highly constrained environments (e.g. treadmill), attached special markers to patients which are not practical for general mobility in order to identify limbs and joints accurately, and have a large number of cameras from different angles in order to triangulate a 3-D model. These are appropriate in order to get absolutely accurate analysis for detailed diagnosis and root-cause analysis of gait issues in a laboratory setting, however, they are not practical for day to day or week to week monitoring of patients gait in an institutional setting (e.g. walking in a hallway).

We deliberately restricted ourselves to a low cost (less than $500) solution with 2 cameras, no markers, and natural walking environment in our approach. Our approach is complementary to the more specialized approaches. We have sufficient consistency and accuracy of basic temporal and spatial parameters in order to measure overall stride, swing, etc. in order to track gradual improvement and flag any detonation of gait when observing patients in an institutional hallway. If a problem is suspected, then follow up can happen with more detailed and accurate analysis in the other methods using a controlled environment with markers and many cameras.

In the table on the next page, one can see that our deep-learning approach (which helps compensate for the lack of markers and reduce the uncertainty caused by the insufficient number of cameras for true 3d modelling) is comparable to two of the best approaches we could find in the literature in terms of the average error rate. The other approaches have an error rate of 2 frames while ours is 4 frames.

Table 48 Comparison to Related Work

Paper	Walking Type	Ground truth	Keypoints Detection	Foot Strike Timing Algorithm	Number of Cameras for 3-D Modeling	Filters	subjects	Average Error
Two simple methods for determining gait events during treadmill and overground walking using kinematic data [23]	Treadmill	Force Plate	Markers	Coordinate-based algorithm Velocity-based algorithm	6 cameras	NA	Mixed, 18	60hz, 98% of events were within two frames
Comparison of methods for kinematic identification of foot strike and toe-off during overground and treadmill running	Treadmill	8 Vicon Cameras / Force Plate	Markers	Multiple Algorithms	8 Vicon Cameras	12 Hz with a fourth-order zero-lag Butterworth filter	20 runners	2-5 Frames
Thesis	Free walking in a lab	Manually Rated	Markerless Deep-Learning	Coordinate-based algorithm [67] Velocity-based algorithm[70]	2 Cameras	4 Hz with a fourth-order zero-lag Butterworth filter + RANSAC	1	4 Frames

5.3 Assumptions, Limitations and Threats to Validity

5.3.1 Assumptions

The first assumption for this study has been that the institute is equipped with two RGB cameras in one of their hallways. Next, the hallway has a good lighting condition (enough for the algorithm to detect the subjects), and the residents can move independently or with an assistive device throughout the hallway. It has been considered that the lighting condition, subject race, and background color are not affecting the outcome. Finally, it has been assumed that at a time, only one patient walks through the hallway, and the reported result is solely based on a single patient per time.

5.3.2 Limitations

The trials were captured in a lab with a static setup for cameras, and due to limited access to the lab, because of the COVID-19 pandemic, we could not simulate different types of camera positions, angles and heights. Moreover, we could not use another reference system (e.g., Vicon System, Force Plates) to compare and verify our outcomes against the system's results; hence we reported errors using manual verifications. We have also estimated parameters such as stride length based on the number of steps and the known length of our lab space.

5.3.3 Threats to Validity

As earlier mentioned, due to a limited number of subjects (only one), it would be challenging to consider our findings as a generalized conclusion—further studies with more diverse subjects, especially patients with sensory and motor disorders. Furthermore, RGB cameras are susceptible to various lighting situations; in this study, we have not tested our findings against different lighting conditions. Also, color contrast plays a significant role in image-

based posture detection frameworks, and pathway color, walls, and patients' outfit colors might affect the accuracy positively or negatively.

6 Conclusion and Future Work

6.1 Research Summary

Gait analysis and gait abnormality detection allows early intervention and treatment to prevent underlying conditions developing that might cause a fall. It can also evaluate the recovery progress of the physical therapy.

The method consists of three stages. First, the event detection module records the gait event video clip while a person walks through the camera. Second, pose estimation is applied to extract sequence of skeleton and joints in the video. Then feature extraction and gait classification is performed to calculate gait and postural parameters. These outcomes helps the physicians to classify if the gait is normal or abnormal.

This thesis provides a comprehensive overview of gait analysis and posture measurement, and some significant research in this area to help developing the foundation required for implementing and evaluating the research objective. The method for marker-less stride parameters analysis with two cameras in a smart hallway shows promise in terms of the preliminary results we have obtained. Referring to the main questions of the research, they can be answered with the following conclusion:

- Would it possible to extract clinically usable gait parameters in 3-D from two cameras installed in an institutional hallway?
    - Yes, it is possible, but at this stage the results are not sufficient enough to monitor patients clinically, moreover they cannot be used for diagnosis. However, it enables the physicians to monitor subjects progress over a period with an acceptable accuracy. (which ones are green, which ones are not)

- Which pose estimation model would provide the most accurate result for the planned setup with the considered restrictions?
    - In terms of frameworks, OpenPose with PAF algorithm provides the highest accuracy.
    - However, in terms of data-model selection, having a model which can estimate position of feet segments is essential, and at this stage the only model which can detect feet and the full body is BODY-25(COCO or MPII alone are not sufficient).
    - The results might be improved if the models were not restricted to use 2-D RGB data to estimate the poses. At the pose estimation level depth data are not considered.

6.2 **Future Work**

The research offered in this thesis is a novel human pose estimation using an AI that can demonstrate results in real-time, with the ability to be used in different set up. Contributions of this thesis include an accurate, easy-to-access, reliable, and live solution to quantify human pose using AI. The successful smart hallway opens the door for many new research opportunities for clinical and none-clinical purposes.

One of the future applications can be that a multi-person household or facility may be incorporated with the face recognition module to automatically accept the identification of the person in a video and then apply derived gait characteristics to their recordings. If a person's gait abnormality has been observed in the system, a medical warning is produced and stored in their profile. In addition, prospective systems will illustrate that a predictive

model for forecasting future falls can be trained on this data and a project would be one step forward in creating a framework capable of predicting and thereby helping to minimise falls in older adults with dementia. Finally, we have noticed that some algorithms including shank angular velocity [67] and the method proposed by Salim Ghoussayni [68] showed promising results in some controlled cases, future research to use hybrid algorithms to detect gait phases based on the subject and movement type could be useful to enhance the reported results.

References

[1] J. Wang, Y. Chen, S. Hao, X. Peng, and L. Hu, “Deep learning for sensor-based activity recognition: A survey,” *Pattern Recognit. Lett.,* 2019.

[2] Z. Cao, T. Simon, S. E. Wei, and Y. Sheikh, “Realtime multi-person 2D pose estimation using part affinity fields,” in *Proceedings - 30th IEEE Conference on Computer Vision and Pattern Recognition, CVPR 2017*, 2017.

[3] A. H. Snijders, B. P. van de Warrenburg, N. Giladi, and B. R. Bloem, “Neurological gait disorders in elderly people: clinical approach and classification,” *Lancet Neurology*. 2007.

[4] E. Jaspers, K. Desloovere, H. Bruyninckx, G. Molenaers, K. Klingels, and H. Feys, “Review of quantitative measurements of upper limb movements in hemiplegic cerebral palsy,” *Gait and Posture*. 2009.

[5] M. Coluccini, E. S. Maini, C. Martelloni, G. Sgandurra, and G. Cioni, “Kinematic characterization of functional reach to grasp in normal and in motor disabled children,” *Gait Posture,* 2007.

[6] Y. Li, J. Zeng, S. Shan, and X. Chen, “Occlusion Aware Facial Expression Recognition Using CNN With Attention Mechanism,” *IEEE Trans. Image Process.,* 2019.

[7] M. Belshaw1, B. Taati, D. Giesbrecht, and A. Mihailidis, “Intelligent vision-based fall detection system: preliminary results from a real world deployment.,” in *RESNA/ICTA 2011: Advancing Rehabilitation Technologies for an Aging Society (June 5-8, 2011 : Toronto, Ontario, Canada),* 2011.

[8] S. Basiratzadeh, E. D. Lemaire, M. Dorrikhteh, and N. Baddour, “Fiducial marker approach for biomechanical smartphone-based measurements,” in *BioSMART 2019 -*

Proceedings: 3rd International Conference on Bio-Engineering for Smart Technologies, 2019.

[9] M. Saleh and G. Murdoch, "In defence of gait analysis. Observation and measurement in gait assessment," *J. Bone Jt. Surg. - Ser. B*, 1985.

[10] M. Iosa *et al.*, "The Golden Ratio of Gait Harmony: Repetitive Proportions of Repetitive Gait Phases," *Biomed Res. Int.*, vol. 2013, p. 918642, 2013.

[11] K. Peffers, T. Tuunanen, M. A. Rothenberger, and S. Chatterjee, "A design science research methodology for information systems research," *J. Manag. Inf. Syst.*, 2007.

[12] F. Achilles, A. E. Ichim, H. Coskun, F. Tombari, S. Noachtar, and N. Navab, "Patient MoCap: Human pose estimation under blanket occlusion for hospital monitoring applications," in *Lecture Notes in Computer Science (including subseries Lecture Notes in Artificial Intelligence and Lecture Notes in Bioinformatics)*, 2016.

[13] N. Zahradka, K. Verma, A. Behboodi, B. Bodt, H. Wright, and S. C. K. Lee, "An Evaluation of Three Kinematic Methods for Gait Event Detection Compared to the Kinetic-Based 'Gold Standard,'" *Sensors*, vol. 20, no. 18, 2020.

[14] A. Kharb, V. Saini, Y. Jain, S. Dhiman, M. Tech, and Scholar, "A review of gait cycle and its parameters," *IJCEM Int J Comput Eng Manag*, vol. 13, 2011.

[15] P. Connor and A. Ross, "Biometric recognition by gait: A survey of modalities and features," *Comput. Vis. Image Underst.*, vol. 167, pp. 1–27, 2018.

[16] E. Ceseracciu, Z. Sawacha, and C. Cobelli, "Comparison of Markerless and Marker-Based Motion Capture Technologies through Simultaneous Data Collection during Gait: Proof of Concept," *PLoS One*, vol. 9, no. 3, pp. 1–7, 2014.

[17] R. Mc Ardle, S. Del Din, P. Donaghy, B. Galna, A. J. Thomas, and L. Rochester, "The Impact of Environment on Gait Assessment: Considerations from Real-World Gait

Analysis in Dementia Subtypes," *Sensors*, vol. 21, no. 3, 2021.

[18] P. Catalfamo, S. Ghoussayni, and D. Ewins, "Gait Event Detection on Level Ground and Incline Walking Using a Rate Gyroscope," *Sensors*, vol. 10, no. 6, pp. 5683–5702, 2010.

[19] K. Aminian, B. Najafi, C. Büla, P.-F. Leyvraz, and P. Robert, "Spatio-temporal parameters of gait measured by an ambulatory system using miniature gyroscopes," *J. Biomech.*, vol. 35, no. 5, pp. 689–699, 2002.

[20] C. C. Monaghan, W. J. B. M. van Riel, and P. H. Veltink, "Control of triceps surae stimulation based on shank orientation using a uniaxial gyroscope during gait," *Med. Biol. Eng. Comput.*, vol. 47, no. 11, p. 1181, 2009.

[21] J. Rueterbories, E. G. Spaich, B. Larsen, and O. Andersen, "Methods for gait detection and analysis in ambulatory systems," *Med. Eng. Phys.*, vol. 32, pp. 545–552, 2010.

[22] J. Rueterbories, E. G. Spaich, and O. K. Andersen, "Gait event detection for use in FES rehabilitation by radial and tangential foot accelerations," *Med. Eng. Phys.*, vol. 36, no. 4, pp. 502–508, 2014.

[23] C.-C. Yang and Y.-L. Hsu, "A review of accelerometry-based wearable motion detectors for physical activity monitoring," *Sensors (Basel).*, vol. 10, no. 8, pp. 7772–7788, 2010.

[24] R. T. Lauer, B. T. Smith, D. Coiro, R. R. Betz, and J. McCarthy, "Feasibility of gait event detection using intramuscular electromyography in the child with cerebral palsy," *Neuromodulation Technol. Neural Interface*, vol. 7, no. 3, pp. 205–213, 2004.

[25] R. T. Lauer, B. T. Smith, and R. R. Betz, "Application of a neuro-fuzzy network for gait event detection using electromyography in the child with cerebral palsy," *IEEE Trans. Biomed. Eng.*, vol. 52, no. 9, pp. 1532–1540, 2005.

[26] M. M. Skelly and H. J. Chizeck, "Real-time gait event detection for paraplegic FES walking," *IEEE Trans. neural Syst. Rehabil. Eng.*, vol. 9, no. 1, pp. 59–68, 2001.

[27] B. T. Smith, D. J. Coiro, R. Finson, R. R. Betz, and J. McCarthy, “Evaluation of force-sensing resistors for gait event detection to trigger electrical stimulation to improve walking in the child with cerebral palsy,” *IEEE Trans. Neural Syst. Rehabil. Eng.*, vol. 10, no. 1, pp. 22–29, 2002.

[28] T. P. Andriacchi, J. A. Ogle, and J. O. Galante, “Walking speed as a basis for normal and abnormal gait measurements,” *J. Biomech.*, 1977.

[29] J. M. Hausdorff, D. A. Rios, and H. K. Edelberg, “Gait variability and fall risk in community-living older adults: A 1-year prospective study,” *Arch. Phys. Med. Rehabil.*, 2001.

[30] C. Prakash, R. Kumar, and N. Mittal, “Recent developments in human gait research: parameters, approaches, applications, machine learning techniques, datasets and challenges,” *Artif. Intell. Rev.*, 2018.

[31] M. Nieto-Hidalgo, F. J. Ferrández-Pastor, R. J. Valdivieso-Sarabia, J. Mora-Pascual, and J. M. García-Chamizo, “A vision based proposal for classification of normal and abnormal gait using RGB camera,” *J. Biomed. Inform.*, 2016.

[32] M. Khokhlova, C. Migniot, A. Morozov, O. Sushkova, and A. Dipanda, “Normal and pathological gait classification LSTM model,” *Artif. Intell. Med.*, 2019.

[33] E. van der Kruk and M. M. Reijne, “Accuracy of human motion capture systems for sport applications; state-of-the-art review,” *Eur. J. Sport Sci.*, vol. 18, no. 6, pp. 806–819, 2018.

[34] K. M. Bell *et al.*, “Verification of a portable motion tracking system for remote management of physical rehabilitation of the knee,” *Sensors*, vol. 19, no. 5, p. 1021, 2019.

[35] C. Ezeh, C. Holloway, and T. Carlson, “MoRe-T2 (mobility research trajectory tracker): validation and application,” *J. Rehabil. Assist. Technol. Eng.*, vol. 3, p. 2055668316670552, Jan. 2016.

[36] L. H. Sloot, J. Harlaar, and M. M. van der Krogt, “Self-paced versus fixed speed walking and the effect of virtual reality in children with cerebral palsy,” *Gait Posture*, vol. 42, no. 4, pp. 498–504, 2015.

[37] P. Sale, M. Franceschini, A. Waldner, and S. Hesse, “Use of the robot assisted gait therapy in rehabilitation of patients with stroke and spinal cord injury,” *Eur. J. Phys. Rehabil. Med.*, vol. 48, pp. 111–121, Mar. 2012.

[38] L. N. Awad, A. Esquenazi, G. E. Francisco, K. J. Nolan, and A. Jayaraman, “The ReWalk ReStore™ soft robotic exosuit: a multi-site clinical trial of the safety, reliability, and feasibility of exosuit-augmented post-stroke gait rehabilitation,” *J. Neuroeng. Rehabil.*, vol. 17, no. 1, p. 80, 2020.

[39] N. Kumar, N. Kunju, A. Kumar, and B. Sohi, “Active marker based kinematic and spatio-temporal gait measurement system using LabVIEW vision,” *J. Sci. Ind. Res. (India).*, vol. 69, Aug. 2010.

[40] N. Zahradka, A. Behboodi, H. Wright, B. Bodt, and S. Lee, “Evaluation of Gait Phase Detection Delay Compensation Strategies to Control a Gyroscope-Controlled Functional Electrical Stimulation System During Walking,” *Sensors (Basel).*, vol. 19, no. 11, p. 2471, May 2019.

[41] C. J. C. Lamoth, O. G. Meijer, A. Daffertshofer, P. I. J. M. Wuisman, and P. J. Beek, “Effects of chronic low back pain on trunk coordination and back muscle activity during walking: changes in motor control,” *Eur. Spine J.*, vol. 15, no. 1, pp. 23–40, 2006.

[42] D. H. Sutherland, “The evolution of clinical gait analysis: Part II Kinematics,” *Gait Posture*, vol. 16, no. 2, pp. 159–179, 2002.

[43] H. J. Woltring and E. B. Marsolais, “Optoelectric (Selspot) gait measurement in two-and three-dimensional space--a preliminary report.,” *Bull. Prosthet. Res.*, vol. 10, pp. 46–52,

1980.

[44] J. Shotton *et al.*, “Real-time human pose recognition in parts from single depth images,” in *Proceedings of the IEEE Computer Society Conference on Computer Vision and Pattern Recognition*, 2011.

[45] Y. Yang and D. Ramanan, “Articulated human detection with flexible mixtures of parts,” *IEEE Trans. Pattern Anal. Mach. Intell.*, 2013.

[46] M. Andriluka, L. Pishchulin, P. Gehler, and B. Schiele, “2D human pose estimation: New benchmark and state of the art analysis,” in *Proceedings of the IEEE Computer Society Conference on Computer Vision and Pattern Recognition*, 2014.

[47] W. Tang, P. Yu, and Y. Wu, “Deeply Learned Compositional Models for Human Pose Estimation,” in *Lecture Notes in Computer Science (including subseries Lecture Notes in Artificial Intelligence and Lecture Notes in Bioinformatics)*, 2018.

[48] X. Liu, M. I. Sarker, M. Milanova, and L. O’Gorman, “Video-Based Monitoring and Analytics of Human Gait for Companion Robot BT - New Approaches for Multidimensional Signal Processing,” 2021, pp. 15–33.

[49] P. C. Bala, B. R. Eisenreich, S. B. M. Yoo, B. Y. Hayden, H. S. Park, and J. Zimmermann, “Automated markerless pose estimation in freely moving macaques with OpenMonkeyStudio,” *Nat. Commun.*, vol. 11, no. 1, p. 4560, 2020.

[50] J. L. Schönberger and J.-M. Frahm, “Structure-from-Motion Revisited,” *2016 IEEE Conf. Comput. Vis. Pattern Recognit.*, pp. 4104–4113, 2016.

[51] M. W. Whittle, “Clinical gait analysis: A review,” *Hum. Mov. Sci.*, vol. 15, no. 3, pp. 369–387, 1996.

[52] A. Alamdari and V. N. Krovi, “Chapter Two - A Review of Computational Musculoskeletal Analysis of Human Lower Extremities,” J. Ueda and Y. B. T.-H. M. for

B.-I. R. Kurita, Eds. Academic Press, 2017, pp. 37–73.

[53] A. D. Likens and N. Stergiou, “Chapter 2 - Basic biomechanics,” N. B. T.-B. and G. A. Stergiou, Ed. Academic Press, 2020, pp. 17–63.

[54] T. Stöckel, R. Jacksteit, M. Behrens, R. Skripitz, R. Bader, and A. Mau-Moeller, “The mental representation of the human gait in young and older adults,” *Front. Psychol.*, 2015.

[55] R. Drillis, R. Contini, and M. Bluestein, “Body segment parameters,” *Artif. Limbs*, vol. 8, no. 1, pp. 44–66, 1964.

[56] C. E. Clauser, J. T. McConville, and J. W. Young, “Weight, volume, and center of mass of segments of the human body,” Antioch Coll Yellow Springs OH, 1969.

[57] T.-Y. Lin *et al.*, “Microsoft coco: Common objects in context,” in *European conference on computer vision*, 2014, pp. 740–755.

[58] H. Dong *et al.*, “Tensorlayer: a versatile library for efficient deep learning development,” in *Proceedings of the 25th ACM international conference on Multimedia*, 2017, pp. 1201–1204.

[59] S. Albawi, T. A. Mohammed, and S. Al-Zawi, “Understanding of a convolutional neural network,” in *2017 International Conference on Engineering and Technology (ICET)*, 2017, pp. 1–6.

[60] M. Mateen, J. Wen, S. Song, and Z. Huang, “Fundus image classification using VGG-19 architecture with PCA and SVD,” *Symmetry (Basel).*, vol. 11, no. 1, p. 1, 2019.

[61] Connor J.C. McGuirk, “A Multi-view Video Based Deep Learning Approach for Human Movement Analysis,” University of Ottawa, 2021.

[62] “OpenCV: Camera Calibration and 3D Reconstruction.” [Online]. Available: https://docs.opencv.org/3.4/d9/d0c/group__calib3d.html#ga61585db663d9da06b68e70cf. [Accessed: 06-Jun-2021].

[63] M. A. Fischler and R. C. Bolles, “Random sample consensus: a paradigm for model fitting with applications to image analysis and automated cartography,” *Commun. ACM*, vol. 24, no. 6, pp. 381–395, 1981.

[64] K. Derpanis, “Overview of the RANSAC Algorithm,” 2005.

[65] I. W. Selesnick and C. S. Burrus, “Generalized digital Butterworth filter design,” *IEEE Trans. signal Process.*, vol. 46, no. 6, pp. 1688–1694, 1998.

[66] G. Ellis, “Chapter 9 - Filters in Control Systems,” G. B. T.-C. S. D. G. (Third E. Ellis, Ed. Burlington: Academic Press, 2004, pp. 171–189.

[67] M. Grimmer, K. Schmidt, J. Duarte, L. Neuner, G. Koglnov, and R. Riener, “Stance and Swing Detection Based on the Angular Velocity of Lower Limb Segments During Walking,” *Front. Neurorobot.*, vol. 13, pp. 1–15, 2019.

[68] S. Ghoussayni, C. Stevens, S. Durham, and D. Ewins, “Assessment and validation of a simple automated method for the detection of gait events and intervals,” *Gait & posture*, vol. 20, no. 3, p. 266—272, Dec. 2004.

[69] A. Peruzzi, U. Della Croce, and A. Cereatti, “Estimation of stride length in level walking using an inertial measurement unit attached to the foot: A validation of the zero velocity assumption during stance,” *J. Biomech.*, vol. 44, no. 10, pp. 1991–1994, 2011.

[70] J. A. Zeni Jr, J. G. Richards, and J. S. Higginson, “Two simple methods for determining gait events during treadmill and overground walking using kinematic data,” *Gait \& posture*, vol. 27, no. 4, pp. 710–714, 2008.